7th International Conference
on Cellular Materials

CellMAT 2022

Book of Abstracts

Chairpersons

Prof. Dr.-Ing. Peter Quadbeck
University of Applied Science Offenburg

Vice Chairperson

Prof. Dr. Dirk Enke
Leipzig University

Dr.-Ing. Tobias Fey
Friedrich-Alexander-Universität Erlangen-Nürnberg (FAU)

Prof. Dr. Michael Scheffler
Otto von Guericke University Magdeburg

Program Committee

Jörg Adler
Fraunhofer Institute for Ceramic Technologies and Systems IKTS

Prof. Dr. Volker Altstädt
University of Bayreuth

Dr. Olaf Andersen
Fraunhofer Institute for Manufacturing Technology and Advanced Materials IFAM

Prof. Dr.-Ing. Christos G. Aneziris
TU Bergakademie Freiberg

Prof. Dr. John Banhart
Helmholtz-Zentrum Berlin für Materialien und Energie

Dr. Ulf Betke
Otto von Guericke University Magdeburg

Prof. Dr. Paolo Colombo
University of Padova

Prof. Dr. Ernesto Di Maio
University of Naples Federico II

Prof. Dr. David C. Dunand
Northwestern University

Prof. Dr. Claudia Fleck
TU Berlin

Prof. Dr. Hans-Peter Heim
University of Kassel

Dr. Thomas Hipke
Fraunhofer Institute for Machine Tools and Forming Technology IWU

Prof. Dr. Yuji Iwamoto
Nagoya Institute of Technology

Prof. Dr. Klaus D. Jandt
Friedrich Schiller University Jena

Dr. Thomas Konegger
TU Wien

Prof. Dr. Carolin Körner
Friedrich-Alexander-Universität Erlangen-Nürnberg (FAU)

Prof. Dr. Andreas Mortensen
École Polytechnique Fédérale de Lausanne EPFL

Dr. Afsaneh Rabiei
North Carolina State University

Prof. Dr. Miguel Angel Rodríguez Pérez
University of Valladolid

Prof. Dr. Thomas Scheibel
University of Bayreuth

Dr.-Ing. Franziska Schmidt
Charité - Universitätsmedizin Berlin

Dr. Hartmut Traut
Trexel GmbH

Mike Tromm
University of Kassel

Dr. Michaela Wilhelm
University of Bremen

Table of contents

Cellular bioactive scaffolds for bone regeneration

Bone consists of a natural composite of organic (collagen) and inorganic (bone mineral Hydroxyapatite) phase with a highly porous structure. For bone regeneration in case of trauma or illness, researchers therefore try to mimic the hieratical, porous and/or material structure of bone. Artificial bone replacement materials should fulfill several requirements, such as: mechanical properties should match the original tissue, the applied material should be at least bioinert or better bioactive (i.e. dissolution of the material will enhance the self-healing properties of the surrounding tissue), and the geometry should mimic that of natural bone (i.e. high porosity coupled with high specific surface area and good mechanical strength). An open porous structure encourages cell adhesion, proliferation and the transport of nutrients. If mesoporous ceramic powders are employed a hierarchical porosity can be achieved, ranging from nanometer to mm pores.

Open macroporous scaffolds can be achieved by conventional processing, such as freeze casting, or by additive manufacturing, such as robocasting, laser-based powder bed fusion or stereolithography. We employed freeze casting to produce Bioactive Glass- Chitosan-Gelatin composite scaffolds with high porosity and good elastic properties. Freeze-casting is a cost-effective, easy to use technique for the fabrication of macroporous ceramics. It relies on the formation and subsequent sublimation of ice crystals that act as pore templates in frozen particulate dispersions. By variation of processing parameters, such as freezing rate and slurry composition pore size distribution and pore shape can be controlled.

Additive manufacturing on the other hand allows complete control over geometry, pore size, pore structure, and such factors, but requires equipment. For AM of pure ceramics and composites the ceramic powders are generally combined with organics, either as sacrificial or non-sacrificial binders.

Component design for foamed thermoplastic injection molded parts

Roman Hofer
2LIMIT GmbH
r.hofer@2-limit.com

Thermoplastic foam injection molding has its advantages and disadvantages. In this lecture you will learn how to use the advantages in component design and avoid typical stumbling blocks.

Innovative polypropylene solutions for injection moulded, foamed parts showing excellent surface appearance

Cornelia Tranninger, Thomas Lummerstorfer, Daniela Mileva, Georg Grestenberger
Borealis Polyolefine GmbH, Linz, Austria

There is a constant seeking for down gauging and light-weighing opportunities within the automotive industries to address more and more demanding legislations on Green-House-Gas emissions while in parallel there is an increasing demand for safety-and comfort enhancing features which might result in increased curb weight. Polymers and in particular polypropylene (PP) are therefore already the material of choice for many interior and exterior applications. This material is a key enabler for light weight design in cars, but also offers other advantages like increased design freedom, functional integration and manufacturing costs. The development of alternative car concepts like cars with electric engines (including heavy batteries) where the distance, which can be driven between recharging cycles, depends among others on the weight of the car, further increases the need for additional curb weight reduction. Consequently, the increasing use of polymeric foams and plastic foam structures is the logical next step.

Plastic parts obtained from the foam injection moulding process offer an additional weight saving potential of up to 30% compared to compact plastic parts (see figure 1). Apart from the obvious weight reduction, this process also allows the production of parts showing high dimensional stability (low warpage) and minimised sink marks. However, achieving good impact performance and surface appearance for parts produced using foam injection moulding is typically rather challenging.

In this study, it will be shown how reducing the density applying short shot and core back foaming technology affects the mechanical properties of PP-compounds based on a heterophasic PP-copolymer and 10% mineral filler. The density of the specimen covered a range from 980 g/cm³ for the compact material to app. 650 g/cm³ for the core back foam injection moulded specimen. Charpy notched impact strength as well as tensile modulus and puncture tests were done in order to systematically study the change of impact stiffness balance as a function of the density. The impact strength of conventional materials is significantly reduced already at moderate foaming levels. Consequently, there is a need to develop specific materials for foaming applications fulfilling the need of excellent surface appearance and good mechanical properties.

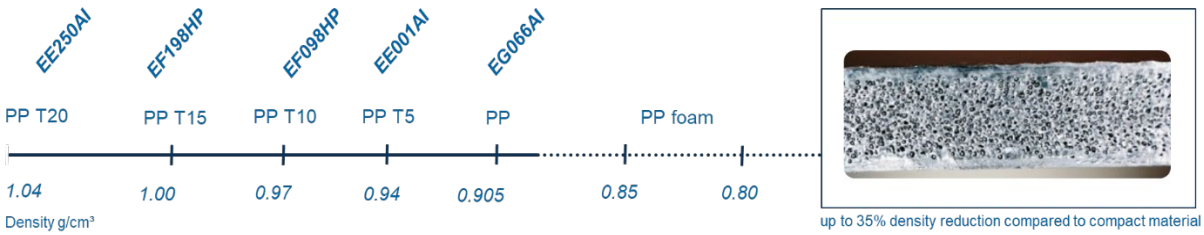

Figure 1: Daplen™ innovations for automotive interior applications & foamed PP as a function of their density.

Metallic porous materials as key component for the efficient electrolysis of water to green hydrogen

C. I. Bernäcker[1*], T. Rauscher[1], S. Loos[1], T. Büttner[1], J. Albers[1], T. Weißgärber[1,2]

[1] Fraunhofer Institute for Manufacturing Technology and Advanced Materials IFAM, Winterbergstraße 28, Dresden, Germany
[2] Technische Universität Dresden, Institute for Materials Science, Dresden, Germany
* Christian.Bernaecker@ifam-dd.fraunhofer.de

Hydrogen is a safe and versatile energy carrier, which can be produced via water electrolysis using renewable energy sources ("green hydrogen"). For a future GW-industry of alkaline electrolysers (AEL), the efficiency has to be improved and the costs (euro per installed kW [€/kW]) have to drop. While the last point in particular is currently receiving a lot of attention and many projects are starting to ramp up mass production of electrolysers, the efficiency point is not sufficiently considered. This is negligent since the total cost of ownership for an operator of a hydrogen production plant is determined by the cost of electricity. This in turn is directly dependent on the efficiency.
Therefore, it is important to develop scalable materials that significantly increase efficiency. Here, the cell architecture and the electrode coating are the main influencing factors.
Modern AEL systems use a zero-gap architecture, in which the electrode is pressed directly onto the separators. The use of porous structures is crucial so that gas bubbles can evolve in the aqueous electrolyte and also be removed from the reaction chamber. These structures, which are often also referred to as porous transport layer, gas diffusion layer or gas diffusion electrode, must have the following properties:
- open porosity for gas bubble removal and electrolyte supply
- optimal pore size for gas-electrolyte exchange (large pores) and for large electrode area or catalyst layer contacting (small pores)
- electrical conductivity
- mechanical stability
- corrosion stability

The presentation will give an overview of the use of porous materials for AEL applications and discuss new developments from IFAM (see Figure 1).

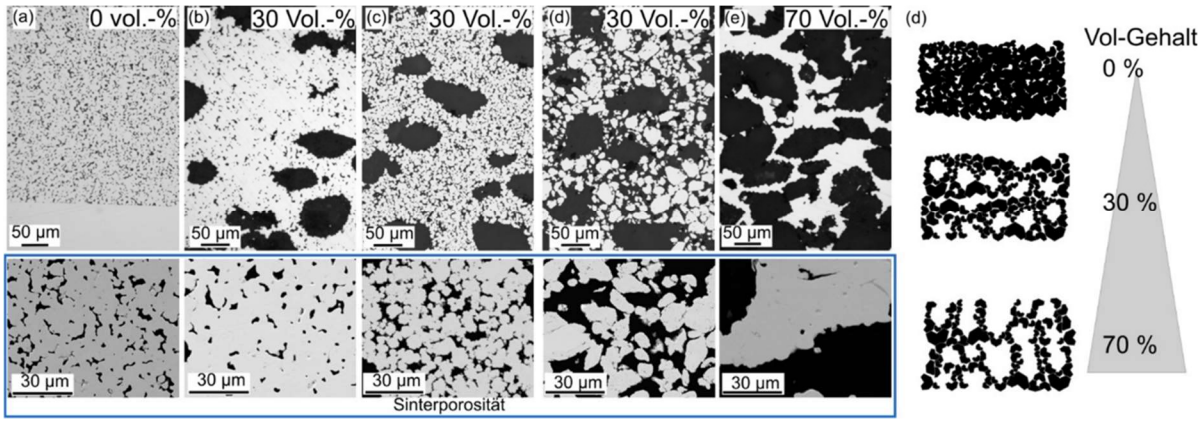

Figure 1. Optical micrographs of IFAM materials revealing a bimodal pore structure.[1]

References

[1] T. Rauscher, C.I. Bernäcker, S. Loos, M. Vogt, B. Kieback, L. Röntzsch, *Electrochimica Acta*, 2019, *317*, 128-128.

Open-cell foam glass with additional nanoporosity

S. Carstens[1*]

[1] Universität Leipzig, Institut für Technische Chemie
*simon.carstens@uni-leipzig.de

Foam glass is an innovative and sustainable material for various applications. Using waste glass as starting material, the production of foam glass is an upcycling process, yielding a durable, non-flammable, highly porous lightweight material. The process uses finely ground waste glass alongside a foaming agent, which releases a gas – most often CO_2 – during its thermally induced decomposition process. Depending on the nature of the foaming agent, which may be either a solid or a liquid, the process is labelled as dry or wet foaming.

Currently, the most prominent foam glass applications are lightweight construction as well as thermal and acoustic insulation. Beyond that, catalysis may also become a relevant field of application for this thermally and chemically stable material with a total porosity of up to 95 %. However, these disparate applications necessitate varying degrees of open or closed foam cells, respectively. This can be controlled by precisely choosing the foaming conditions, which besides the particle size and the nature and amount of foaming agent also include the temperature program.

The effects of different dry foaming agents such as manganese oxides in varying oxidation states (MnO_2, Mn_2O_3, Mn_3O_4), as well as the influence of the temperature program were investigated. This is not limited to the foaming temperature as such but also the heating and cooling rates. Thus, glass foams with a share of open cells as high as 99 % can be obtained.

In another line of study, sodium borosilicate (*sbs*) glasses were used as starting material. *sbs* glasses exhibit a unique behaviour when a second tempering plateau is added after the foaming step itself. This second tempering step occurs within the range of glass transition with high ion mobility in the glass body. Depending on the temperature and duration, a phase separation can thus be induced, yielding a silicate phase and a sodium-rich borate phase. The latter may afterwards be removed by acid leaching. Applying this idea to foam glass, additional nanoporosity may be introduced within the walls of the glass foam. The surface area is thus enhanced, and possible applications as catalysts or filters arise. Since the phase separation process can be controlled precisely, the nanopores are adjustable. [1]

Reference

[1] C.S. de Oliveira, R. Kohns, F. Meyerhöfer, S. Carstens, D. Enke, R.B. Wehrspohn, J. Martins de Souza e Silva *Mater. Chem. Front.*, 2021, *5*, 4615.

Porous ceramics – from processing to novel applications

T. Fey[1*]

[1] Friedrich-Alexander-Universität Erlangen-Nürnberg (FAU)
* tobias.fey@fau.de

Porosity in ceramics is usually avoided because porosity leads to a reduction in strength. However, there are a variety of applications where the use of porous materials is necessary.

The spectrum of applications ranges from catalyst carrier structures, filters, lightweight construction materials, energy adsorption or energy storage materials to bone replacement materials in the medical field. A variety of established and novel manufacturing methods are available. With these, a wide range of material properties, e.g. thermal conductivity, mechanical strength or damping, can be adjusted by using different materials. By saving material and thus resources, porous ceramic materials make an important contribution to CO2 savings and resource efficiency.

Invited talks

Sprayable Glass Bubble insulation for sustainable and energy efficient building insulation

T. Gerdes[1*], A. Rosin[1], S. Zelder[1],

[1] University of Bayreuth, Keylab Glass Technology
*gerdes@uni-bayreuth.de

In 2018, 117 Mt of CO_2 emissions in Germany originated from the building sector. This corresponds to 14% of the total greenhouse gas emissions in Germany. The climate goals cannot be achieved with the current rate of energy refurbishment.
Despite a variety of current insulation concepts, different properties of the materials used, which go beyond the primary goal of insulation, are often inadequate or problematic. In addition, a payback of the investment through savings in energy costs is not feasible in all cases.
This contribution examines a micro hollow glass sphere-based interior and exterior insulation as an alternative to existing thermal insulation composite systems, which is characterised by a special combination of open and closed pores. The so-called ecosphere system is a cement-based sprayable insulation material with a volume fraction of approximately 90% micro hollow glass beads (glass bubbles). Glass bubbles are thin-walled (0.3-2.0 µm) spherical glass particles with a diameter of 30-200 µm (see fig. 1, left). For decades glass bubbles are an important product in niche markets. With this new application, the bubbles will enter the mass market.
The processing technology is of crucial importance for the outstanding properties of the insulation. By improving existing spraying technologies for plasters it is now possible to apply this composite material to façades with a thickness of 15 cm without damaging the filigree glass bubbles. The compressed air-driven spraying process introduces additional porosity into the insulation, and thus further reduces thermal conductivity. Because of the high amount of porosity (93%), the glass bubble insulation has a density of just 125 kg/m^3 and thermal conductivity of 0.040 W/mK. Moreover, because ecosphere is a purely mineral insulation material, it can be reused at the end of its life cycle as an aggregate for hydraulically binding building materials after crushing and moderate heat treatment.

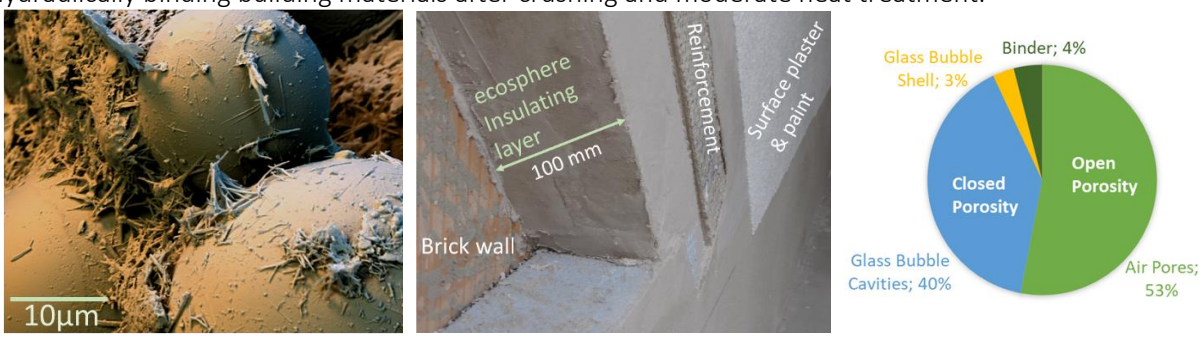

Figure 1. Bonding between the glass bubbles and the cement phase needles (left) and the layered structure of the ecosphere insulation on the building façade (middle), Composition of the ecosphere insulation (right)

Till the end of 2021, about 55,0000 m^2 of ecosphere insulation has been applied to buildings by the development partner Maxit.
Within the talk, the crucial role of glass in the insulation material will be discussed, as well as the required energy for production (“Grey Energy”).

References

[1] https://www.bmu.de/fileadmin/Daten_BMU/Download_PDF/Klimaschutz/klimaschutz_zahlen_2019_fs_gebaeude_de_bf.pdf

Additive manufacturing

Additive cellular material design by UV-induced polymer hydrogel inter-crosslinking

T. A. Neuendorf[1], N. Weigel[1], M. Vigogne[1], J. Thiele[1*]

[1] Leibniz Institute of Polymer Research Dresden
*thiele@ipfdd.de

In recent years, stimuli-responsive hydrogels have gained tremendous interest in designing smart 4D materials for applications ranging from biomedicine[1] to soft electronics[2] that can change their properties on demand over time. However, at present, a hydrogel's response is often induced by merely a single stimulus, restricting its broader applicability. Here, we show the controlled hierarchical assembly of various hydrogel building blocks, each with a tailored set of mechanical and physicochemical properties as well as programmed stimulus response that may potentially enable the design and fabrication of multi-responsive polymer-based cellular materials that process complex operations.

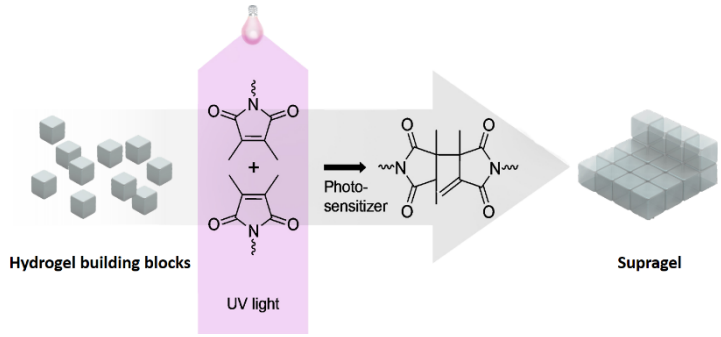

Figure 1. Schematic representation of the supragel's fabrication.

To build up discontinuous soft matter based on hydrogel building blocks, the inter-connection stability of such building blocks is equally crucial as their property since it is directly associated with the transfer of information between the building blocks. Although multiple approaches of inter-connection[3,4] and assembly[5,6] have been described, they either miss out on the controlled stacking of assemblies into 3D objects or mostly rely on unsaturated moieties of the respective base material to inter-connect their hydrogel structures instead on a strong building block inter-connection.

We address these challenges using a separate crosslinking mechanism based on UV-induced 2,3-dimethylmaleimide (DMMI) dimerization to inter-connect hydrogel-based building blocks. To demonstrate its versatility, we inter-connect acrylamide-based and *N*-isopropylacrylamide-based millimeter-sized cubic building blocks, respectively, yielding dual-crosslinked freestanding assemblies. With this work, we want to pave the way towards cellular materials based on hydrogel building blocks with the capability of tuning material properties at the micrometer-scale, allowing topologically complex, multi-functional materials.

References

[1] S. H. Aswathy *Heliyon*, 2020, *6*, e03719.
[2] X. Sun *ACS Appl. Bio Mater.*, 2021, *4*, 140-162.
[3] I. Antoniuk *Polymers*, 2018, *10*, 566.
[4] J. C. Gaulding *Macromolecules*, 2012, *45*, 39-45.
[5] F. G. Downs *Nat. Chem.*, 2020, *12*, 363-371.
[6] M. A. Skylar-Scott *Nature*, 2019, *575*, 330-335.

Additively manufactured high-manganese steel lattice structures for energy absorption applications

D. Kibaroglu[1*], P. Köhnen[2], C. Haase[1], U. Krupp[1], C. Drebenstedt[3], C. Hannemann[3], Thomas Hipke[3]

[1] RWTH Aachen, [2]GKN Additive, [3]Fraunhofer Institute for Machine Tools and Forming Technology
*dilay.kibaroglu@iehk.rwth-aachen.de

Additive manufacturing (AM) is a novel manufacturing technique that allows rapid production of net-shaped components for automotive, aerospace, and biomedical applications [1]. Parts with complex geometries such as lattice structures for lightweight applications with high energy-absorption capacity can be produced by AM. In this regard, laser powder bed fusion (LPBF) stands out as one of the feasible AM techniques due to its high resolution (small laser spot size) and flexible processing (powder-bed approach), which allows production of geometrically complex structures with small strut thickness [2].

As a member of second generation advanced high-strength steels (AHSS), high-manganese steels (HMnS) have been reported as suitable alloys for production of lattice structures by LPBF [3]. By alloy design approach, different deformation mechanisms, e.g., transformation-induced plasticity (TRIP) and twinning-induced plasticity (TWIP), can be activated in HMnS. For this purpose, addition of different Al amounts (1 and 5 wt.%) was utilised to manipulate the deformation mechanisms by changing the stacking fault energy (SFE) of the alloy. Then the lattice structures of X30Mn22, X30MnAl22-1, and X30MnAl22-5 alloys with $f_2$cc,z unit cells were produced by LPBF and their deformation behaviour under compression was investigated. The results revealed that the HMnS lattice structures have higher weight-specific energy absorption than the benchmark alloys (Ti6Al4V and AISI 316L), as shown in **Figure 1.a** [3]. However, it can be seen in **Figure 1.b** that strain localisation at z-strut nodes (parallel to load direction) of X30Mn22 lattice occurs under compression, which leads to formation of brittle martensite at the early stages of deformation and consequently collective failure of the structure.

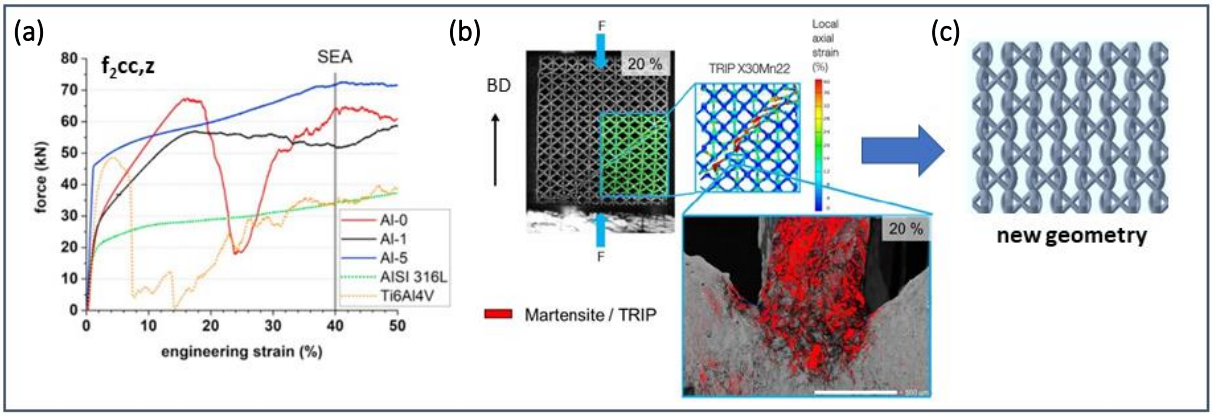

Figure 1. Cell design approach for HMnS lattice structures: (a) Compression curves of $f_2$cc,z structures. (b) Drawbacks of $f_2$cc,z design. (c) Proposed geometry.

In order to prevent strain localisation at the nodes of the structures under load while improving the microstructural and mechanical characteristics, a new geometry, that is illustrated in **Figure 1.c**, was proposed. In this contribution, the combined alloy and geometry design approach for HMnS lattice structures with enhanced energy-absorption capacity is presented.

References

[1] D. L., Bourell *Annual Review of Materials Research)*, **2016**, *46*, 1-18.
[2] B. Hanks, J. Berthel, M. Frecker, T.W. Simpson *Additive Manufacturing*, **2020**, *35*, 101-301.
[3] P. Köhnen, S. Ewald, J.H. Schleifenbaum, A. Belyakov, C. Haase *Additive Manufacturing*, **2020**, *35*, 101-389.

Computational 3D modelling of Calcium diffusion and gelling front migration in hydrogels blend for bioprinting

J. Palma[1], M. Bertuola[1], É. Hermida[1]

[1] Instituto de Tecnologías Emergentes y Ciencias Aplicadas (ITECA), UNSAM, CONICET, Escuela de Ciencia y Tecnología (ECyT), San Martín, 1650 Buenos Aires, Argentina
*jpalma@unsam.edu.ar

Natural hydrogels are widely used for 3D-bioprinting of scaffolds that emulate the extracellular matrix of different human tissues; Alginate based gels are among the most broadly used. Crosslinking by Ca^{2+} ions is a key issue for achieving the proper mechanical response; the dynamics of this process has been reported for alginate and alginate-gelatine systems [1,2] however, 3D modelling of scaffolds of any shape, with calculated diffusion parameters is not already implemented.

The aim of this work was study the kinetics of the gelling front and the diffusion of Calcium ions within the matrix of the Alginate-Gelatine-Hyaluronic acid (Alg-Gel-HA) tripartite ink (4.5% w/v of each polymer in PBS1X) using a simple and low-cost method (video record and image analysis by ImageJ®). Experimental data could be well fitted by a numerical model (Python script) that predicts the time for maximum cross-linking, according to the dimension and shape of the scaffolds.

Samples were prepared by placing a drop of Alg-Gel-HA ink onto a glass slide, and pressing with a coverslip until the ink reaches the edge of the coverslip. Each sample was mounted above a black base and a USB camera with red light was used to enhance contrast in the video. Once the video recording was started, 0.5M of Ca^{2+} was injected at one edge of the coverslip; the ink becomes opaque as the the Ca^{2+} diffuses. The diffusion front was followed and recorded for 40min at 22°C; the advance of the crosslinking front (x) at the time (t) was determined using the software image J®. These data could be fitted by the equation: $x = A*t^{1/2}$, where A is a constant, following the typical relation for a diffusion process. This A value was included in a numerical code in Phyton, developed to model how the crosslinking proceeds in an any shape sample, just using the .STL file as the input of the code. This model was validated using circular samples as shown in the Fig 1.

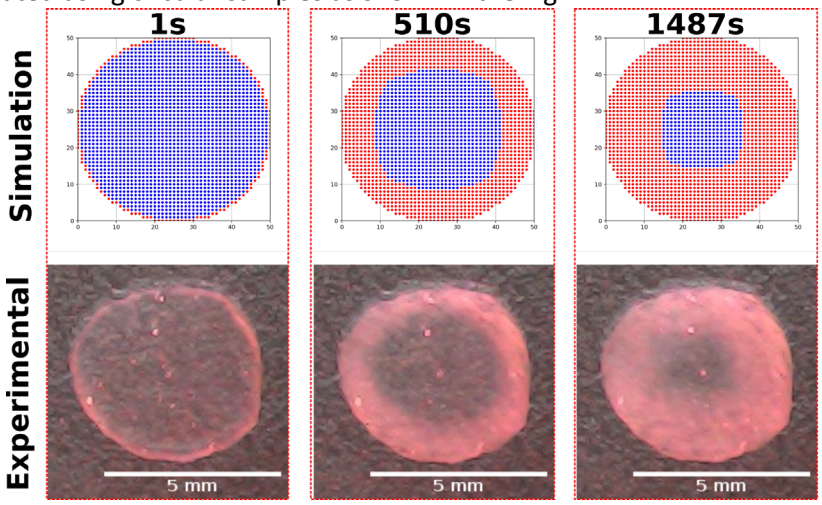

Figure 1. Results of Python simulation of crosslinking cylinder scaffold at 22°C (0.5M $CaCl_2$) and experimental validation.

Processing the time evolution of the crosslinking front (border of the opaque outer area) shown in Fig 1, A=(0.039±0.004)mm/$s^{1/2}$ arises. Introducing this value in the Python code we programmed we could simulate the advance of the crosslinking front and validate the results using circle shaped scaffold (Fig. 1). Therefore, the experimental device and the image analysis have become proper to predict how the crosslinking process takes place even in complex structures. However, the numerical model fits very well the beginning of the diffusion process, but changes in the boundary conditions deviate the prediction when more than 50% of the samples has been crosslinked. For instance, the time needed to fully crosslink the sample of Fig 1 cylinder was t=(2700 ± 300)s while the simulation predict t=(4400±700)s.

References

[1] A. Posbeyikian, et al., *Carbohydrate Polymers*, **2021**, *269*, 1-10.
[2] M.S. Chavez, et al., *Journal of food science*, **1994**, *59*, 1108-1110.

Resorbable and biocompatible scaffolds made of a bacterial biopolymer

Daiana Nygaard, Marcos Bertuola, Oxana Yashchuk, Élida B Hermida

Instituto de Tecnologías Emergentes y Ciencias Aplicadas, UNSAM, CONICET, Escuela de Ciencia y Tecnología, Laboratorio de Biomateriales, Biomecánica y Bioinstrumentación (Lab3Bio), San Martín, Provincia de Buenos Aires, Argentina.

3D printing allows to build scaffolds for tissue regeneration with controlled porosity. By adjusting the percentage and pattern of infill, and the printing velocity, scaffolds can be manufactured with the porosity that mimics the extracellular matrix (ECM) of each type of tissue (bone, cartilage, skin, etc.). The elastic modulus of Poly(3-hydroxybutyrate-co-3-hydroxyvalerate) (PHBV), a biodegradable polymer produced by microorganisms, make it suitable to resemble the ECM of cartilage and bone. In fact, the excellent combination of its attributes: thermoplastic, resorbable and biocompatible, encourages 3D printing of PHBV-products for biomedical applications. Fused deposition modeling with PHBV filaments has the drawback of the narrow working window between the melting point (160°C) and the thermal decomposition temperature (220°C). Thus, the aim of this work is to formulate a viscous ink made of PHBV that allows to build scaffolds using a bioprinter.

The PHBV-ink was obtained by dissolving PHBV in chloroform (12.7% m/v) at 70°C and slowly cooled to room temperature; the ink was poured into one of the two cartridges of the bioprinter LifeSi 3D Res (Argentina) (Fig 1A). Printing was performed at room temperature using a 514um blunt-tipped 21G needle. A single layer model with square pores was generated with 10% of infill (.gcode) generating porous scaffold (porous dimension of 2mm x 2mm).

The printed layer, shown in Fig. 1B, has filaments of 648±7um thickness and 22±5um height. The printing fidelity (Pr) of the ink was calculated as $Pr=L^2/(16*A)$, where L = 2mm and A are the length and area of the pores, respectively. Fig 1C remarks the well-defined square shape of the pores, with Pr= (0.9845±0.0025).

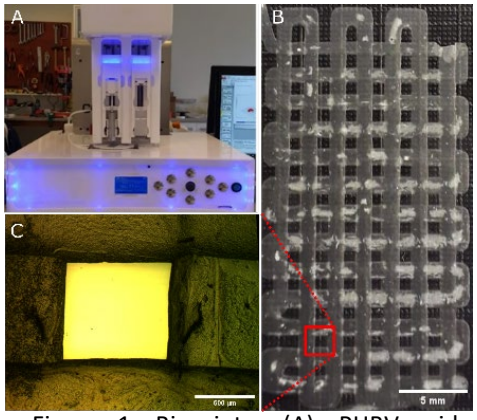

Figure 1: Bioprinter (A), PHBV grid printed with 10% infill (B). Optical microscopy at 40X of grid pores (C).

Regarding the PHBV production, it was performed by *Cupriavidus necator* in culture medium with residual glycerol (35g/l) and propionic acid (1g/l) as carbon sources. Bacterial cells were observed at 72h by optical, scanning electron and transmission microscopies (Fig. 1). The production of bacterial cells and biopolymers was quantified by gravimetry and UV spectrophotometry. Then, the produced polymer was extracted from the lyophilized bacterial cells with hot chloroform, purified in two steps with methanol and hexane at 4°C, and characterized by H^1 and C^{13} NMR. Kinetic measurement of the production process established the maximum value of 3.4g/l PHBV copolymer at 72 h, corresponding to 63% of the cell dry weight, with a hydroxyvalerate monomer molar fraction of 7.6%.

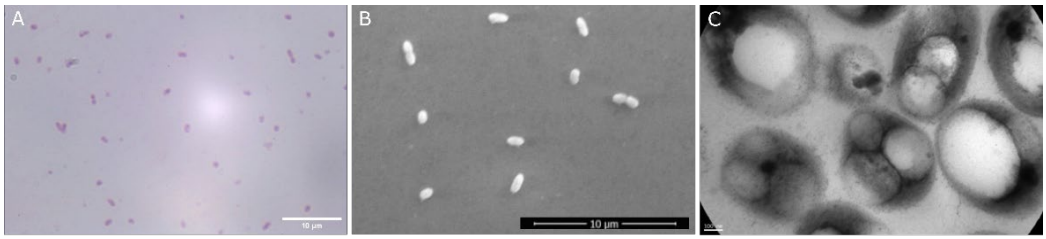

Figure 2: *Cupriavidus necator* cells observed at 1000X (A), 10000X (B) and 85000X (C).

The effect of porosity and heat treatment on the mechanical behavior of regular open-cell C95500 Cu alloys

A. Soleimani[1], M. Jafari Esfad[1], A. Moloodi[1*]

[1] Materials Research Group, Iranian Academic Center for Education, Culture and Research (ACECR), P.O. Box 91779-49367, Mashhad, Iran
*ahmad_moloodi@yahoo.com

Investment casting is one of the common methods of producing metal foam [1-2]. In this research, the relationship between the strength and porosity and also the effect of the heat treatment on the strength of the C95500 bronze foam was investigated.
For this purpose, the first porous samples with Kelvin pattern [3-4] with three types of porosity include of 80, 85, and 90% were designed. Then the designed regular open-cell patterns were produced via the 3D printer method with a polymer made of PLA. Finally, the printed samples were produced via the investment casting method in the dimensions of 2×2×2 cm^3.
To investigate the effect of heat treatment on the strength of bronze foams, the following operation heat treatment cycles were performed on the samples:
- The first cycle is heating at 900 °C for 2 hours and quenching in water.
- The second heating cycle is at 590 °C for 1 hour and then quenching in the air.

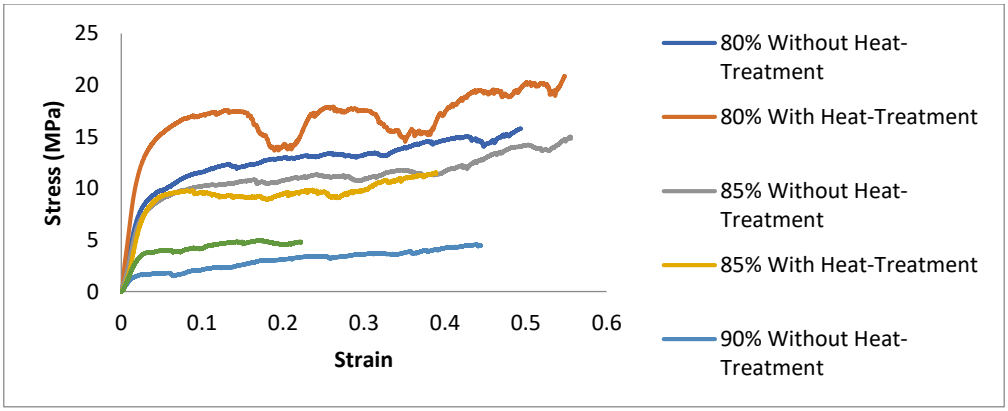

Figure 1. Stress-Strain curves of all produced samples

As it was shown in figure 1, a relatively linear increase in the strength of metal foams with a decrease in porosity was found. The lowest strength of the plateau stress was for the sample with the 90% porosity (4.42 MPa) and the highest one was for the sample with 80% porosity (15.65 MPa). It is because of more cell wall thickness in the samples with the lowest porosity [5-6]. Also, the amount of the strain in the breaking stress point was almost the same for all samples. This indicates that changes in the amount of porosity have a more effect on the strength of the metal foams produced in this method.
The effect of the heat treatment on all samples was also determined. By performing heat treatment, the strength of samples was increased about 5 MPa and their ductility of them was almost constant. It is also determined that in the sample with the lowest porosity (80%), heat treatment has led to the ridged stress-strain curve behavior in the plastic region. This indicates brittle behavior in the foam samples produced with low porosity. In fact, in the samples with low porosity, as the cell wall of the foam metal produced increases, the effect of the heat treatment is greater and led to the brittle behavior.

References

[1] Z. Sarajan, M. Soltani, J. Kahani Khabushan, *Mater Manuf Processes*, 2011, 26, 1293-1298.
[2] X. F. Tao, L.P. Zhang, Y.Y. Zhao, *Materials & Design*, 2009, 30, 2732-2736.
[3] D. Weair, R. Phelan, *Philosophical Magazine Letters*, 1994, 69, 107-110.
[4] R. Kusner, J. M. Sullivan, *Forma*, 1996, 11, 233-242.
[5] S. f. Fan, et al., *Transactions of Nonferrous Metals Society of China*, 2017, 27, 117-124.
[6] C. H. Liao, et al., *Materials Letters*, 2018, 215, 152-156.

Additive manufacturing 1

Session Chairs

Prof. Dr.
Matej Vesenjak

Additive manufacturing based hybrid processes for the development of carbon-bonded filters for steel melt filtration

T. Wetzig[1*], B. Bock-Seefeld[1], M. Schwarz[2], L. Schöttler[2], C. G. Aneziris[1]

[1] TU Bergakademie Freiberg, [2] Deutsche Edelstahlwerke Specialty Steel GmbH & Co. KG
*tony.wetzig@ikfvw.tu-freiberg.de

State-of-the-art steel casting processes like continuous casting or ingot casting by bottom teeming are the backbone of the modern steelmaking industry supplying countless industries with high-performance steel products. In this regard, the ever-increasing quality requirements by customers demand the research of new approaches to improve the steel melt cleanliness beyond today's standards. One popular approach is the so-called steel melt filtration. In the framework of this study, hybrid processes based on additive manufacturing were investigated as a basis for advancements in established filter manufacturing approaches. Different foam templates with tailored composition and geometry were designed and constructed by selective laser sintering. The additive manufacturing of foam templates provides an adaptive alternative to commercially available reticulated foams with random anisotropic macrostructure.

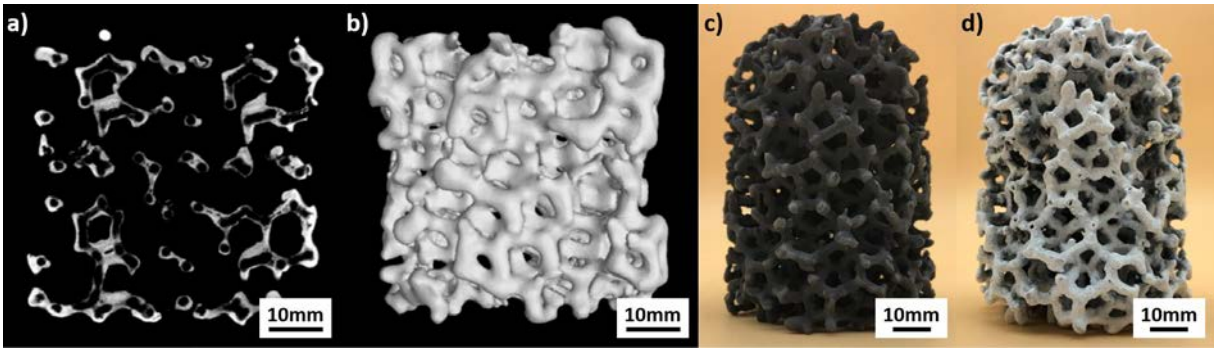

Figure 1. Reconstructed 2D cross-section (a) and 3D volume image (b) by means of microfocus computed tomography of alginate-gel-coated filters based on PVA templates with hollow filter struts and two additional alginate-free coatings before pyrolysis; [1] Replicated carbon-bonded foam filter on the basis of tailored polyurethane templates constructed by means of selective laser sintering before (c) and after (d) flame spraying. [2]

On the one hand, water-soluble polyvinyl alcohol (PVA) filter templates were fabricated and investigated. The PVA templates were coated with alginate-containing slips and subsequently treated in an aqueous solution containing Ba^{2+} ions. The solution simultaneously triggers the sol-gel transition of the alginate and initiates the dissolution of the PVA template. Thus, the template material is removed before firing. The hollow base filters are recoated and/or functionalized with alginate-free slips and subsequently fired. [1]
Furthermore, selective laser sintering was applied to fabricate polyurethane filter templates with tailored geometry for ingot casting. Different coating routines and pitch reinfiltration were investigated in order to replicate the filter structure. Final filter prototypes were functionalized with flame-spray coatings and tested in industrial ingot casting. [2]

References

[1] B., Bock-Seefeld; T., Wetzig; J., Hubálková; G., Schmidt; M., Abendroth; C. G., Aneziris: *Advanced Engineering Materials*, 2022, *24 (2)*, 2100655
[2] T., Wetzig; M., Neumann; M., Schwarz; L., Schöttler; M., Abendroth; C. G., Aneziris: *Advanced Engineering Materials*, 2022, *24 (2)*, 2100777

Electron beam based additive manufacturing of auxetic structures composed of shape memory Nitinol as catalyst carrier

A. Fink[1*], D. Rudolf[2], Z. Fu[1], H. Freund[2], C. Körner[1]

[1] Friedrich-Alexander-University Erlangen-Nürnberg, [2] TU Dortmund University
*alexander.fink@fau.de

Periodic open cellular structures (POCS) show an emerging interest as support structures in the research field of heterogeneous catalysis. Regarding the heat management of chemical fixed-bed reactors, metallic POCS reveal promising characteristics compared to conventional packed beds in tubular reactors, e.g. perfused beds of spherical particles. In such a case, due to point-to-point contact, heat conduction contributes only a small amount to the overall heat transport. With strong exothermic reactions, undesired local overheating may occur. By superior heat conduction, POCS enable an improved heat transport within the fixed bed. However, inserted into a tube, a small gap between reactor tube wall and POCS maintains, impairing the heat removal [1].

Designing POCS with an auxetic effect is a promising approach for closing this gap. These structures show a negative Poisson's ratio, i.e. applying a compression load, their size in one or several of the perpendicular directions decreases. As the main deformation mechanism, the nodes of the auxetic structures rotate and generate a complex stress field and high local strains [2]. Nitinol (NiTi) is able to bear the high strains since it offers 8 % reversible strain due to the shape memory effect (compared to 0.2 % elastic strain of normal metallic materials) [3]. In addition, the degrees of freedom unlocked by electron beam powder bed fusion (EB-PBF) make it possible to fabricate auxetic structures [2].

This study displays the progress of producing NiTi auxetic structures (see Fig. 1a) on a freely programmable EB-PBF machine *Freemelt One*. Moreover, it covers mechanical and thermal simulations computed with the software *COMSOL Multiphysics* combined with compression tests of EB-PBF built NiTi specimens to determine the reversible strains, maximum stresses and displacements (see Fig. 1b). The aim is to reach an optimization of the geometric parameters of NiTi auxetic re-entrant hexagon structures in terms of improving the heat transfer of tubular reactor systems.

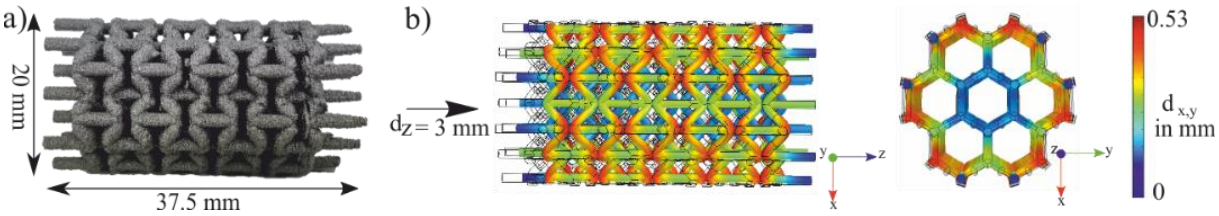

Figure 1. ABAB re-entrant hexagonal POCS for compression tests built on a freely programmable *Freemelt One* (a). *COMSOL Multiphysics* compression test model (b). With a defined z-displacement of 3 mm a maximum x, y-displacement of 0.53 mm is calculated at the outermost nods.

References

[1] G. Littwin, S. Röder, H. Freund, *Industrial & Engineering Chemistry Research*, 2021, *60*, *6753-6766*.
[2] C. Körner, Y. Liebold-Ribeiro, *Smart Materials and Structures*, 2015, 24, 025013.
[3] J.V. Humbeeck, *Advanced Engineering Materials*, 2001, 11, 837-850.

Homogenization and de-homogenization of strut-based lattice cores in sandwich panels

H. Georges[1*] , C. Mittelstedt[2] , W. Becker[1]

[1] Technical University Darmstadt, Institute of Structural Mechanics, Franziska-Braun-Str.7, 64287 Darmstadt, Germany
[2] Technical University Darmstadt, Institute for Lightweight Construction and Design, Otto-Berndt-Straße 2, Darmstadt 64287, Germany
*georges@fsm.tu-darmstadt.de

The freedom of design provided by additive manufacturing enables the fabrication of filigree structures such as strut-based lattices. Strut-based lattices exhibit outstanding mechanical properties and a low density, simultaneously. Therefore, these open-cell structures can be used as cores in sandwich panels. In comparison with honeycomb structures, strut-based lattices allow heat transfer through the core and can be customized to the requirements of the given load case.

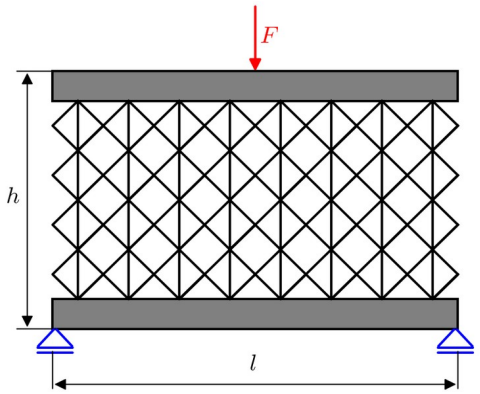

Figure 1. Sandwich structure with strut-based lattice core subjected to a transverse load

Generally, strut-based lattices are composed of a unit cell, which is periodically repeated in all directions. The unit cell is also known as representative volume element (RVE). The topology and the dimensions of the RVE determine the mechanical properties of the lattice. To reduce the modeling and computing time, the lattice core is frequently replaced by a homogeneous material, which shows the effective elasticity parameters of the RVE (homogenization).

The lightweight advantage of sandwich panels is due to the separation of the high-strength face sheets by a low-density material. However, the difference in the core and face sheet material stiffness and localized loads cause highly localized deformations and stresses, which are not considered in the classical sandwich theories. Moreover, using homogenization does not enable the consideration of local effects. Hence, a detailed analysis of the lattice struts is required to obtain the local stresses. In this work, a computational model is presented, which enables the calculation of localized stresses and deformations in the struts of lattice cores with acceptable computational effort using de-homogenization methods. To outline the advantage of using additively manufactured strut-based lattices, the strut diameter of the lattice core is varied through the core thickness. Thus, the stress distribution in the graded core can be controlled and adapted through the core thickness.

Influence of different filter materials and coatings on removal of iron in a secondary aluminum-silicon alloy using a laboratory filtration apparatus

J.P. Schoß [1*], H. Becker[2], A. Keßler[1], A. Leineweber[2], M. Szucki[1], G. Wolf[1]

[1] Foundry Institute, [2] Institute of Materials Science, TU Bergakademie Freiberg
*Johannes.Schoss@gi.tu-freiberg.de

In this study, the influence of different coatings and filter materials on the removal of iron from secondary aluminum-silicon alloys was investigated. Based on three chemical compositions with different initial contents of iron (≈1.2 and 2.0 wt% Fe), manganese (≈0.35 and 1.2 wt% Mn) and chromium (≈0.05 and 1.2 wt% Cr), a two-stepped procedure consisting of (1) conditioning in order to bond Fe in primary Fe-containing intermetallic particles and (2) metal melt filtration using a laboratory filtration apparatus to remove these particles was applied.[1] Four ceramic foam filter (CFF), consisting of aluminum oxide (Al_2O_3), Al_2O_3 with a coating of Disperal (AlOOH), carbon-bonded (C) Al_2O_3 filter, and C-bonded Al_2O_3 with MgAlON coating, were tested.[2, 3]

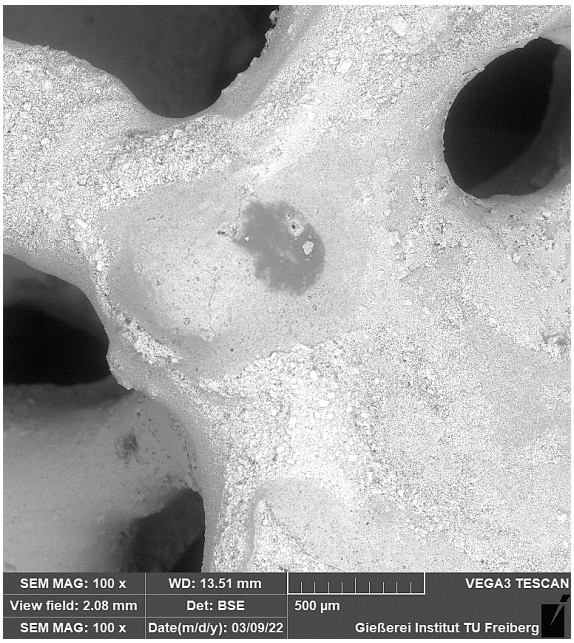

Figure 1: SEM image in backscattered electron contrast (BSE) of the surface of a C-bonded Al_2O_3 CFF with MgAlON coating at a magnification (MAG) of 100 times and a working distance (WD) of 2.08 mm.

For determining interaction effects between the Fe-containing intermetallics and the filter materials, the overall microstructure after filtration was analyzed by optical light microscopy. Scanning electron microscopy (SEM) with energy dispersive spectroscopy was performed to obtain the elemental distribution on the filter cake and the filter interior. Electron backscatter diffraction was conducted for phase identification of Fe-rich intermetallics at the filters interfaces. Whereas the intermetallic β-phase preferentially attached to the dispersal-coated filter surfaces, a favorable adhesion effect was revealed for intermetallic α-phase at the interfaces of the C-bonded Al_2O_3 and MgAlON coated filters. The Fe content was reduced by about 80% due to the multi-functional filter coatings.

References

[1] J.P. Schoß, H. Becker, A. Keßler, A. Leineweber, G. Wolf: *Adv. Eng. Mat.* 2022, *24*, 2100695, 1-15.
[2] K. Schwartzwalder, A. V. Somers: *(General Motors Co., Ltd.) US3090094A*, 1961.
[3] A. Schramm, V. Recksiek, S. Dudczig, C. Scharf, C.G. Aneziris: *Adv. Eng. Mat.* 2022, *24*, 2100519, 1-12.

Influence of scanning pattern on Electron Beam Powder Bed Fusion processed Inconel 718 filigree structures

T. Arold[1], D. Kotzem[2] F. Walther[2], T. Niendorf[1]

[1] University Kassel, [2] TU-Dortmund
[1] arold@uni-kassel.de

Additive Manufacturing includes a broad range of different processing techniques. Most of these techniques enable realization of complex and filigree structures like fine struts or periodic lattices, which cannot be processed by conventional techniques like milling or drilling. Due to a very high design flexibility and hardly any constraints, powder bed fusion processes have shown to be suitable for manufacturing of periodic lattice structures. Especially because of the very high process temperatures and slow cooling rates only low thermally induced residual stresses remain in Electron Beam Powder Bed Fusion (PBF-EB/M) processed periodic lattice structures.

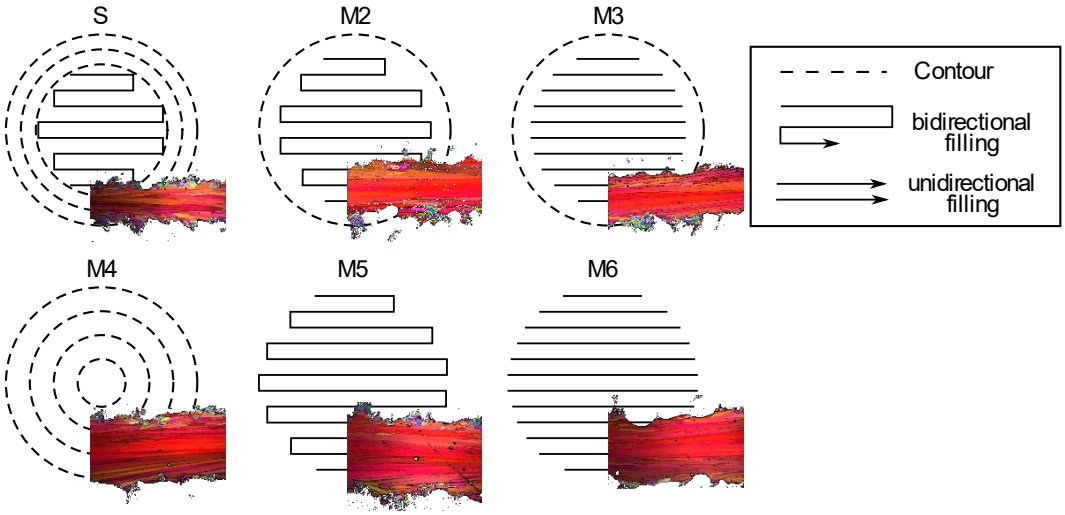

Figure 1: Scanning pattern used in this work for filigree struts and their resulting microstructures, visualized by grain orientation maps obtained by EBSD data and induced for build direction, respectively longitudinal axes of the struts.

Focusing on the deformation behavior of such fine structures, fatigue life is significantly affected by surface roughness. Additionally, inner defects or, considering specific alloys like IN718, heterogeneous microstructures have to be considered as well [1]. The smaller the structures, the higher is the contribution of surface roughness to the fatigue life. For complex geometries post processing of surface features is hard to realize. However, it is known, that the adaption of process parameters and scanning strategies can effectively alter surface roughness [2], relative density, microstructure, or final feature size, as shown in Figure 1. Thus, one should consider in advance the correct process settings to minimize the effort needed for post processing. What can be done to optimize IN718 lattice structures processed via PBF-EB/M, and how sensitive small features react to process adaptations, like different scanning pattern will be scope of this work.

References

[1] D. Kotzem, *Mater. Sci. Eng. A*, 2020, *772*, 138785.
[2] C. Körner, *Modelling Simul. Mater. Sci. Eng. A*, 2013, *21*, 085011 (18pp)

Stereolithography-based additive manufacturing of polymer-derived catalyst carrier structures

Johannes Eßmeister[1*] (J. Eßmeister), **Lisa Schachtner**[1] (L. Schachtner), **Altan Alpay Altun**[2] (A.A. Altun), **Martin Schwentenwein**[2] (M. Schwentenwein), **Eva Szoldatits**[3] (E. Szoldatits), **Karin Föttinger**[3] (K. Föttinger), **Thomas Konegger**[1] (T. Konegger)

[1] TU Wien, Institute of Chemical Technologies and Analytics; [2] Lithoz GmbH; [3]TU Wien, Institute of Materials Chemistry
*johannes.essmeister@tuwien.ac.at

Heterogeneous catalysts are used under increasingly harsh conditions, requiring the use of high-performance ceramics with high thermal and chemical stability as carrier material. In addition, a high surface area for an effective reaction at the active sites and well-tailored macroporous structures for high product flow are required. Currently, conventional ceramic processes are highly limited in meeting these shaping requirements, which calls for additive manufacturing in the form of stereolithography. Polymer-derived ceramics exhibit outstanding thermal properties and allow for a direct introduction of metal centres into the ceramic matrix through chemical modification, rendering them ideal candidate materials for catalysis applications. This study investigates the fabrication of complex lattice structures via stereolithography of polysiloxane and further thermal conversion into SiOC ceramics. Two approaches to modifying the photoactive polysiloxane printing system were developed.
On the one hand, the addition of SiC particles to the printing resin significantly increased the stability of the specimens and the freedom of design during the process. This combination allowed the production of defect-free, dense SiOC/SiC composite material with a characteristic strength of 325 MPa obtained with a biaxial ball-on-three-balls testing methodology. Secondly, chemical modification of the base material was carried out using metalorganic compounds to create metal-ceramic hybrid materials, as depicted in Figure 1. Thus, nanoscale nickel particles could be generated in-situ during the polymer-to-ceramic conversion. In combination with the modification via the nickel complexes, phase separation phenomena were observed, which led to the formation of micelles in the printing system. This separation subsequently led to the generation of hierarchical porosity, in addition to the printed macrostructure. The synergies of both approaches are used to produce stable ceramic catalyst support materials containing a catalytically active phase. By selecting the process parameters during the production of the printing resin, the printing process and the pyrolytic conversion, phase development and microstructural evolution of the metallic phases as well as the generation of the porosity, were elucidated. Furthermore, the influence of these parameters on the catalytic activity of the produced materials regarding CO_2 methanation was determined.

Figure 1. Manufacturing of metal-modified, polymer derived ceramic lattice structures via stereolithography

Virtual Prototyping of Foam Structures for Metal Melt Filtration

E. Werzner[1], H. Lehmann[2], A. Malik[3], M. Abendroth[3], B. Jung[2], S. Ray[1*]

Technische Universität Bergakademie Freiberg, 09599 Freiberg, Germany
[1] Institute of Thermal Engineering, Chair of Gas and Heat Technology, [2] Institute of Informatics, [3] Institute of Mechanics and Fluid Dynamics
*ray@iwtt.tu-freiberg.de

The application of additively manufactured templates during manufacturing of ceramic foam filters for metal melt filtration using the replica technique has considerably extended the scope for the design of improved filter geometries [1,2]. While the production and testing of novel filters in real trials is time-consuming and expensive, virtual prototyping allows the generation and screening of a huge number of variants at comparatively low cost. For the present study, an automated workflow for the computer generation and efficient evaluation of novel filter geometries has been developed [3]. Three different geometric modifications to a reference foam structure, as shown in Fig. 1a, were considered: the elliptical elongation and flattening of the strut cross section obeying a prescribed aspect ratio (i), the addition of finger-like struts protruding into the pore (ii), and the deliberate closing of pore windows (iii), as depicted in Fig. 1b. All modifications were parametrically varied and implemented for macroscopic porosities between 70 % and 90 %, resulting in a total of 45 geometry variants. The different structures were characterized by the relevant hydraulic effective properties, namely, the hydraulic tortuosity, the permeability and the Forchheimer coefficient, which have been obtained from detailed pore-scale simulations of the flow field using the lattice-Boltzmann method. In order to assess the filtration performance, the filtration coefficient has been evaluated for conditions present during continuous casting of aluminium employing Lagrangian tracking of inclusions.
The investigation shows that the geometry modifications affect the hydraulic characteristics and filtration behaviour quite differently. Among all modifications which improve filtration, the addition of finger-like struts is associated with the smallest increase in pressure gradient, rendering it the most efficient measure, while the partial closing of windows is the least efficient one (see Fig. 1c). A comparison of the filtration coefficient with different geometric and hydraulic effective properties for all samples shows a correlation with the hydraulic tortuosity and also the inverse of Forchheimer coefficient, but no consistent correlation with the specific surface area.

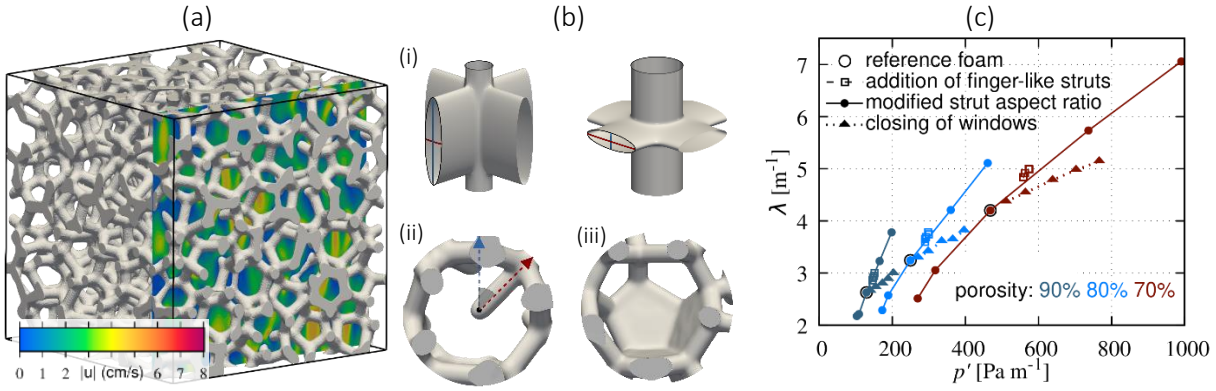

Figure 1. (a) Reference foam with 80 % porosity, serving as basis for the geometry modifications, and distribution of velocity magnitude $|u|$ for conditions present during continuous aluminium casting, (b) investigated geometry modifications, (c) variation of filtration coefficient λ with respect to pressure gradient p' for all investigated geometries.

References

[1] A. Ortona, C. DAngelo, S. Gianella, D. Gaia *Materials Letters*, 2012, *80*, 95-98.
[2] A. Herdering, M. Abendroth, P. Gehre, J. Hubálková, C. G. Aneziris *Ceramics International* 2019, *45*, 153-159.
[3] H. Lehmann, E. Werzner, A. Malik, M. Abendroth, S. Ray, B. Jung *Advanced Engineering Materials* 2021, *24*, 2100878.

Automotive, aerospace and transportation

Lightweight design for inland container vessels using aluminium foam sandwiches

F. Schneider[1*], Dr. J. Hohlfeld[2]

[1,2] Fraunhofer Institute for Machine Tools and Forming Technology IWU (Chemnitz)
*frank.schneider@iwu.fraunhofer.de

There is a need for more sustainability in the transport industry. To reduce freight traffic on road it is necessary to shift cargo load on train or inland water transportation. This demand is supported at national, international and European level [1]. However, to make the things more difficult, especially inland water transportation is also faced with an increasing occurrence of climatic extremes, such like very hot and dry summers. According to that, there are long times low water levels in the rivers, forcing inland sailors to reduce their cargo load. Therefore, it is a lot to do, to make inland water transportation more appealing.

Figure 1. Prototype – Load section of an inland container vessel made with aluminium foam-sandwiches.

In a project funded by the Bundesministerium für Wirtschaft und Energie (BMWi), the aim was to enable inland container vessels to load and unload containers in the port, independently, using its own handling unit. The resulting additional mass of the crane unit should be compensated by lightweight design on the ship's hull (Fig. 1). The task was mastered by a consortium consisting of shipbuilders, crane and steel constructors as well as two Fraunhofer Institutes [2]. Results, got there, can also help to make ship hulls lighter in other projects.

To achieve the aim of mass reduction, adaptations in the structure of ship hull were made, so that in a second step lightweight materials like aluminium foam-sandwiches could be integrated. The adaptation include a separation from load-carrying parts and inferior parts in the structure. Secondary components from a structural point of view are, for example, the walls and covers of ballast tanks, which make up large parts of the ship's hull. Sandwich elements, in this case with an aluminium foam core, are ideal for this. They have a large area moment of inertia and can easily dissipate bending loads, such as those caused by water pressure. Load-carrying parts however, are made using massive materials, like steel, furthermore. So a mass reduction of 20% for a load-section was achieved, for the whole vessel 50-60 tons seems to be possible.

References

[1] Commission of the European Community; White paper “Fahrplan zu einem einheitlichen europäischen Verkehrsraum”, 2011.
[2] Bundesministerium für Wirtschaft und Energie (BMWi); Förderkennzeichen 03SX404A-E.

Preparation and characterization of low density composites by spark plasma sintering method

Vitalijs Abramovskis[1*] (V. Abramovskis), Jurijs Ozolins[1*] (J. Ozolins), Ints Steins[2*] (I. Steins), Andrei Shishkin[1*] (A. Shishkin).

[1] Rudolfs Cimdins Riga Biomaterials Innovations and Development Centre of RTU, Faculty of Materials Science and Applied Chemistry, Riga Technical University, Pulka 3, K-3, Riga, LV-1007, Latvia.
[2] Faculty of Materials Science and Applied Chemistry, RTU, Paula Valdena 7, Riga, LV-1048, Latvia.
*vitalijs.abramovskis@rtu.lv, jurijs.ozolins@rtu.lv, *ints.steins@rtu.lv, *andrejs.siskins@rtu.lv.

Today, several industries are trying to reduce the use of energy materials while maintaining or improving the properties and quality of the product. Obtaining materials with reduced weight is beneficial for both the manufacturer, as he saves raw materials and the final consumer, who spends less on the purchase and maintenance of the final product. One of the methods to reduce weight can be the production of a composite as a syntactic foam. Cenospheres (CS) can be used as a closed cell matrix [1]. Cenospheres have many important properties, such as low heat transfer coefficient, high hardness, lack of electrical conductivity and complete chemical inertia, low density: the real 0.65-0.7 g/cm^3 and bulk density 0.39-0.42 g/cm^3 [2], [3].
In the experimental work CS can was coated using physical vapor deposition method (PVD) by metal – Ti6Al4V alloy which acts as a binder during the sintering process. Second divertive are coated by titanium (Ti6Al4V) and titanium nitride. The lightweight composite material, using spark plasma sintering method was produced. The influence of the SPS process parameters (different sintering temperatures) on the apparent density of the composite, compressive strength was investigated.

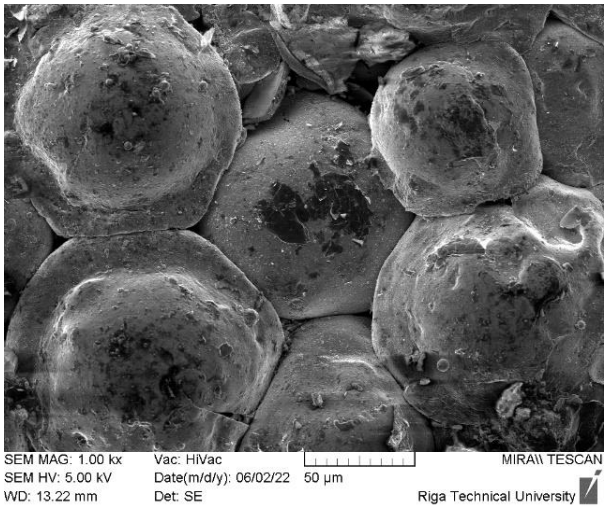

Figure 1. Ti-TiN@CS composite sintered at 1220 ° C, SEM image under magnification X1000.

On the figure 1 is represented sintered together CS coated by the titanium nitride and Ti alloy. Is clearly seen that cenospheres are incac and tightly located one to each other. The obtained material is specified by the from 26 to 91 MPa of the compression stress and form 0,42 g·cm^{-3} bulk density.

References

[1] N. Gupta and D. Pinisetty, "A review of thermal conductivity of polymer matrix syntactic foams - Effect of hollow particle wall thickness and volume fraction," *JOM*, vol. 65, no. 2. 2013. doi: 10.1007/s11837-012-0512-0.
[2] D. S. Nakonieczny, M. Antonowicz, and Z. K. Paszenda, "Cenospheres and their application advantages in biomedical engineering - A systematic review," *Reviews on Advanced Materials Science*, vol. 59, no. 1. 2020. doi: 10.1515/rams-2020-0011.
[3] N. Ranjbar and C. Kuenzel, "Cenospheres: A review," *Fuel*, vol. 207. Elsevier Ltd, pp. 1–12, 2017. doi: 10.1016/j.fuel.2017.06.059.

Bio and chemical engineering and conversion

Pharmaceutical applications of cellular structures

A. Szoboszlai[4], Á. Haimhoffer[1], G. Vasvári[1], M. Béresová[2], J. Tóth[3], F. Fenyvesi[1], I. Budai[4]*

[1]University of Debrecen, Department of Pharmaceutical, [2]University of Debrecen, Department of Medical, Imaging Technology, [3]University of Debrecen, Department of Laboratory Medicine, [4]University of Debrecen, Faculty of Engineering
*budai.istvan@eng.unideb.hu

Cellular materials have many known applications, from aerospace technology [1] to food production and pharmaceuticals. There is a wide range of beneficial applications for the user of this type of structure. The pharmaceutical industry has also recognised the benefits e.g. low density, buoyancy, carrier and drug volume reduction, controllable drug delivery, extended residence time, matrix material type. Low density floating formulations can increase gastric residence time of the drugs; therefore the drug release will be sustained [2]. Our aim was to produce stable floating formulations by foaming. The main criterion for the selection of matrix was minimal irritation [3] and a natural plant source was an additional consideration. Firstly, we used polyethylene glycol (PEG), and plant-derived polysaccharide: agar agar. Another option was to produce a swelling mould that swells in the stomach to ten times its original size so that it does not escape from the stomach, thus increasing the residence time. In this case the matrix was carrageenan. The produced solid foam was dried to reduce its size considerably, making it easy to dose. According to our experiments a stable foam could be produced by rapid homogenisation (shorter than 1 minute) without any surfactant material [4-6].

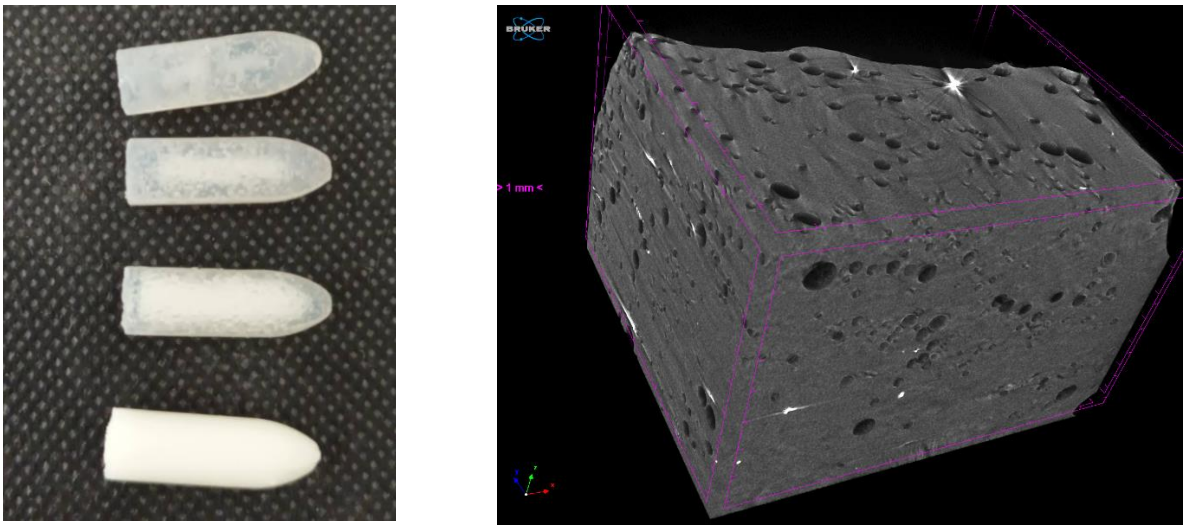

Figure 1. Representative pictures (floating foam) and microCT image of the solid foams.

References

[1] I.N Orbulov, A. Szlancsik, A. Kemény, D. Kincses, *J. of Mat. Engineering and Performance*, 2022, 1-9
[2] Z. Shariatinia Chapter 2. *Natural Polysaccharides in Drug Delivery and Biomedical Applications*, 2019, 15-57
[3] P. Sellaturay, S. Nasser S, P. Ewan *The Journal of Allergy and Clinical Immunology: In Practice*, 2021, *9(2)*,670
[4] G. Vasvári, Á. Haimhoffer, L. Horváth, I. Budai, et al. *AAPS PharmSciTech*, 2019, *20*:290
[5] Á. Haimhoffer, G. Vasvári, I. Budai, F. Fenyvesi, et al. AAPS *PHARMSCITECH* 2021, *22:5*, 187,
[6] Á. Haimhoffer, G. Vasvári, J. Tóth, I. Budai, et al. *PHARMACEUTICS,* 2021, *13:10*, 1571

Design and architecture 1

Session Chairs

Dr.-Ing.
Franziska Schmidt
TU Berlin

Genetic algorithm based inverse design of cellular materials within and beyond orthotropy

Nikolaos Karathanasopoulos[1*]

[1] New York University, Department of Engineering, Abu Dhabi Campus, UAE
*n.karathanasopoulos@nyu.edu

The inverse design of cellular materials that can meet multiple macroscale performance objectives constitutes a significant engineering challenge, primarily due to the high computational cost required for the exploration of broad design spaces. In the last decades, the development of machine learning methods along with the substantial enhancement of the computational limits has opened new frontiers in the analysis and design of materials. In the current work, machine learning methods are employed along with homogenization analysis techniques to inversely identify cellular material patterns that optimally meet the entire set of mechanical parameters contained within a fully populated elasticity tensor. The genetic algorithm modulates the inner material distribution to optimally meet both the stiffness objectives and relative density macroscale constraints posed. The approach allows for the identification of both isotropic and highly anisotropic cellular designs with positive, zero or auxetic Poisson's ratio values. Its accuracy is verified using periodic, Abaqus-based finite element models. Moreover, dedicated 3D-printed specimens are manufactured and experimentally tested, highlighting its robustness and potential for wide-applicability.

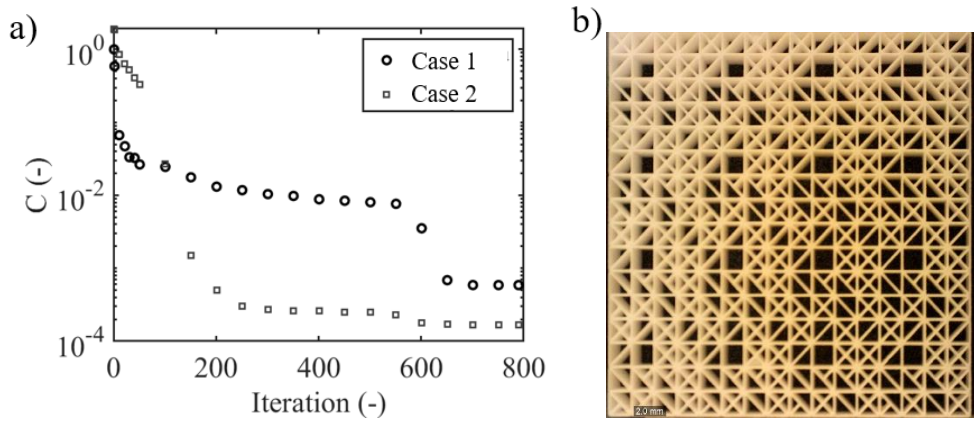

Figure 1. Cost function evolution for two case target metamaterial objectives (A) along with an example of an inversely identified 3D-printed unit-cell design (B)

References

[1] N. Karathanasopoulos, F. Dos Reis, P. Hadjidoukas, J-F. Ganghoffer "LatticeMech: A discrete mechanics code to compute the effective static properties of 2D metamaterial structures", SoftwareX, 11, 100445, 2020

Wood in Top Form - New Perspectives in Wood Construction

P. Haller[1],

[1] Technische Universität Dresden
peer.haller@tu-dresden.de

Moulded wood profiles from solid wood are novel structural elements for architecture, civil and mechanical engineering. The idea is based on wood as a cellular material that undergoes large deformations when heated and compressed. With the help of moisture and temperature the deformation can be released and used for shaping [1].
The presentation will show the thermo-hygromechanical behaviour of wood and its particularities such as recovery when moistened and fixation when dried. For structural use wooden tubes can optionally be reinforced with technical fibres and textiles from glass, aramid and carbon.

Figure 1. Fibre reinforced moulded wood profiles. Foto L. Sprenger 2009

Within this research particular attention is paid to the use soft and hardwood such as beech. It could be shown that this specie is suitable for moulding perpendicular to the grain. Consequences regarding sylviculture and environment are being discussed.
Experimental test results of components and connections will be presented as well as environmental impact assessments.
Structural tubes showed outstanding load bearing capacities. Special applications from the building sector and plant engineering such as solar and wind power stations are also dealt with. Within the project BEECHPOLE, a lightning pole is being developed [2] [3]. The study of its impact behaviour on a test track with a car showed excellent results regarding the frangibility criteria.
The same physical principles are used for the shaping of sandwich cores from wood, especially Balsa. This approach uses end grain panels from bi-axially compressed wood that allow the manufacturing of double curved shells. In addition with high performance fibres one obtains sandwich elements with a high potential in lightweight design.

References

[1] KUTNAR, A.; SANDBERG, D.; HALLER, P.;: Compressed and moulded wood from processing to products – a review; Holzforschung, 01/2015
[2] J. U. HARTIG; J. WEHSENER; P. HALLER; Experimental and theoretical investigations on moulded wooden tubes made of beech (Fagus sylvatica L.) Construction and Building Materials 126 (2016) 527–536
[3] J. U. HARTIG; S. FACCHINI; P. HALLER; Investigations on lateral vehicle impact on moulded wooden tubes made of beech (Fagus sylvatica L.) Construction and Building Materials 174 (2018) 547–558

Energy and thermal management

Lattice structures versus heat – Increased cooling performance inside the thermal management of battery systems

C. Hannemann[1*], M. Uhlig[1], Prof. Dr. H.-G. Schweiger[2], D. Koch[2]

[1] Fraunhofer Institute for Machine Tools and Forming Technology, [2] Technische Hochschule Ingolstadt (THI)
*christian.hannemann@iwu.fraunhofer.de

The cooling of power electronics is increasingly becoming the focus of economic interest. That is caused by continuously growing power density and thus rejected heat of those electronic components. Examples are the aimed reduction in charging time of electric driven vehicles, which is associated with an increase in charging current, or the growing performance of computer processors with a trend toward decreasing dimensions.
The potential of metal foam structures for use as heat sinks in thermal management is one component of the battery development in the EC-funded MARBEL project, in which 16 partners from 8 countries are working on the next generation of battery systems. The targeted 300-thousand kilometer service life along with shortened charging times are in reach through precise temperature control of the battery cells. For fast and comprehensive heat transfer under load, not only the pressure and quantity but also the shape of the flow of the cooling liquid plays a decisive role. The integration of cellular structures inside channels and cooling areas increases the internal surface area and creates turbulences in the cooling liquid. Within the project the extent of the effect and influence of density, cell size and connection to the heat source are investigated.
Knowledge of the behavior and flow resistance of the foam structures will enable a defined selection and adaptation of these cellular structures to the individual requirements of each application.

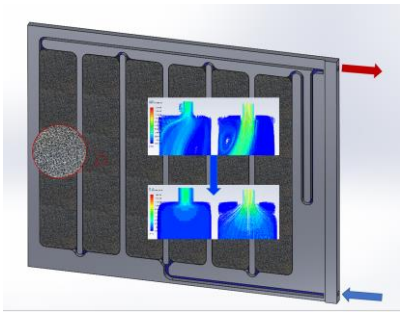

Figure 1. Metal foam application in a heatsink

In contrast to the increase in heat generation per surface area, the available installation space for cooling usually decreases. Therefore the demand on the efficiency of the systems increases. The approaches pursued are a fundamental building block on the way to an industrially suitable solution to this challenging task. By optimizing the integration and connection of the foam structure, adjusting the density up to a defined variation of the porosity within a component and a clever choice of materials, the cooling effect was significantly increased. Meanwhile the complexity and thus the costs of the components can be reduced. The development is accompanied by considerations of sustainability and recyclability and generates findings that not only form the next generation of battery technology, but also the basis for further development and simulation projects from other fields of application to meet the increasing requirements of power electronics.

Energy and thermal management 1

Session Chairs

Dr.-Ing.
Daniela Haase
Fraunhofer Institute for Cerami...

Cooling of fuel-cell stacks by air flow in open-cell aluminium foam

N. Dukhan[1*], A. Hmad[2]

[1]University of Detroit Mercy, [2] University of Detroit Mercy
*dukhanni@udmercy.edu

Fuel cells have been considered for powering cars [1] among other applications. The chemical reaction in fuel cells is exothermic, and if the generated heat is not removed, the efficiency of fuel cells will decrease [8]. Moreover, higher temperatures can damage fuel cells' membranes [9]. A new numerical and experimental work investigating the cooling potential of open-cell aluminum foam (using airflow) for fuel cell stacks is described. A model for metal-foam cooling design based on a commercial 500-W proton exchange membrane fuel cell (PEM) stack was simulated and tested experimentally. The new design of the current investigation replaces the existing liquid-cooling channels with compressed aluminum foam having a porosity of 60%, Fig. 1. The study considered symmetric and asymmetric heated foam channels subjected to constant heat flux of 1.56 W/cm^2, and cooled by airflow at hydraulic-diameter Reynolds numbers in the range 87 to 657. In the simulations, the thermal energy equations were solved invoking the local thermal non-equilibrium model, which is a more realistic treatment for airflow in metal foam. Local temperatures in the stack, local and length-

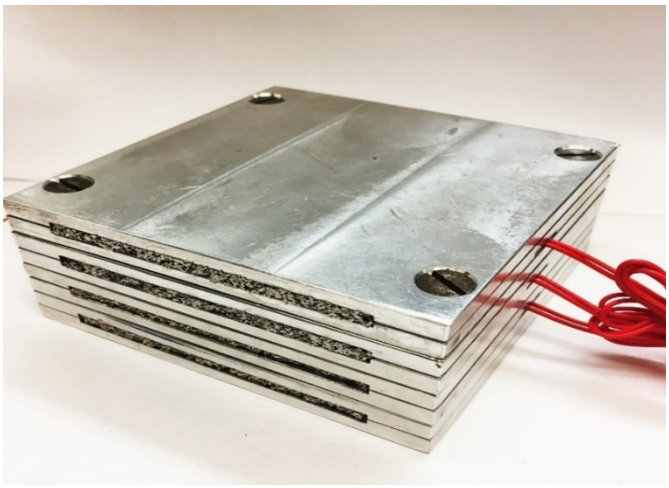

Figure 1. Metal-foam experimental model with cooling channels filled with aluminium foam, and heaters inserted between each two adjacent plates to provide the heat generated by fuel cells

averaged Nusselt numbers, and friction factors were determined numerically and experimentally. Good agreement between the simulation and experiment was obtained for the local temperatures. The local Nusselt number slightly decreased with distance along the cooling channel, and the length-averaged Nusselt number increased with Reynolds number. As for the friction factors predicted by simulation and obtained experimentally, there was an average difference of about 18.3%. This difference has been attributed to the poor correlation used by the CFD package for pressure drop in metal foam. The new cooling system could remove the 500 watts of waste heat of the stack, and would keep the stack within the safe range of operating temperature: 60-90 ^{O}C.

References

[1] ____ Fuel cell handbook, 5th ed., EG&G Services, Parsons Inc., US Department of Energy, Office of Fossil Energy, National Energy Technology Laboratory, 2000, West Virginia.
[2] A. Faghri and Z. Guo, Int. J. Heat Mass Transf., 2005, 48, 3891–3920,
[3] B. S. Parajón-Costa, C. C. Wagner, E. J. Baran, "Fuel cell handbook,", 2003, 629, 1085–1090.

FEM-Simulation of heat transfer properties of thermal paste layers with integrated metal structures

WEISE Jörg[1, a], KNOLL Arthur[1,b], BAUMEISTER Joachim[1,c] and MYSLICKI Sebastian[1,d]

[1]Fraunhofer Institute IFAM, Wiener Strasse 12 D-28359 Bremen, Germany

[a]joerg.weise@ifam.fraunhofer.de, [b]knoll.arthur@gmx.net, [c]joachim.baumeister@ifam.fraunhofer.de, [d]sebastian.myslicki@ifam.fraunhofer.de

Keywords: FEM, simulation, heat transfer, E-mobility, wire structures.

Abstract. Thermal control is an essential issue for the safety and endurance of the drive battery pack of electric vehicles. A main parameter for the heat flow from the battery elements to the cooling system (e.g. cooling channels) is the thermal resistance in the gap between the battery element and the housing. Current solutions for improving heat transfer are based on thermal paste fillings in the gap. Those "gap fillers" feature typically thermal conductivities of 2-4W/m/K. Adjustment of gap thickness variations is done by viscous flow. Those gap filler pastes lead, however, to increased weight and costs and to difficulties during assembly or disassembly of the battery pack. Therefore, an alternative approach was investigated – the combination of metal structures (like pins, wire structures, corrugated sheets or expanded metal) with gap filler pastes. In this case the metal structure has to show the same flexibility regarding the gap thickness as the paste. The significantly higher intrinsic thermal conductivity of the metal structures can offer higher freedom for the paste optimisation regarding assembly. One example is the combination of metal structures with injectable pastes of lower thermal conductivity. In the presented work the thermal behaviour of metal structures embedded in gap filler paste was simulated by means of FEM-calculations. For this, typical detail elements of such structures were identified and investigated regarding their influence on thermal transport. Special attention was given the influence of the heat transfer coefficient between paste and metal. The FEM-simulations showed that this coefficient dominates the metal structures' efficiency. Therefore, in order to improve thermal flow the embedded metal structures should feature: a) a large portion of metal oriented no less than 30° from the target thermal flow direction, b) small interface areas transverse to the target flow direction, c) large interface areas parallel to the target flow direction.

Functionalization and Surface modification

Anti-leishmanial evaluation of AmB loaded solid lipid nanoparticles coated with vitamin B12-stearic acid conjugate

A. Singh, G. Yadagiri, S. Parvez, O.P. Singh, A. Verma, S. Sundar, S. L. Mudavath*

Institute of Nano Science and Technology, Sector-81, Mohali, Punjab 140306, India

Abstract

Surface functionalized VB_{12} biocompatible nanoparticles exploit the well characterized uptake absorption pathway of VB_{12} shielding it from enzymatic degradation and inadequate absorption. In this perspective, subsequent to escalated mucus interaction and diffusion analysis, the nanoparticles were investigated by immunostaining with anti CD320 antibody and internalization mechanisms were examined by selectively blocking specific uptake processes, we saw internalization to be energy dependent clathrin mediated, simultaneously highlighting the remarkable ability to bypass P-glycoprotein efflux. In particular, synthesized nanoparticles were evaluated for cytocompatibility by analysing cellular proliferation, membrane viscoelasticity and fluidity analysis by FRAP and oxidative stress detection making them well suited for successful translation to clinical setups. Our previous *in vitro* antileishmanial results paramount for further *in vivo* and toxicity analysis paving for targeted therapeutic efficiency. The augmented surface hydrophilicity attributed by VB_{12} and monomerization of AmB within the lipid core strengthen the oral bioavailability and stability as evidenced by FRET analysis.

1. Characterization of Vitamin B_{12} stearate modified solid lipid nanoparticles encapsulating Amphotericin B

Vitamin B_{12} stearate (VBS) modified solid lipid nanoparticles encapsulating Amphotericin B (VBS-AmB-SLN) were synthesized and substantiated as an eminently stable orally administrated anti-leishmanial SLNs and a graphical abstract representing the same is illustrated in Fig. 1 (A).[1] VBS-AmB-SLN were synthesized through double emulsion solvent evaporation method, and a schematic diagram is demonstrated in Fig. 1 (B). SLNs were spherical in shape, 250-300 nm in diameter with a zeta potential of 0.350 ± 4.5 mV. TEM results are illustrated in Fig. 1 (C). Furthermore, our studies demonstrated that AmB was effectively loaded into SLNs (% EE = 98.5 ± 3.4 % and % DL = 39.5 ± 2.6 %) respectively and efficiently internalized by macrophage cells as advocated by cellular uptake studies Fig. S1 (A) which were further quantitatively validated by fluorescence-activated cell sorting (FACS) analysis Fig. S1 (B). Furthermore, it was discerned that characteristic peaks of AmB, VB_{12}, stearic acid, VBS and VBS-AmB-SLN (supplementary information) did not change after FTIR analysis Fig. 1 (D), henceforth it was deduced that AmB is in the free form and there is no interaction with the excipients used.[1]

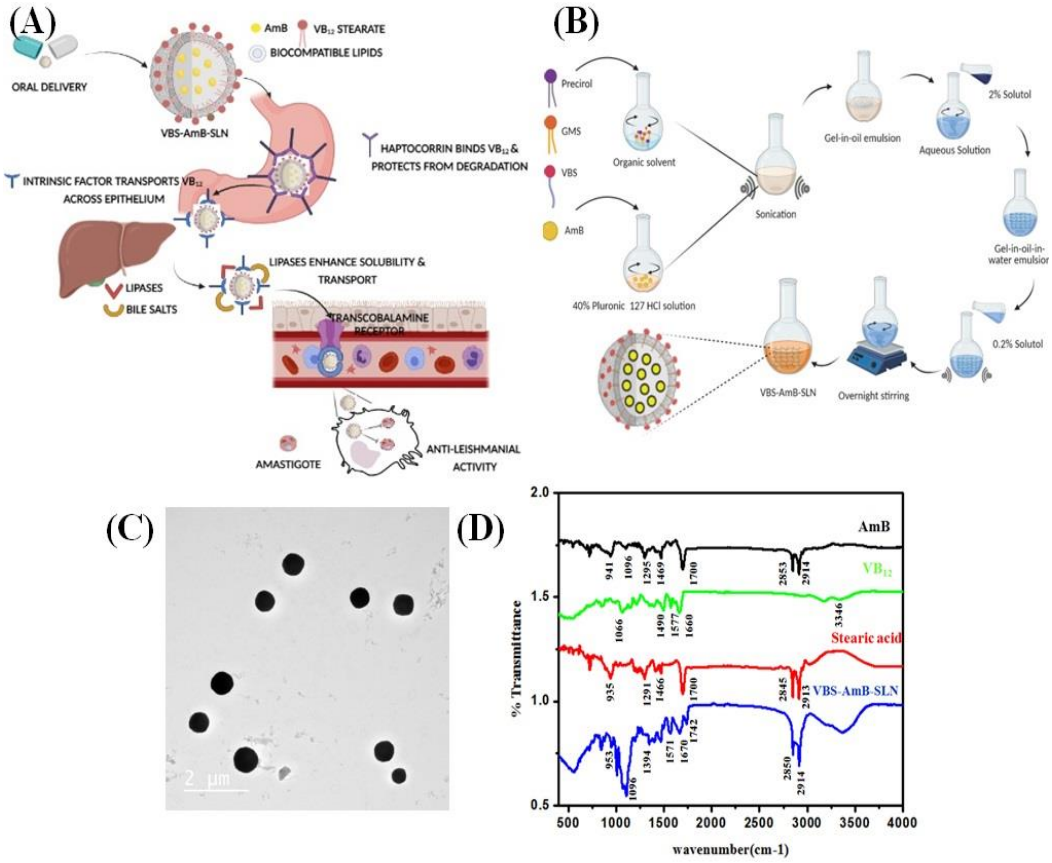

Fig. 1 (A) VBS-AmB-SLN as a stable oral anti leishmanial carrier, (B) Synthesis of VBS-AmB-SLN by double emulsion solvent evaporation method, (C) TEM microphotograph of VBS-AmB-SLN, (D) FTIR spectrum of AmB, VB_{12}, stearic acid and VBS-AmB-SLN.

2. Wettability analysis

VB_{12} is a hydrophilic molecule with high molecular weight and it is arduous to anchor this hydrophilic molecule on the surface of lipophilic SLNs.[2] On that account, to improve its lipid compatibility our previous study reported successful esterification of VB_{12} to stearic acid by modified oxyma method resulting in the synthesis of VBS.[1] The conjugation of VB_{12} on the surface of SLNs was confirmed by evaluating the wettability of unmodified and VB_{12} modified SLN (VBS-AmB-SLN) by measuring the contact angle by sessile drop method using drop shape analyzer. Contact angle of water on AmB-SLN coated glass slide was around 48.15 ± 2.47°, which reduced to 29.5 ± 0.77° in the case of VBS-AmB-SLN as illustrated in Fig. 2 (A). Almost 40% reduction in contact angle indicated VBS-AmB-SLN was more hydrophilic than AmB-SLN. This enhanced hydrophilicity can be attributed to the presence of hydrophilic VB_{12} on the surface of nanoformulation.

3. Aggregation state analysis

AmB is the first line drug used for the treatment of VL. It is a highly efficacious drug in the Indian subcontinent with 99% cure rates.[3] The characteristics hydrophobic and hydrophilic groups in AmB result in spontaneous self-association in aqueous environment.[4] However, its water soluble oligomers are highly toxic due to its relatively high affinity to host cell's cholesterol while the monomeric form specifically binds to ergosterol abridging host cell toxicity.[5] Achieving monomerization of AmB generally relies on employing biocompatible lipid carriers which induce disaggregation with longer chain surfactants. Additionally, previous reports revealed a more effective monomerization of AmB by micellar stearates as present in VBS coated on SLNs for improving the lipid compatibility of hydrophilic VB_{12}. The polyene chain with seven conjugated double bonds result

in dipole-dipole interactions of AmB with neighbouring molecules and since the λ_{max} of drug is dependent on molecular organization, therefore monitoring the spectrum of AmB presents an effective approach in evaluating drug interactions. The UV spectrum of AmB exhibits intense peaks where peak I depicts the aggregated form while peak IV represents the monomeric form while the ratio of peak IV/peak I represents the state of AmB monomerization. As demonstrated in Fig. 2 (B), the ratio of peak values suggested significant monomerization of AmB, when entrapped inside VBS-AmB-SLN nanoformulation.

4. MTT assay

MTT reduction assay was conducted to evaluate the cytotoxic effects of SLNs against macrophage cells. The results demonstrated in Fig. 2 (C) showed that in the absence of drug, SLNs were not cytotoxic in the concentration range evaluated; the cell viability was above 90% at the highest concentration tested. When AmB was incorporated into SLNs, cellular viability was 80% at the highest concentration tested in contrast to the comparatively higher cytotoxicity of free drug at the same concentration. Therefore, it can be concluded that after encapsulation of drug within the SLNs the cell viability was remarkably enhanced *in vitro*. Untreated cells were used as control with 100% cellular viability.

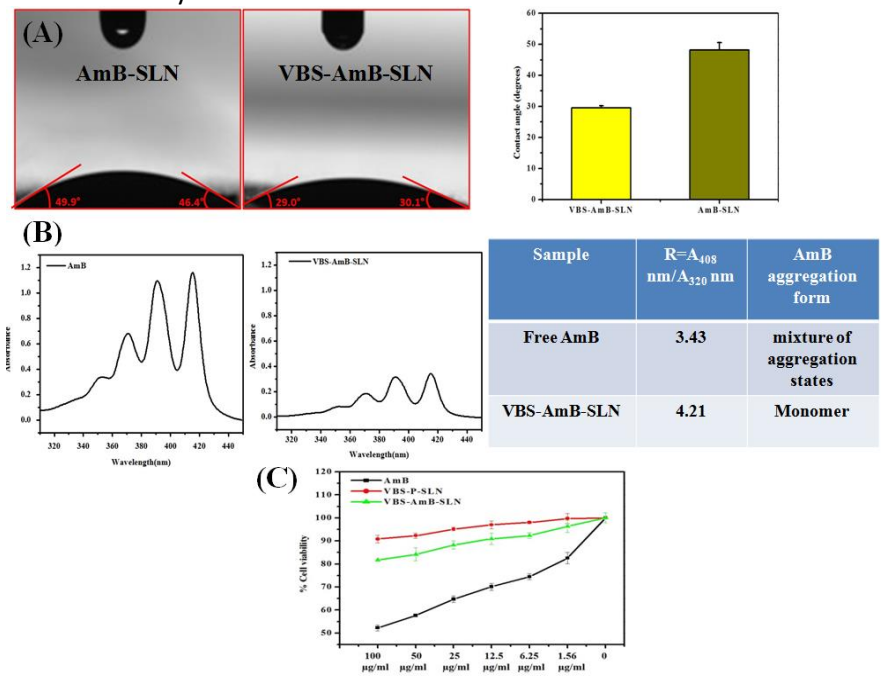

Sample	R=$A_{408\ nm}/A_{320\ nm}$	AmB aggregation form
Free AmB	3.43	mixture of aggregation states
VBS-AmB-SLN	4.21	Monomer

Fig. 2 (A) Contact angle measurement through sessile drop method AmB-SLN and VBS-AmB-SLN and its bar graph representation, (B) aggregation state analysis through UV-visible spectroscopy of AmB, VBS-AmB-SLN, and their peak ratio values, (C) Evaluation of cell viability of macrophage cells upon treatment with VBS-AmB-SLN, VBS-P-SLN and free drug, for AmB concentrations of (0-100 µg/mL).

5. Internalization and transport studies

Surface engineered nanoparticles administered orally are modified due to interaction and adsorption of corona of molecules to satisfy the 'bare surface free energy' of nanoparticles in complex biological environments.[6,7] Subsequently, the composition of corona endows a distinct entity to nanoparticles leading to exploration of unique physiochemical properties including mechanism of cellular uptake, antileishmanial efficacy, and toxicity. As demonstrated by the 'Vroman effect', the low affinity adsorbed molecules or soft corona can be replaced by high affinity or hard corona that binds more tightly to the nanoparticle surface with a longer exchange lifetime.[8] Whilst, hard corona are distinctively stable but they are not completely reversible. Therefore, coating the nanoparticles

with a well-established dissociable mucus inert hydrophilic material would facilitate mucus permeation and subsequently mediate uptake through epithelium. Several studies have successfully validated N-(2-hydroxypropyl) methacrylamide polymer (pHPMA) as a dissociable carrier which assists in overcoming the mucus barrier, whilst separating in time for subsequent transport through epithelial cells.[9] Furthermore, to attain mechanistic insights into minimizing mucoadhesion, we focused on our understanding of specific physiochemical properties that regulate the transport of viruses, which have been able cause infection for over thousands of years.[10] The findings demonstrated that highly dense hydrophilic surface curtails hydrophobic entanglement in mucus and the net neutral charge might facilitate mucus transport by evading strong covalent interaction.[11] Therefore, we rationalized that the highly dense hydrophilic molecules with net neutral surface charge on VBS-AmB-SLN (zeta potential: 0.350 ± 4.5 mV) might minimize adhesion to mucus.

5.1 Mucus interaction analysis

Orally administered nanoparticles encapsulating therapeutic agent needs to permeate through the mucus to reach the underlying epithelial membrane and be eventually absorbed into systemic circulation. Although, not restricted certain macromolecules are highly susceptible to be trapped or degraded by enzymes. Therefore, we hypothesized that by disguising the nanoparticles beneath the dissociable mucus inert pHPMA coating could minimize aggregation and subsequent washing out of VBS-AmB-SLN from the mucus layer. Therefore, we analysed the mucoadhesion of VBS-AmB-SLN by quantifying relative fluorescent intensity of TRITC tagged pHPMA VBS-AmB-SLN following incubation with mucin at different time intervals. Furthermore, a consistent mucoadhesion can prolong its residence time, thereby augmenting systemic absorption and subsequently its bioavailability. Withal, the intestinal mucosal turnover being 0.8 to 4.5 h, VBS-AmB-SLN administered orally ought to remain adhered to mucus layer for approximately 5 h to avoid clearance and undergo systemic absorption. As illustrated in Fig. 3 (A), VBS-AmB-SLN displayed consistent mucin retention ability.

Evaluating biomaterials for mucoadhesion or ability to adhere to intestinal mucosa interestingly enables its development as a transmucosal drug delivery carrier for prolonged efficacy of active pharmaceutical ingredient. ITC is a complementary technique to mechanistically understand and thermodynamically characterize the binding interactions.[12,13] Herein, we employ ITC for the very first time to characterize the binding of mucin to VBS coated on the surface of VBS-AmB-SLN. The interaction between biological molecules predominantly consists of four types of forces comprising of hydrogen bonds, electrostatic interactions, vander Waals forces, and hydrophobic interactions. Furthermore, the thermodynamic parameters (ΔH and ΔS) associated with these interactions have been previously characterized by Ross and Subramanian [14,15]. If $\Delta H>0$ and $\Delta S>0$, the major contributing interaction is hydrophobic, conversely when $\Delta H<0$ and $\Delta S<0$, hydrogen and vander Waal forces are more dominant. Nonetheless, when $\Delta H<0$ and $\Delta S>0$, electrostatic forces are domineering. We used ITC to obtain insights into the mechanism of interaction. The ITC data as shown in Fig. S2 (A) did not fit any classical binding model. However, according to the values of thermodynamic parameters for binding interactions, indicated an exothermic reaction as manifested by negative enthalpy change accompanied by a positive entropy change. This characteristic behaviour suggested that the gradual addition of VBS to mucin was an exothermic spontaneous process, resulting from electrostatic interactions between VBS and mucin.

Additionally, to further analyze the diffusion of VBS-AmB-SLN in mucin through multiple image photography (MIP), the mucin VBS-AmB-SLN dispersion was placed in sealed microscopy chambers of defined thickness of upto 120 µm, similar to thickness of intestinal mucosa.[16] Using 3D imaging CLSM microscopy, it was discerned that FITC labeled VBS-AmB-SLN were uniformly distributed throughout the mucin layer as illustrated through Fig. 3 (B) and supplementary videos 3 and 4.

5.2 Immunostaining transcobalamine II receptor

Fluorescent immunostaining was performed to investigate the cellular uptake of VBS-AmB-SLN by transcobalamine receptors present in macrophage cells. To visualize internalization, cells were immunostained with anti CD320 or anti transcobalamine receptor that specifically binds to

transcobalamine bound vitamin B_{12} followed by immunolabeling with Rhodamine tagged secondary antibody. CLSM images revealed that, after 48 h incubation with FITC tagged VBS-AmB-SLN, the majority of immunolabeled antibody colocalized with internalized nanoparticles as demonstrated in Fig. 3 (C). Fluorescence was not evident in control where treatment with primary antibody was excluded. Immunostaining for transcobalamine was significant revealing expression in macrophage cells.

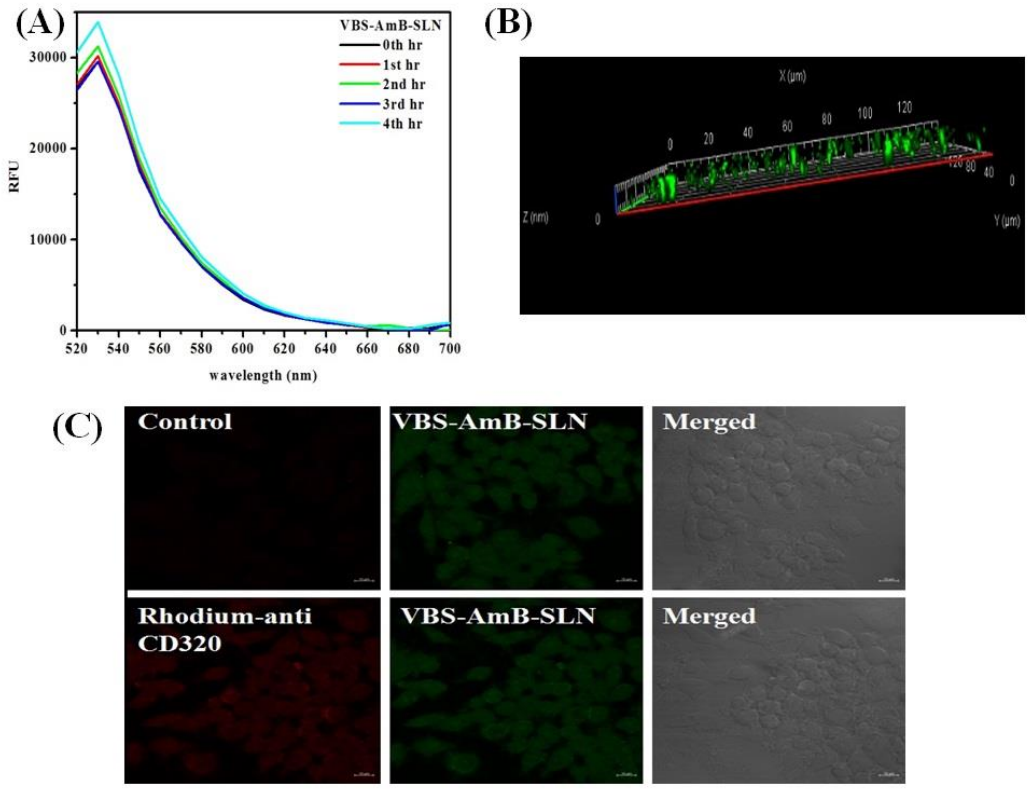

Fig. 3 (A) Relative fluorescent intensity of TRITC tagged pHPMA VBS-AmB-SLN following incubation with mucin at different time intervals (0-4 h), (B) CLSM microscopic images of FITC labeled VBS-AmB-SLN in mucin dispersion after incubation in sealed microscopy chambers, (C) CLSM images of colocalization of FITC labeled VBS-AmB-SLN after 48 h, Red signal from rhodamine labeled anti-CD320 antibody (immunostaining for TCII, a carrier protein involved in the binding and transport of vitamin B_{12} through the enterocytes), and bright field images.

5.3 Endocytosis pathway investigation

Understanding the cellular uptake of engineered nanoparticles plays a crucial role in drug delivery applications and furthermore aids in assessing its potential toxicity. Nanoparticles can enter the cells through various mechanisms, with receptor mediated endocytosis being one of the most effective internalization pathway.[17] Extensive research previously revealed that size and surface properties have profound influence on internalization mechanism.[18,19] To understand the dynamics of endocytosis, we used confocal microscopy imaging to examine the underlying mechanisms of internalization of fluorescently tagged VBS-AmB-SLN. Fig. 4 (A) shows the relative amount of nanoparticles that were taken up by macrophage cells after inhibitory treatments with pharmacological inhibitors that specifically suppress a particular endocytic pathway. Additionally, the results illustrated that macrophage cells treated with chloropromazine, an inhibitor of clathrin mediated endocytosis,[20] significantly abridged the internalization of FITC labeled VBS-AmB-SLN when compared to control cells along with sodium azide, an inhibitor of energy dependent active transport.[21] Contrarily, genistein, an inhibitor of caveolae mediated endocytosis[22] and nocodazole, an inhibitor of microtubular endocellular transport process[23] showed no impact on

uptake and internalization of FITC labeled VBS-AmB-SLN. Similar results were obtained from FACS assay which were consistent with confocal study as shown in Fig. 4 (B). Consequently, the uptake of VBS-AmB-SLN was mediated by clathrin dependent endocytosis and was energy dependent. Withal, the effect of pharmacological inhibitors on cell viability was assessed using MTT assay. As illustrated in our previous study, the pharmacological inhibitors (100 µg/mL) exhibited no significant cytotoxicity on macrophage cells even after 24 h of treatment Fig. S2 (B).

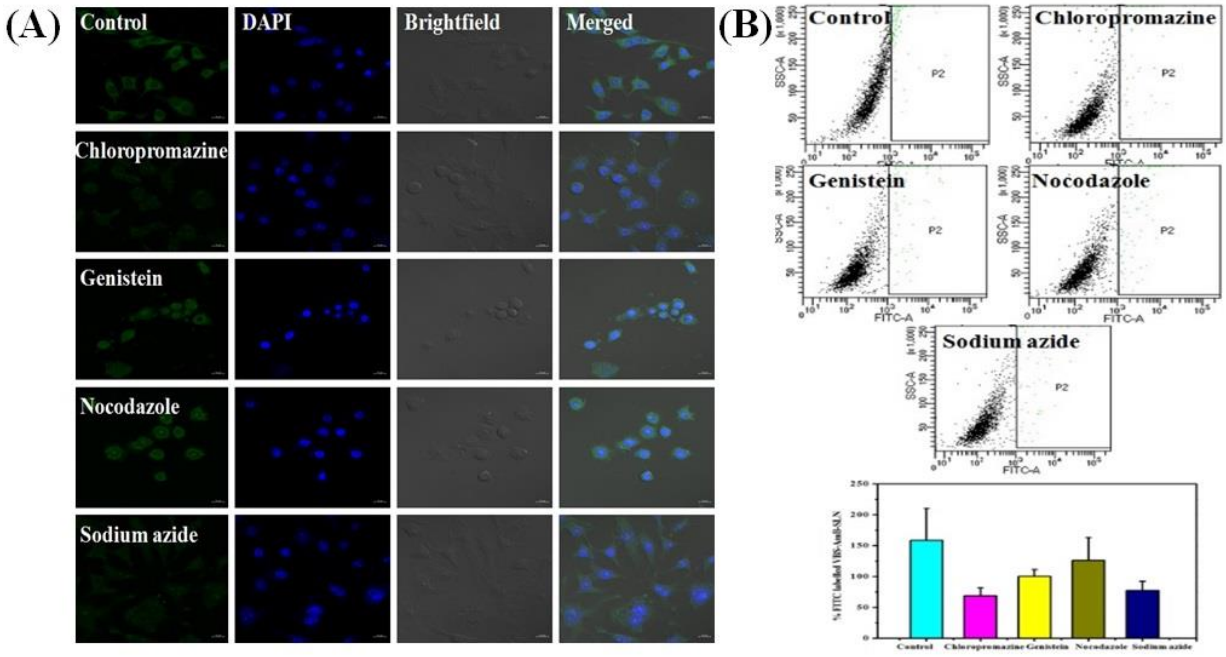

Fig. 4 (A) CLSM images DAPI (λ_{ex}: 405 nm) stained nucleus of macrophage cells, colocalization of FITC (λ_{ex}: 488 nm) labeled VBS-AmB-SLN after treatment with no inhibitor (control), chloropromazine, genistein, nocodazole, and sodium azide, bright field images, and merged images. (B) Dot plot FACS analysis and bar graph representation of internalized FITC labeled VBS-AmB-SLN after treatment with inhibitors.

5.4 Exocytosis pathway investigation

Cells take in nanoparticles through endocytosis and secrete the ingested contents via exocytosis through the cell membrane and into extracellular space through specific secretory translocation vesicles[24]. Thus, it is crucial to evaluate exocytosis of internalized nanoparticles from macrophage cells to evaluate their biosafety. To investigate whether VBS-AmB-SLN can be transported out of cells via exocytosis pathways, we incubated macrophage cells transfected with FITC VBS-AmB-SLN with specific pharmacological exocytosis inhibitors. Exocytosis of nanoparticles reduces the number of accumulated nanoparticles, which of course reduces its efficacy and therapeutic effect. Therefore, the possible use of exocytosis inhibitors could give us valuable insights into the relative percentage of accumulated nanoparticles. Thus, we incubated macrophage cells for 24 h with brefeldin A, an inhibitor of ER-Golgi trafficking[25] and monensin, an inhibitor of Golgi-plasma membrane transport.[26] We found that in exocytosis inhibitor treated groups the cytoplasmic fluorescence was relatively higher than control groups after a prolonged incubation of 24 h as demonstrated in Fig. 5 (A). Similar results were obtained from FACS study Fig. 5 (B), further confirming the obvious effect of exocytosis inhibitors on macrophage cells. In summary, our findings imply that considerable amount of nanoparticles are transported out of macrophage cells, preventing prolonged accumulation and henceforth its phagocytic ability.

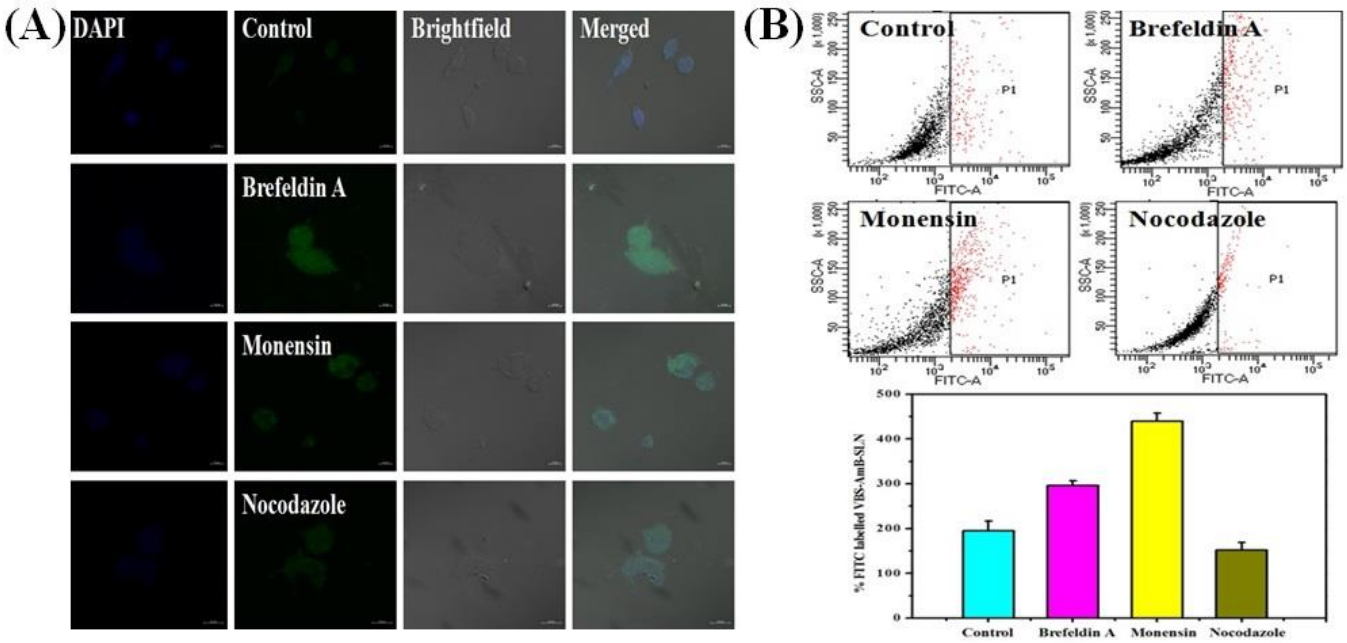

Fig. 5 (A) CLSM images of DAPI (λ_{ex}: 405 nm) stained nucleus of macrophage cells, colocalization of FITC (λ_{ex}: 488 nm) labeled VBS-AmB-SLN treatment with no inhibitor (control), and inhibitors like brefeldin A, monensin, and nocodazole, bright field images, and merged images. (B) Dot plot analysis and bar graph representation of internalized FITC labelled VBS-AmB-SLN after treatment with exocytosis inhibitors.

5.5 P-glycoprotein efflux assay

P-glycoprotein (P-gly) is one of the most studied and well characterized ABC multidrug transporters whose overexpression is responsible for multi-drug resistance by expelling drugs out of cells at the expense of ATP hydrolysis.[27] Encapsulation of AmB inside VBS-AmB-SLN could bypass this purging mechanism as opposed to free drug and restore the intracellular drug concentration required for parasite clearance. Potent P-gly inhibitors like verapamil hydrochloride possess the ability of rescind drug expulsion, resulting in increased therapeutic concentration of the drug without affecting the expression level of P-gly.[28] Additionally, Rhodamine 123 (R123) is the typical representative P-gly substrate and a sensitive dye used for representing P-gly function. Therefore, R123 was used as a marker for evaluating P-gly efflux kinetics.[29] Furthermore, to investigate the retention of FITC labeled VBS-AmB-SLN and R123, 100 µM verapamil, P-gly inhibitor was added to test group as opposed to control group and P-gly activity was assayed using confocal microscopy and further quantified by FACS analysis. As expected, verapamil significantly increased the intracellular content of R123 in macrophage cells, whereas VBS-AmB-SLN accumulation was only marginally higher than verapamil free control group Fig. 6 (A). As evident by FACS assay, verapamil caused a significant accumulation of R123 which is attributed to binding of verapamil in the active site of P-gly and thereby inhibiting its efflux out of cells Fig. 6 (B).

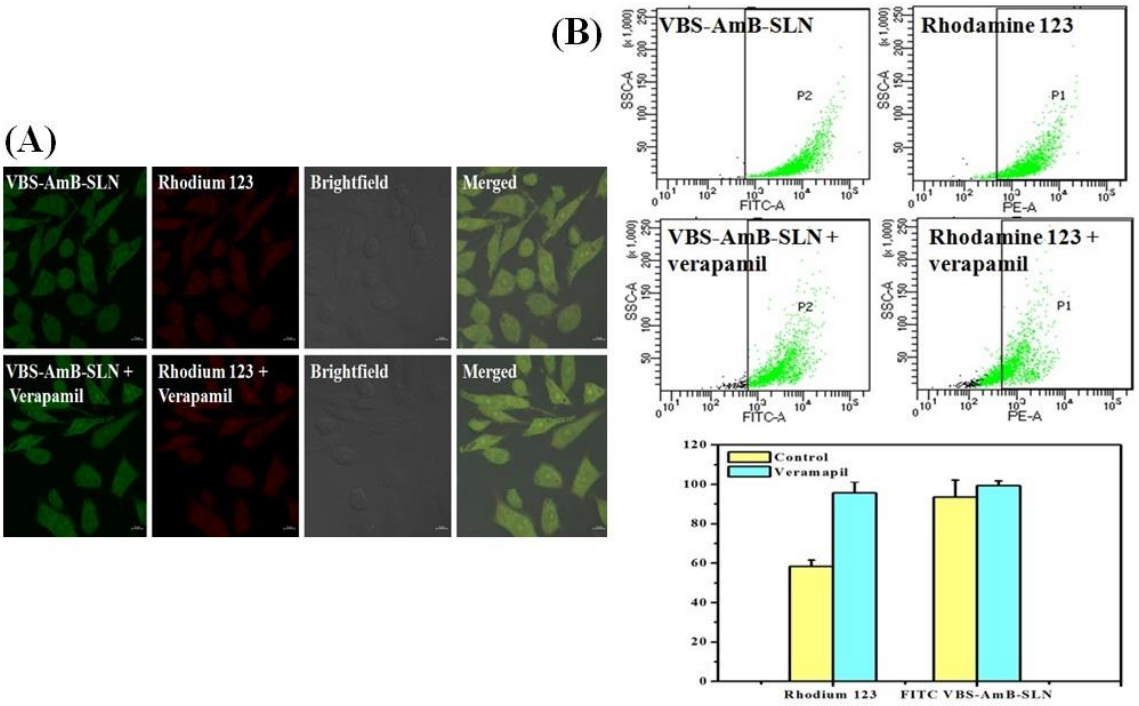

Fig. 6 (A) CLSM images of Rhodium 123 (5µM) treated macrophages cells without verapamil, and with 2mM verapamil, colocalization of FITC (λ_{ex}: 488 nm) labeled VBS-AmB-SLN (100 µg/mL) after 24 h of treatment without verapamil, and with 2mM verapamil, bright field images, and merged images. (B) Dot plot analysis and bar graph representation of internalized rhodium 123 and FITC labeled VBS-AmB-SLN as control and after treatment with verapamil.

6. Reactive oxygen species (ROS) and nitric oxide (NO) production

ROS production assessment in macrophage cells might provide insightful information whether VBS-AmB-SLN addition could induce oxidative stress and lead to disturbances in cellular metabolism.[30] DCFH-DA method (10 µM) was used to investigate ROS generation, which was considerably low as illustrated in Fig. 7 (A) and (B). Conclusively, VBS-AmB-SLN addition did not induce any oxidative stress in macrophage cells.

Additionally, we investigated the effect of VBS-AmB-SLN addition on macrophage cells by focusing on the production of nitric oxide (NO). NO is the principal effector molecule produced enzymatically by nitric oxide synthase in macrophage cells.[31] *In vitro* quantification of NO production was evaluated by Griess colorimetric nitrite assay which is based on the conversion of NO to a stable azo compound (λ_{ex} 540 nm).[32] With the aid of standard curve, the production of nitric oxide was calculated for free drug in comparison to encapsulated drug after an exposure of 48 h. As expected, the encapsulated drug VBS-AmB-SLN (100 µg/mL) as shown in Fig. 7 (C), resulted in slightly reduced production of NO. For antileishmanial applications, it is desirable to have a controlled release of NO to prevent proliferation of parasites.

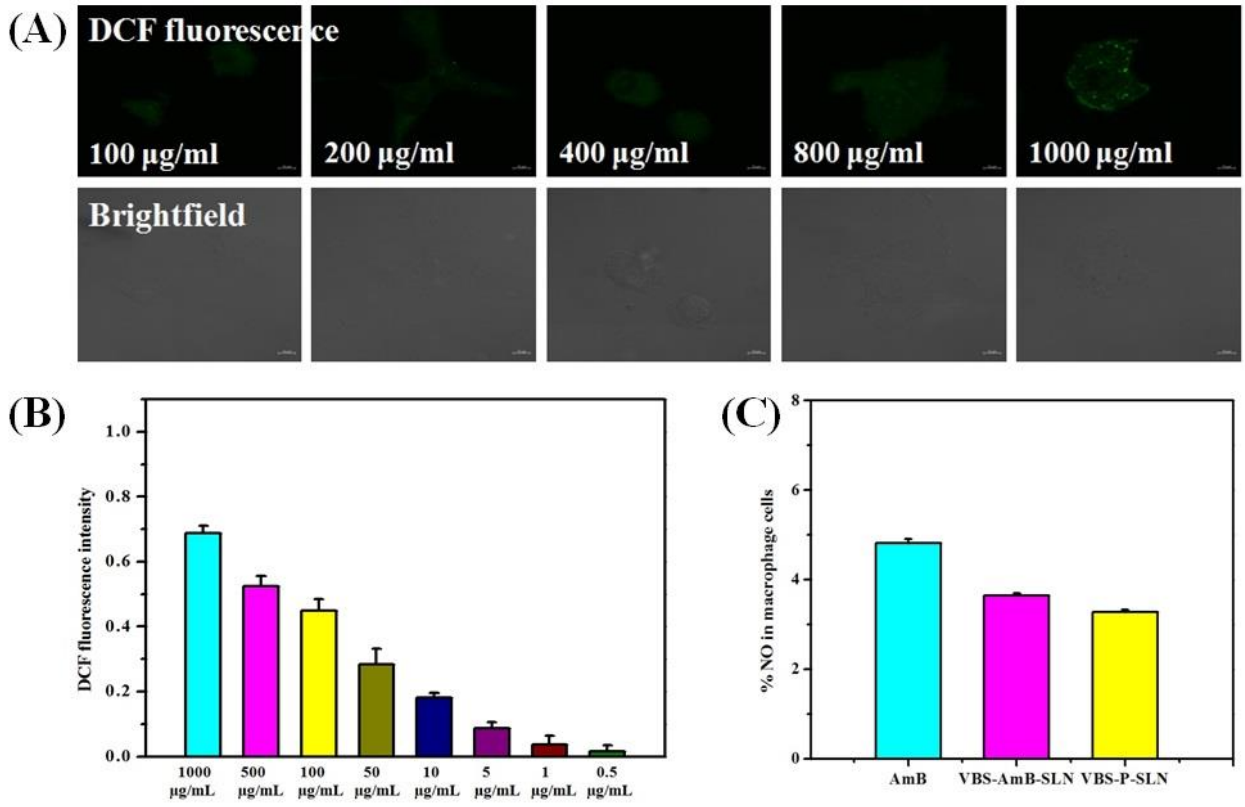

Fig. 7 (A) CLSM images after detection of ROS species by oxidation of non-fluorescent H_2DCFDA into highly fluorescent 2',7'-dichlorofluorescein (DCF) as indicated by green fluorescence after treatment with 100 µg/mL of VBS-AmB-SLN, and brightfield images. (B) Bar graph representation of detection of ROS species after treatment with (0-100 µg/mL) of VBS-AmB-SLN for 48 h by DCFH-DA method. (C) NO levels in macrophages after exposure of AmB, VBS-AmB-SLN and VBS-P-SLN for 48 h. Griess reagent reacts with nitrite in samples to form a purple azo product, (540 nm), which can be quantified by spectrofluorometry.

7. FRAP and FRET analysis

Plasma membrane maintains electrochemical balance and henceforth the activity of membrane bound carriers and enzymes.[33] It has been previously reported that ROS and NO production affects membrane fluidity and viscoelasticity.[34,35] Furthermore, addition of VBS-AmB-SLN might affect the plasma membrane, we desired to evaluate the changes in plasma membrane fluidity using fluorescence recovery after photobleaching (FRAP) technique. FRAP, is a powerful technique for assessing the diffusion of nanoparticles and dynamics of plasma membrane.[36] In FRAP experiments; fluorescently tagged lipids of plasma membrane are selectively photobleached by a strong intensity laser which leads to blighting of fluorophores in that defined region. Subsequently, recovery of fluorescence in the photobleached region occurs over time as fluorophores molecules diffuse into it. The procedure for FACS and the representative illustrating images at different steps including prebleaching, bleaching and recovery are demonstrated after treatment with and without VBS-AmB-SLN in Supplementary video 1 and 2. As shown in Fig. 8 (B), plasma membrane fluidity of macrophage cells decreased slightly after VBS-AmB-SLN addition which might be due to the interaction of plasma membrane with VBS-AmB-SLN.

Fluorescence resonance energy transfer (FRET) is a widely used reliable approach most commonly employed in elucidating interactions between biological molecules. The efficiency of FRET, a radiationless nanomechanism is extremely sensitive to changes in intermolecular distance based on the energy transfer mechanism between two fluorophores. When the donor and acceptor moieties are present in close proximity, the donor can transfer energy to acceptor by dipole-dipole

interactions, thereby curtailing its own emission intensity. The nanoparticle intactness can be addressed by entrapping spectrally overlapping fluorophores that act as donor and acceptor pairs for FRET inside the nanoparticle scaffold. A positive FRET fluorescence will suggest that coupling of FRET pairs in close proximity i.e. within 10 nm which would successfully confirm that the nanocarrier is intact whereas lack of FRET would suggest potential leakage or burst of nanocarrier. In this perspective, we fabricated VBS-AmB-SLN loaded with FRET pairs, DiO and DiI to constitute FRET SLNs where the two fluorophores are in close proximity. However, SLNs prepared by entrapping a single fluorophore resulted in recovery of fluorescence of donor molecule. To confirm intactness of VBS-AmB-SLN after internalization by macrophage cells Fig. 8 (C), confocal laser scanning microscopy was used to detect enhanced fluorescence of acceptor moiety that proved the presence of acceptor dye in close proximity to donor dye within the hydrophobic core.

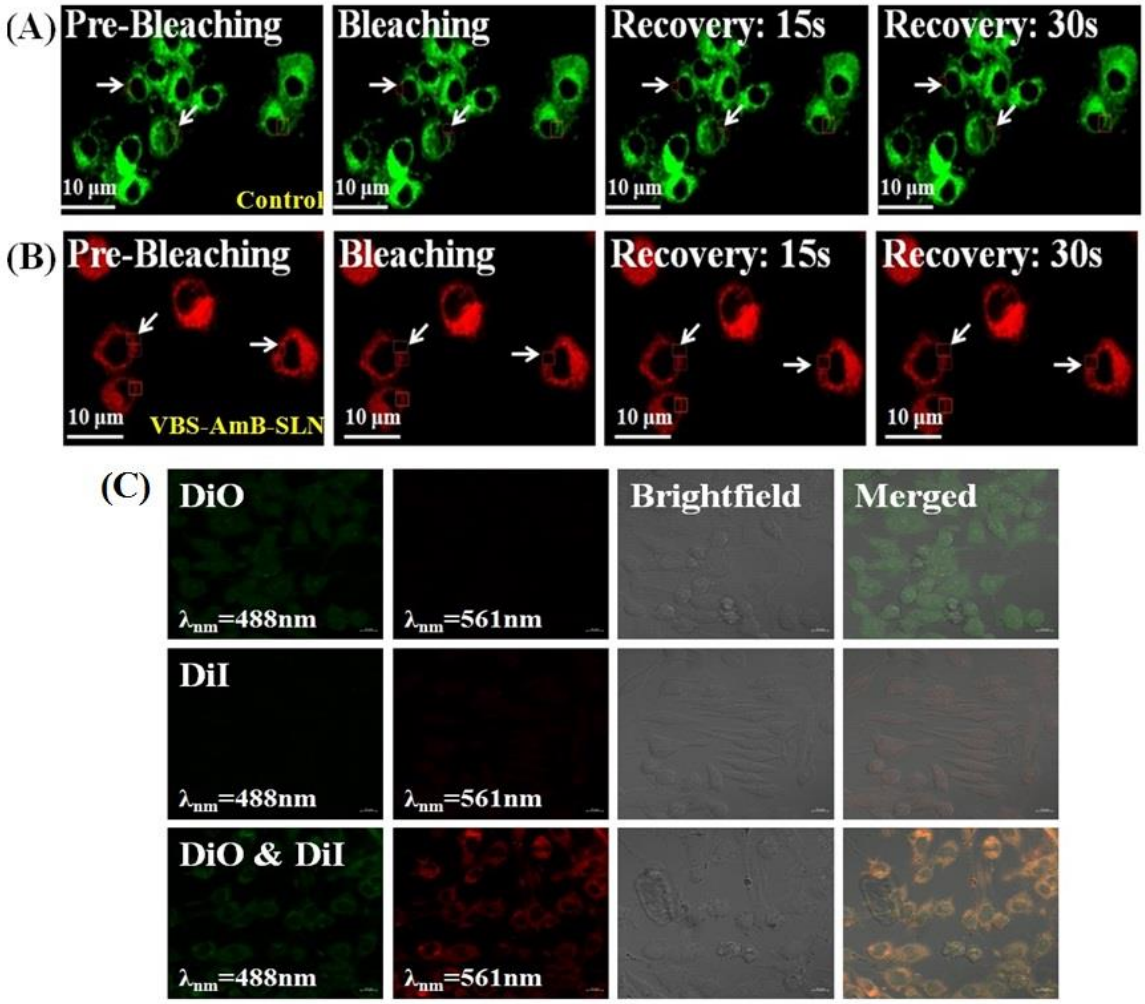

Fig. 8 (A) CLSM images of fluorescence recovery after the photobleaching (FRAP) procedure; without treatment with VBS-AmB-SLN (control) of DiO stained macrophages and (B) after treatment with VBS-AmB-SLN of DiI stained macrophages; bleaching region is marked by red and green rectangle (white arrows), (C) Cellular uptake of DiO loaded nanoparticles, cellular uptake of DiI loaded nanoparticles; cellular uptake of DiO and DiI loaded nanoparticles which showed FRET effect when both were entrapped together representing intact VBS-AmB-SLN formulation, brightfield images, and merged images.

8 *In vivo* study

8.1 Toxicity study

Herein, we designed a study to investigate the acute oral toxicity as well as chronic side effects after single bolus oral administration of different dose of our well optimised formulation VBS-AmB-SLN. According to previous studies, toxicity of AmB is right away related to its aggregation in aqueous solution as a result of interaction between hydrophobic groups. The toxic side effects are attributed to the interaction of AmB with cholesterol present in host plasma membrane while its efficacy is ascribed to its interaction with ergosterol present in parasite cell membrane. Entrapment of drug inside the biocompatible lipid core could intercalate the hydrophobic regions as well as mask the polar groups further stabilizing the monomeric state forestalling aggregation and henceforth toxicity. Interestingly, there was no significant toxicity observed after an oral administration of VBS-AmB-SLN, the swiss albino mice were healthy with no abnormal behaviour or any substantial changes in serum biochemical markers. No considerable changes were observed in hepatic and renal toxicity biomarkers signifying biocompatibility of the components used. However, noticeable alterations in biomarker levels were observed during acute oral AmB toxicity evaluation Fig. 9 (A-D). Therefore, it was evident from *in vivo* toxicity evaluation that VBS-AmB-SLN was biocompatible and safe when administered orally. This was further corroborated with the results obtained from aggregation state analysis of AmB as well as VBS-AmB-SLN. This biocompatibility ensured the application of VBS-AmB-SLN as an effective and potential drug delivery carrier.

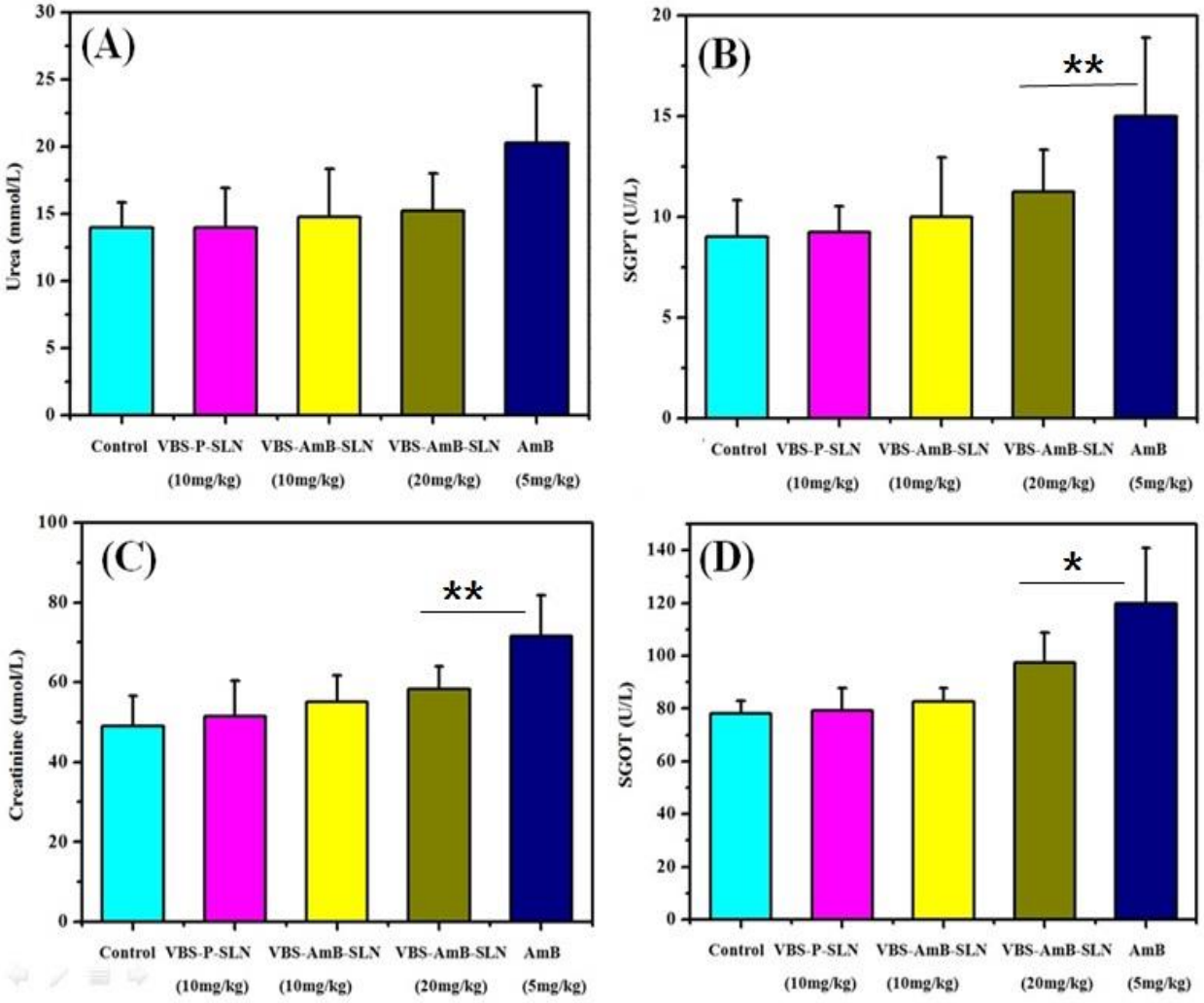

Fig. 9 Serum biochemical analysis of renal and hepatic toxicity biomarkers (A) SGOT (B) SGPT (C) creatinine and (D) urea upon treatment with AmB, VBS-P-SLN, and VBS-AmB-SLN.

8.2 Anti-leishmanial efficacy against *Leishmania* infected BALB/c mice

The efficacy of the therapeutic system was acclaimed by its interaction with the biological system. Hence, *in vivo* efficacy studies has significant importance in evaluating the pharmacological efficiency of VBS-AmB-SLN as it is the pilot step in evaluating its clinical performance. We next investigated the liver parasite burden (LDU) of *Leishmania donovani* infected BALB/c mice after treatment with test and reference therapeutic drugs.[37] VBS-AmB-SLN (10-20 mg/kg) significantly ($P<0.0001$) diminished the intracellular amastigote load in liver tissues (Fig. 10 (D)) compared to negative control (Fig. 10 (C)). Additionally, treatment with VBS-AmB-SLN (20 mg/kg x 5 days; *p.o.*) showed 96.37% inhibition of LDU (Fig. 10 (A)), whereas, VBS-AmB-SLN (10 mg/kg x 5 days) and miltefosine (3 mg/kg x 5 days) showed 79.38% and 50.62% parasite inhibition respectively (Fig. 10 (B)). However, prior to *in vivo* study, our preliminary *in vitro* testing demonstrated an enhanced intracellular parasite killing effect in *L. donovani* infected macrophages with no adverse effects which corroborated with *in vivo* efficacy.

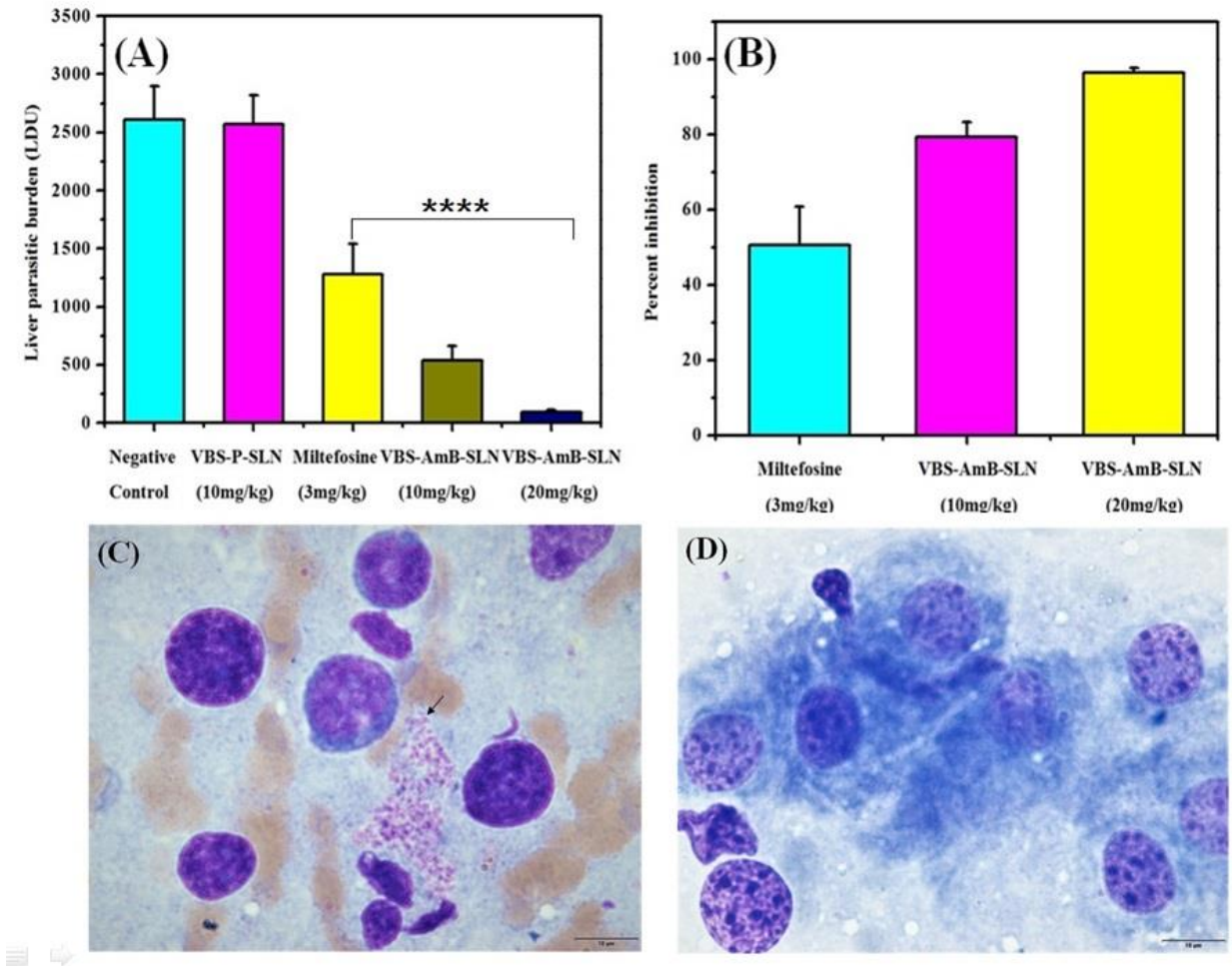

Fig. 10 (A) Liver parasitic burden in *L. donovani* infected mice model upon treatment with VBS-AmB-SLN & Miltefosine (B) Percentage inhibition of VBS-AmB-SLN & Miltefosine against *L. donovani* infected mice model. Microscopic images of *L. donovani* infected hepatic tissue impressions (100X). Black arrows indicate intracellular amastigotes. (C) Negative control, and (D) VBS-AmB-SLN (20 mg/kg; *p.o.*) treatment.

9. Stability study

Despite the great progress, the stability of liposomal formulation of AmB against extreme deteriorating tropical conditions is still a big challenge.[38] We assessed the stability of VBS-AmB-SLN

in neutral, acidic as well as alkaline electrolyte buffers. Evaluation was carried out by adopting different temperature and pH conditions at ambient humidity. For stability study, in order to mimic tropical climatic conditions accelerated temperature conditions were set and preliminary characterization was carried out over a period of 30 days. The long term stability analysis as illustrated in Fig. 11 (A-B) exhibited outcomes similar to our previous stability where release from VBS-AmB-SLN were analysed in simulated gastric and intestinal fluids by rotating basket method.[1] Release was found to negligible in simulated gastric fluids while small amount of drug was released in simulated intestinal fluids while size was not significantly altered. Overall results demonstrated that inert VBS-AmB-SLN were noticeably stable enough to traverse through GIT. Therefore, straightforward strategy of encapsulating the drug inside the robust lipid core significantly improved the stability of VBS-AmB-SLN.

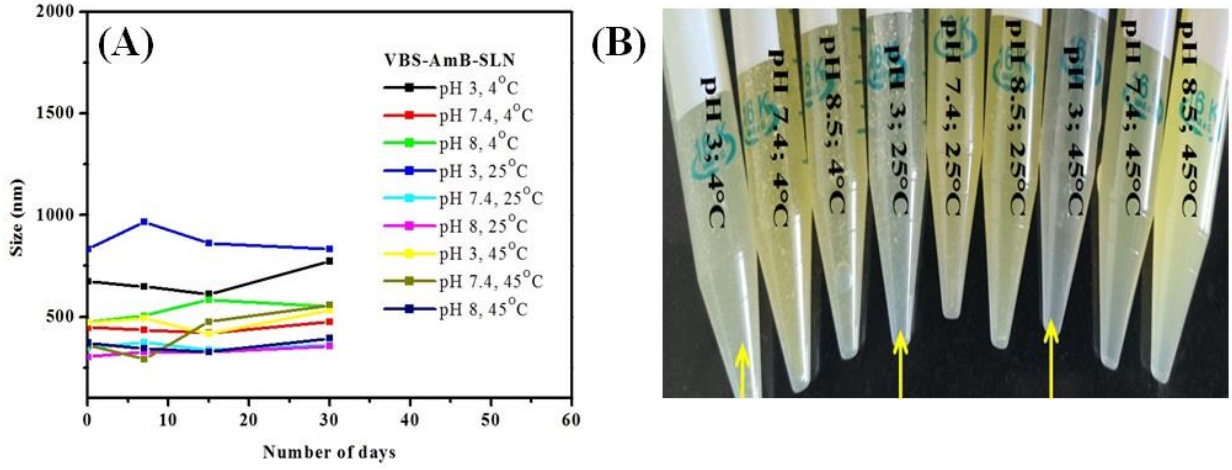

Fig. 11 (A) Average diameter, and (B) release of lyophilized VBS-AmB-SLN when reconstituted with PBS buffer of different pH and temperature conditions.

Conclusion

In the present study, we demonstrated the use of VB_{12} as an exemplary surface functionalization for SLN to enhance the oral bioavailability of encapsulated drug, while maintaining substantially high cellular viability and simultaneously enduring the harsh conditions of GIT. Given that VB_{12} can be recognized by specific transcobalamine receptors, it comes instinctive to wonder whether it can also affect the internalization mechanisms. Moreover, it was essential to investigate the active mechanism associated with VBS-AmB-SLN, which was found to be energy dependent clathrin mediated. We further found that the non invasive oral administration of the formulation to be a promising and highly efficient therapeutic strategy in combating leishmaniasis without causing any cellular toxicity or drastic disruptions in membranes viscoelasticity. The consistent mucus retention ability of formulation has profound effects on systemic absorption and subsequent bioavailability. Our previous *in vitro* studies advocated for highly efficacious therapeutic antileishmanial response *in vivo*. One of the greatest concerns with nanoparticles is whether they remain intact after internalization or dissociate from carrier over time. This concern was comprehensively addressed by stability studies and FRET analysis. Overall, the results clearly highlight the biocompatibility, and stability of formulation. Nevertheless, our findings herein firmly suggested the potential feasibility of the formulation for future applications in anti-leishmanial clinical therapy.

Supporting information

Nuclear changes and live dead assay

The cytotoxic effects on macrophage cells were investigated by changes in morphology of nucleus after long term exposure of VBS-AmB-SLN. Nuclear colocalization of VBS-AmB-SLN for longer

duration might induce DNA damage leading to swelling and hence fragmentation of cell nuclei [39]. Therefore, DAPI stained nucleus of macrophage cells were evaluated using confocal microscopy. Microscopic images of macrophage cells in Fig. 12, showed that the cell nuclei were normal and indistinguishable in cellular morphology even when the cells were exposed to 400 µg/mL. However, cell nuclei swell and fragment when cells were exposed to increased concentration of 800 µg/mL and 1000 µg/mL with slight decrease in cell density.

Live dead assay was used to confirm VBS-AmB-SLN did not negatively influence cell viability. The results demonstrated in Fig. 14, showed no visible effect on cell viability as evidenced by microscopic images of macrophage cells on exposure of 400 µg/mL of VBS-AmB-SLN. However, after incubation at concentration above 800 µg/mL, a considerable number of dead adherent cells were evident indicating cells undergoing cell death. Furthermore, the nuclear staining images were consistent with those of live dead assay.

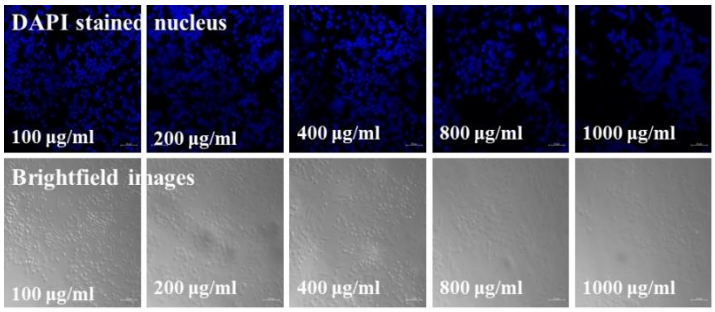

Fig. 12 CLSM images of DAPI (λ_{ex}: 405 nm) stained & bright field images of nucleus of macrophage cells after 48 h exposure of VBS-AmB-SLN (A & F) 100 µg/mL; (B & G) 200 µg/mL; (C & H) 400 µg/mL; (D & I) 800 µg/mL; (E & J)1000 µg/mL.

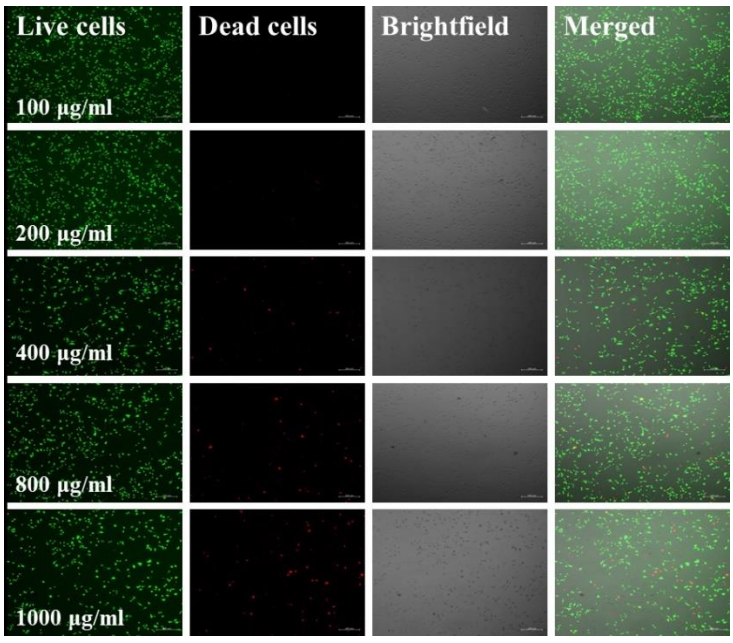

Fig. 13 CLSM images of fluorescein diacetate stained live macrophage cells after treatment with VBS-AmB-SLN (A) 100 µg/mL, (E) 200 µg/mL, (I) 400 µg/mL, (M) 800 µg/mL, and (Q) 1000 µg/mL for 48 h, Propidium iodide stained dead macrophage cells, Bright field images (C,G,K,O, and S), and Merged images (D, H, L, P and T).

Plasma membrane integrity assay

To further substantiate the above results and delineate the effect of VBS-AmB-SLN on plasma membrane integrity, macrophage cells were incubated with FITC labeled VBS-AmB-SLN for 48 h followed by treatment with propidium iodide (PI). Upon VBS-AmB-SLN treatment, macrophage cells with plasma membrane damage allow PI to passively diffuse into cytoplasm and bind with intracellular nucleic acids [39]. Therefore, by estimating PI positive cells one could assess the percentage of cells undergoing plasma membrane damage in the total population. The results showed that membrane integrity was confirmed for macrophage cells and no passive diffusion was observed as displayed in Fig. 14. The results further demonstrated that VBS-AmB-SLN (200 µg/mL) did not compromise the integrity of plasma membrane even after 48 h of exposure.

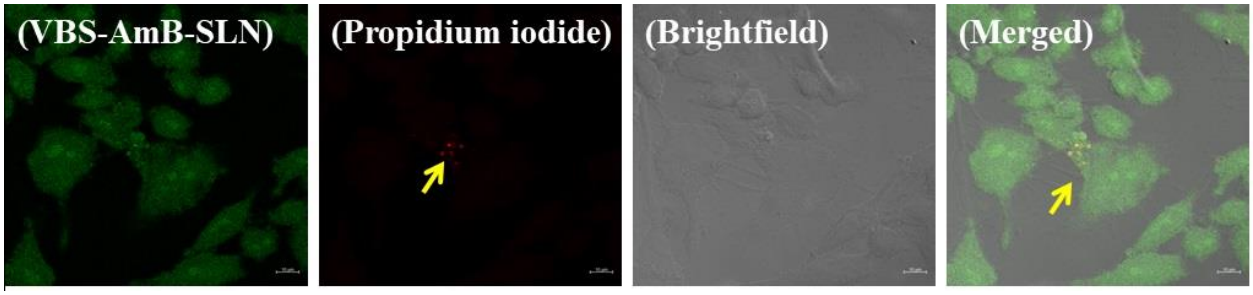

Fig. 14 CLSM images of PI (λ_{ex}: 493 nm) stained (50 µg/mL) macrophage cells, Colocalization of FITC (λ_{ex}: 488 nm) labeled VBS-AmB-SLN (200 µg/mL) after 48 h of treatment, Bright field images, and Merged images.

FTIR Spectra

The characteristic peaks of AmB, Fig. 1(D) at 2914 cm^{-1} represents the C–H stretching vibrations of the alkane and alkene groups. The peak at 1469 cm^{-1} can be assigned to N–H stretching vibration of amine groups and C=C of alkene groups while peak at 1700 cm^{-1} represents C=O stretching vibrations of carboxylic groups. The peak at 1096 cm^{-1} is associated with the C–OH bond present in AmB. The FTIR spectra of VB_{12}, shows characteristic peak at 3346 cm^{-1} which is attributed to O–H stretching of hydroxyl groups and peak at 1660 cm^{-1} is accredited to C=O stretching vibration of propionamide chain of VB_{12}. The peak at around 1577 cm^{-1} is ascribed to C=C double bond. The peak at 1490 cm^{-1} is allocated to the C=C bonds of the corrin ring. The FTIR spectrum of stearic acid shows a carbonyl peak at 1700 cm^{-1}. The peaks at 2845 cm^{-1} and 2913 cm^{-1} are attributed to CH_2 symmetric stretch and CH_2 anti-symmetric stretch. The characteristic peak of VBS at 1742 cm^{-1}, ascribed to the formation of a new band representing the esterification of carbonyl carbon of stearic acid with primary alcohol.

It is discerned that characteristic peaks of AmB and VBS did not change after subjecting the formulation to FTIR analysis, hence it can be concluded that the drug is in the free state and there is no interaction between the drug and the excipients used.

Supplementary Figures

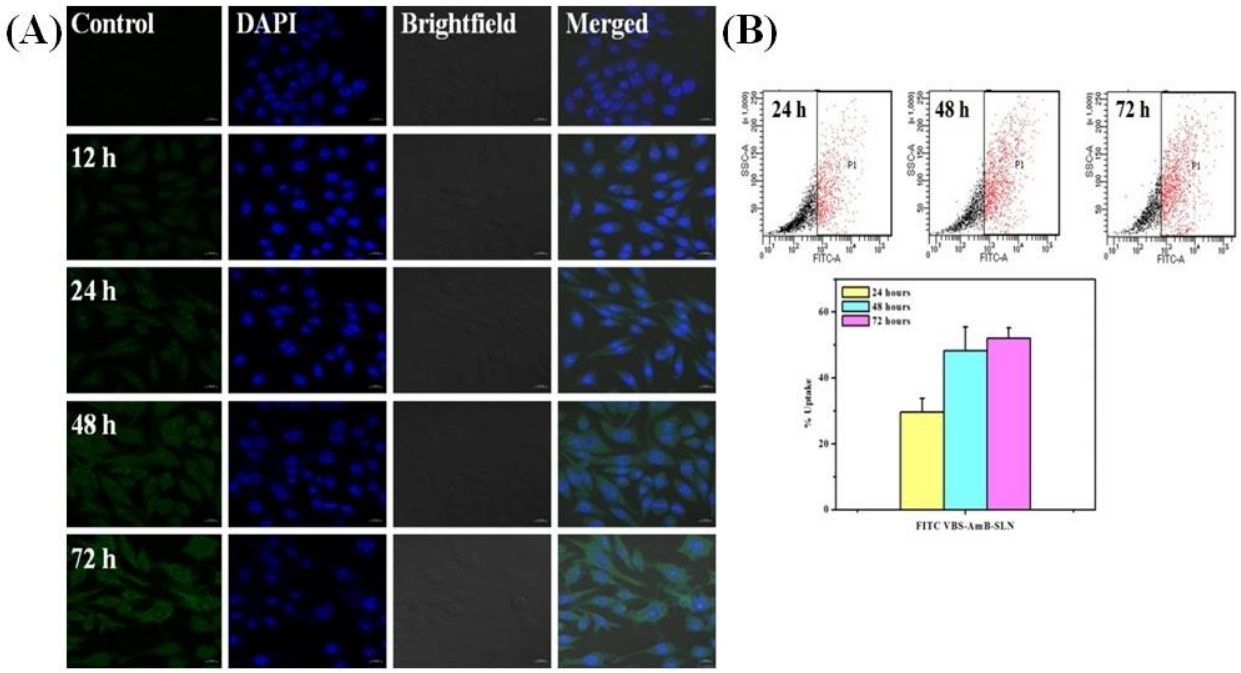

Fig. S1. (A) CLSM images of DAPI (λ_{ex}: 405 nm) stained nucleus of macrophage cells, colocalization of FITC (λ_{ex}: 488 nm) labeled VBS-AmB-SLN after 12 h, 24 h, 48 h, and 72 h of treatment, bright field images, and merged images. Scale bar in 63X is denoted as 10 µm. (B) Dot plot analysis of internalized FITC labeled VBS-AmB-SLN in macrophage cells after 24 h, 48 h, 72 h of incubation, and bar graph representation of internalized FITC VBS-AmB-SLN after 24 h, 48 h, and 72 h incubation.

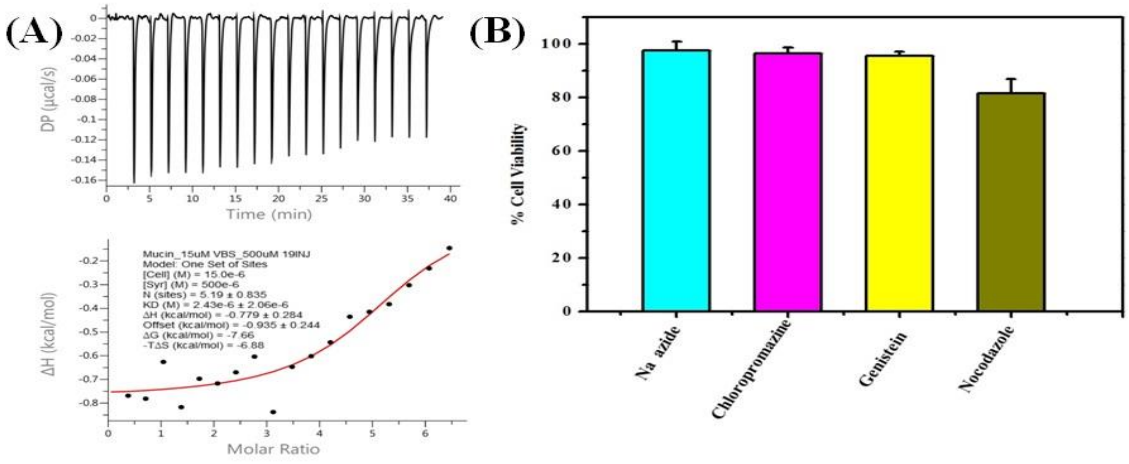

Fig. S2. (A) Isothermal titration calorimetry (ITC) analysis of the interaction between vitamin B_{12} stearate (VBS) and mucin: changes in heat flow over time when 500 µM VBS was injected into 15 µM mucin suspension. (B) Cell viability percentage of macrophage cells treated with sodium azide (100 µg/mL), chloropromazine (100 µg/mL), genistein (100 µg/mL) and nocodazole (100 µg/mL) for 24 h.

Supplementary videos

Supplementary video 1:  Supplementary video 1.mp4

Supplementary video 2:  Supplementary video 2.mp4

Supplementary video 3:  Supplementary video 3.mp4

Supplementary video 4:  Supplementary video 4.mp4

References

[1] A. Singh, G. Yadagiri, S. Parvez, O.P. Singh, A. Verma, S. Sundar, S.L. Mudavath, Formulation, characterization and in vitro anti-leishmanial evaluation of amphotericin B loaded solid lipid nanoparticles coated with vitamin B12-stearic acid conjugate, Mater. Sci. Eng. C. 117 (2020) 111279. https://doi.org/10.1016/J.MSEC.2020.111279.

[2] H. He, P. Wang, C. Cai, R. Yang and X. Tang, VB12-coated Gel-Core-SLN containing insulin: Another way to improve oral absorption, Int. J. Pharm. 493 (2015) 451–459. https://doi.org/10.1016/J.IJPHARM.2015.08.004.

[3] S. Hirve, A. Kroeger, G. Matlashewski, D. Mondal, M.R. Banjara, P. Das, A. Be-Nazir, B. Arana, P. Olliaro, Towards elimination of visceral leishmaniasis in the Indian subcontinent—Translating research to practice to public health, PLoS Negl. Trop. Dis. 11 (2017). https://doi.org/10.1371/JOURNAL.PNTD.0005889.

[4] J. Zielińska, M. Wieczór, T. Baczek, M. Gruszecki, J. Czub, Thermodynamics and kinetics of amphotericin B self-association in aqueous solution characterized in molecular detail, Sci. Rep. 6 (2016). https://doi.org/10.1038/SREP19109.

[5] R. Delhom, A. Nelson, V. Laux, M. Haertlein, W. Knecht, G. Fragneto, H.P. Wacklin-Knecht, The Antifungal Mechanism of Amphotericin B Elucidated in Ergosterol and Cholesterol-Containing Membranes Using Neutron Reflectometry, Nanomater. 2020, Vol. 10, Page 2439. 10 (2020) 2439. https://doi.org/10.3390/NANO10122439.

[6] S. Liu, A. Pandey, J. Duvigneau, J. Vancso, J.H. Snoeijer, Size-Dependent Submerging of Nanoparticles in Polymer Melts: Effect of Line Tension, Macromolecules. 51 (2018) 2411–2417. https://doi.org/10.1021/ACS.MACROMOL.7B02353.

[7] X. Bai, J. Wang, Q. Mu, G. Su, In vivo Protein Corona Formation: Characterizations, Effects on Engineered Nanoparticles' Biobehaviors, and Applications, Front. Bioeng. Biotechnol. 0 (2021) 263. https://doi.org/10.3389/FBIOE.2021.646708.

[8] G. MN, R. I, How Corona Formation Impacts Nanomaterials as Drug Carriers, Mol. Pharm. 17 (2020) 725–737. https://doi.org/10.1021/ACS.MOLPHARMACEUT.9B01111.

[9] W. Shan, X. Zhu, M. Liu, L. Li, J. Zhong, W. Sun, Z. Zhang, Y. Huang, Overcoming the diffusion barrier of mucus and absorption barrier of epithelium by self-Assembled nanoparticles for oral delivery of insulin, ACS Nano. 9 (2015) 2345–2356. https://doi.org/10.1021/ACSNANO.5B00028.

[10] B.M. Boddupalli, Z.N.K. Mohammed, R.A. Nath, D. Banji, Mucoadhesive drug delivery system: An overview, J. Adv. Pharm. Technol. Res. 1 (2010) 381. https://doi.org/10.4103/0110-5558.76436.

[11] Y.Y. Wang, S.K. Lai, J.S. Suk, A. Pace, R. Cone, J. Hanes, Addressing the PEG mucoadhesivity paradox to engineer nanoparticles that "slip" through the human mucus barrier, Angew. Chemie - Int. Ed. 47 (2008) 9726–9729. https://doi.org/10.1002/ANIE.200803526.

[12] O. Mertins, R. Dimova, Binding of Chitosan to Phospholipid Vesicles Studied with Isothermal Titration Calorimetry, Langmuir. 27 (2011) 5506–5515. https://doi.org/10.1021/LA200553T.

[13] B. Menchicchi, J.P. Fuenzalida, K.B. Bobbili, A. Hensel, M.J. Swamy, F.M. Goycoolea, Structure of

Chitosan Determines Its Interactions with Mucin, Biomacromolecules. 15 (2014) 3550–3558. https://doi.org/10.1021/BM5007954.
[14] P.D. Ross, S. Subramanian, Thermodynamics of protein association reactions: forces contributing to stability, Biochemistry. 20 (2002) 3096–3102. https://doi.org/10.1021/BI00514A017.
[15] S. VD, W. LS, G. AH, A. PV, K. GB, Spectroscopic analysis on the binding interaction of biologically active pyrimidine derivative with bovine serum albumin, J. Pharm. Anal. 6 (2016) 56–63. https://doi.org/10.1016/J.JPHA.2015.07.001.
[16] O. SS, P. JL, Y. AI, W. KJ, M. TR, C. RA, Diffusion of macromolecules and virus-like particles in human cervical mucus, Biophys. J. 81 (2001) 1930–1937. https://doi.org/10.1016/S0006-3495(01)75844-4.
[17] M. D, C. V, Endocytosis: The Nanoparticle and Submicron Nanocompounds Gateway into the Cell, Pharmaceutics. 12 (2020). https://doi.org/10.3390/PHARMACEUTICS12040371.
[18] S. Salatin, A.Y. Khosroushahi, Overviews on the cellular uptake mechanism of polysaccharide colloidal nanoparticles, J. Cell. Mol. Med. 21 (2017) 1668–1686. https://doi.org/10.1111/JCMM.13110.
[19] I. Ruseska, A. Zimmer, Internalization mechanisms of cell-penetrating peptides, Beilstein J. Nanotechnol. 11 (2020) 101. https://doi.org/10.3762/BJNANO.11.10.
[20] § Jae-Min Oh, § Soo-Jin Choi, § and Sang-Tae Kim, J.-H. Choy*, Cellular Uptake Mechanism of an Inorganic Nanovehicle and Its Drug Conjugates: Enhanced Efficacy Due To Clathrin-Mediated Endocytosis, Bioconjug. Chem. 17 (2006) 1411–1417. https://doi.org/10.1021/BC0601323.
[21] G.-H. Chai, F.-Q. Hu, J. Sun, Y.-Z. Du, J. You, H. Yuan, Transport Pathways of Solid Lipid Nanoparticles Across Madin–Darby Canine Kidney Epithelial Cell Monolayer, Mol. Pharm. 11 (2014) 3716–3726. https://doi.org/10.1021/MP5004674.
[22] J. Lee, M. Twomey, C. Machado, G. Gomez, M. Doshi, A.J. Gesquiere, J.H. Moon, Caveolae-Mediated Endocytosis of Conjugated Polymer Nanoparticles, Macromol. Biosci. 13 (2013) 913–920. https://doi.org/10.1002/MABI.201300030.
[23] A.M. Bannunah, D. Vllasaliu, J. Lord, S. Stolnik, Mechanisms of Nanoparticle Internalization and Transport Across an Intestinal Epithelial Cell Model: Effect of Size and Surface Charge, Mol. Pharm. 11 (2014) 4363–4373. https://doi.org/10.1021/MP500439C.
[24] X. Zhu, X. Ji, N. Kong, Y. Chen, M. Mahmoudi, X. Xu, L. Ding, W. Tao, T. Cai, Y. Li, T. Gan, A. Barrett, Z. Bharwani, H. Chen, O.C. Farokhzad, Intracellular Mechanistic Understanding of 2D MoS2 Nanosheets for Anti-Exocytosis-Enhanced Synergistic Cancer Therapy, ACS Nano. 12 (2018) 2922–2938. https://doi.org/10.1021/ACSNANO.8B00516.
[25] H. S, H. I, G. E, Y. J, P. S, Y. SH, L. WW, Y. JW, Brefeldin A-sensitive ER-Golgi vesicle trafficking contributes to NLRP3-dependent caspase-1 activation, FASEB J. 33 (2019) 4547–4558. https://doi.org/10.1096/FJ.201801585R.
[26] P.A. Takizawa, J.K. Yucel, B. Veit, D.J. Faulkner, T. Deerinck, G. Soto, M. Ellisman, V. Malhotra, Complete vesiculation of Golgi membranes and inhibition of protein transport by a novel sea sponge metabolite, ilimaquinone, Cell. 73 (1993) 1079–1090. https://doi.org/10.1016/0092-8674(93)90638-7.
[27] C.-H. Choi, ABC transporters as multidrug resistance mechanisms and the development of chemosensitizers for their reversal, Cancer Cell Int. 5 (2005) 30. https://doi.org/10.1186/1475-2867-5-30.
[28] L. KV, G. ME, B. RW, R. AG, Cooperativity between verapamil and ATP bound to the efflux transporter P-glycoprotein, Biochem. Pharmacol. 118 (2016) 96–108. https://doi.org/10.1016/J.BCP.2016.08.013.
[29] S. Forster, A.E. Thumser, S.R. Hood, N. Plant, Characterization of Rhodamine-123 as a Tracer Dye for Use In In vitro Drug Transport Assays, PLoS One. 7 (2012) e33253. https://doi.org/10.1371/JOURNAL.PONE.0033253.
[30] D.B. Zorov, M. Juhaszova, S.J. Sollott, Mitochondrial Reactive Oxygen Species (ROS) and ROS-Induced ROS Release, Physiol. Rev. 94 (2014) 909. https://doi.org/10.1152/PHYSREV.00026.2013.
[31] H. V, K. M, Z. A, P. J, Nitric oxide as a regulatory and effector molecule in the immune system, Mol. Immunol. 38 (2002) 989–995. https://doi.org/10.1016/S0161-5890(02)00027-5.
[32] N.S. Bryan, M.B. Grisham, Methods to Detect Nitric Oxide and its Metabolites in Biological Samples, Free Radic. Biol. Med. 43 (2007) 645. https://doi.org/10.1016/J.FREERADBIOMED.2007.04.026.
[33] J. Alvarez-Malmagro, G. García-Molina, A.L. De Lacey, Electrochemical Biosensors Based on Membrane-Bound Enzymes in Biomimetic Configurations, Sensors 2020, Vol. 20, Page 3393. 20 (2020) 3393. https://doi.org/10.3390/S20123393.
[34] V. Sood, D.S. Katti, Physicochemical changes in plasma membrane mirror nanoparticle-mediated cytotoxicity, (n.d.). https://doi.org/10.1101/2019.12.29.890236.
[35] R. Itri, H.C. Junqueira, O. Mertins, M.S. Baptista, Membrane changes under oxidative stress: the impact

of oxidized lipids, Biophys. Rev. 6 (2014) 47. https://doi.org/10.1007/S12551-013-0128-9.
[36] H.C. Ishikawa-Ankerhold, R. Ankerhold, G.P.C. Drummen, Advanced Fluorescence Microscopy Techniques—FRAP, FLIP, FLAP, FRET and FLIM, Molecules. 17 (2012) 4047. https://doi.org/10.3390/MOLECULES17044047.
[37] S. Parvez, G. Yadagiri, M.R. Gedda, A. Singh, O.P. Singh, A. Verma, S. Sundar, S.L. Mudavath, Modified solid lipid nanoparticles encapsulated with Amphotericin B and Paromomycin: an effective oral combination against experimental murine visceral leishmaniasis, Sci. Reports 2020 101. 10 (2020) 1–14. https://doi.org/10.1038/s41598-020-69276-5.
[38] N.R. Stone, T. Bicanic, R. Salim, W. Hope, Liposomal Amphotericin B (AmBisome®): A review of the pharmacokinetics, pharmacodynamics, clinical experience and future directions, Drugs. 76 (2016) 485. https://doi.org/10.1007/S40265-016-0538-7.
[39] M.R.K. Ali, Y. Wu, D. Ghosh, B.H. Do, K. Chen, M.R. Dawson, N. Fang, T.A. Sulchek, M.A. El-Sayed, Nuclear Membrane-Targeted Gold Nanoparticles Inhibit Cancer Cell Migration and Invasion, ACS Nano. 11 (2017) 3716–3726. https://doi.org/10.1021/ACSNANO.6B08345.

Catalytic exhaust aftertreatment based on cellular materials

F. Hoferecht[1], A. Roppertz[2*]

[1] Blue Fire GmbH, 26683 Ramsloh-Saterland
[2] University of Applied Science Niederrhein, 47998 Krefeld
*Andreas.Roppertz@hs-niederrhein.de

Cellular materials have been used in stoves and small combustion plants for some time. Placed close to the combustion chamber a noticeable dust separation is possible. Recently, the cellular materials are coated with catalysts in order to diminish other harmful emission, being also present in the exhaust. However, as the catalytic materials are temperature-sensitive, the choice of a suitable installation site is much more complicated. This presentation will give an overview of the current developments and challenges in simultaneous dust and emission reduction using cellular materials.

Precision and Lightweight Design - It Does Work!

H. Göhler[1*], U. Jehring[1], J. Hohlfeld[2], S. Siebeck[2], P. Quadbeck[1], Th. Weißgärber[1,3]

[1] Fraunhofer Institute for Manufacturing Technology and Advanced Materials IFAM, Branch Lab Dresden,
[2] Fraunhofer Institute for Machine Tools and Forming Technology IWU,
[3] Technical University Dresden, Faculty Mechanical Engineering, Institute of Materials Science, Chair Powder metallurgy
*hartmut.goehler@ifam-dd.fraunhofer.de

Rhythmic and accelerated movements caused by machining generate vibrations that are transmitted by lightweight, highly rigid structures with low losses. However, lightweight construction is necessary to increase cycle rates and minimize driving power. For several years sandwich constructions with aluminum foam core layers have been used successfully for lightweight construction of moving assemblies of machine tools. On the one hand, the high stiffness of cover layers allows high precision statically, but on the other hand they prevent dynamic deformation of the aluminum foam, which would be necessary for a damping effect. The lighter the assemblies, the greater the excited amplitudes for the same vibration energy. High amplitudes reduce the precision of metal-cutting machining, limit cycle rates as well as component and tool life, and result in noise emission. Therefore, the desired high sandwich stiffness is counterproductive in terms of good damping. A remedy is provided by particle-filled hollow spheres embedded in aluminum foam. The particles, which move freely in the hollow spheres, damp the vibrations of the component even in the case of rigid-body motion. In the poster, the development of the semi-finished product from vibration damping models to prototype applications will be presented.

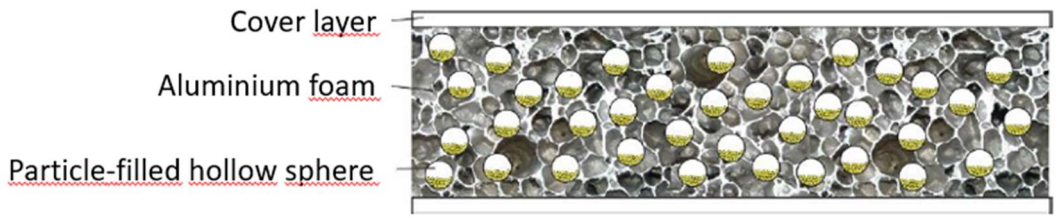

Figure 1. Scheme of a vibration damping sandwich

Surface treatment of Ti6Al4V titanium alloy for medical applications

A. Moloodi[1], H. AminiMashhadi[1], F. Barzegar[1], A. Salehi[*1]

[1] Materials Research Group, Iranian Academic Center for Education, Culture and Research (ACECR), Khorasan Razavi, P.O. Box 91779-49367, Mashhad, Iran.
*am_salehi85@yahoo.com

In this study Ti6Al4V alloy medical grade were subjected to surface chemical treatment. For this purpose cylindrical specimens similar to the standard sizes were machined and then were subjected to sandblast and acid etching. The acid etching process was performed at constant temperature and different times of 5, 10, 15, 20, 25 and 30 minutes. EDX and SEM evaluation were performed on the samples to evaluate the surface changes. SEM evaluations have shown that the best surface structure can be achieved by increasing the acid etching time to 25 minutes.

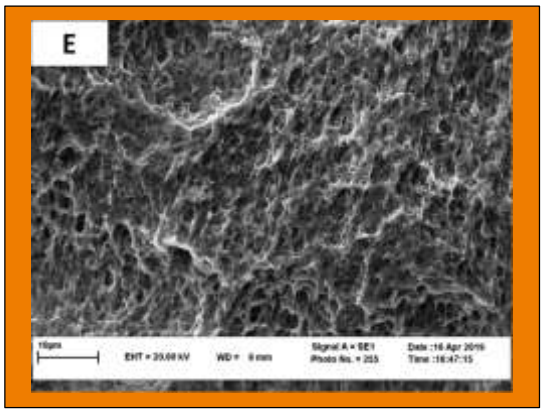

Figure. SEM image of titanium surfaces at 25 minutes of acid etching.

When an implant is placed in a bony area, a series of biological events begins. Osteoconduction first occurs, causing osteogenic cells to migrate to the contact surface of the implant. Then the formation of new bone begins [8]. The sandblasting process increases the macroscopic roughness to some extent. The type of surface structure resulting from the sandlasting process differs from the surface structure of Straumann specimens. Preliminary studies have shown that acid etching process after sandblasting is effective in improving the microscopic roughness of the surface and also increases the hydrophilicity of the surface. Therefore, the samples were etched at 5, 10, 15, 20, 25 and 30 minutes. It is shown after 25 minutes etching, there is not any useful microstructural changes in the surface.

References

[1] Turkyilmaz, Ilser, ed. Implant dentistry: a rapidly evolving practice. BoD–Books on Demand, 2011.
[2] Eldo Koshy, Sonitha Raj Philip, Dental ImplantSurfaces: An Overview, International Journal of clinical implant Dentistry, 2015, 14-22.
[3] Isa ZM, Schneider GB, Zaharias R, et al. Effects of fluoridemodified titanium surfaces on osteoblast proliferation and gene expression. Int J Oral Maxillofac Implants, 2006; 21:203–211.
[4] Mustafa K, Wennerberg A, Wroblewski J, et al. Determining optimal surface roughness of TiO(2) blasted titanium implant material for attachment, proliferation and differentiation of cells derived from human mandibular alveolar bone. Clin Oral Implants Res, 2001, 12:515–525.
[5] Buser D, Broggini N, Wieland M, et al. Enhanced bone apposition to a chemically modified SLA titanium surface. J Dent Res, 2004, 83:529–533.


General manufacturing

Creating powder-metallurgical aluminum foams with improved cell structure by tailored precursor materials

S. Siebeck[1], M. Trautmann[2], H. Ahmad[2], J, Hohlfeld[1], G. Wagner[2]

[1]Functional Integration/Lightweight Design, Fraunhofer Institute for Machine Tools and Forming Technology IWU, Chemnitz
[2]Group of Composites and Material Compounds, Chemnitz University of Technology

Aluminum foams produced by powder metallurgy usually exhibit typical inhomogeneities regarding their pore size distribution. The realized pore sizes range from a few tenths of a millimeter to several centimeters. Discontinuous cell structures lead to discontinuous properties and make the predictability of metal foam-based components difficult. This deficiency subsequently ensures that many applications with high reliability and predictability requirements remain closed to the material. Accordingly, influencing the cellular structure of metallic foams is a popular target of relevant work. Our approach aims to influence the precursor material so that initially, many microscopic pores are formed instead of a few larger ones. The challenge lies in producing starting material with finely distributed blowing agent components and in adapting the foaming process to the new conditions. We want to shed light on both focal points in equal measure within this contribution. We integrated a high-energy ball milling process into the powder metallurgical process line to produce a homogeneous fine-scaled precursor material. Figure 1 shows the distribution of the comminuted TiH_2 particles in dependence of the milling time. The β-value can be used to determine the quality of the distribution of TiH_2 particles on SEM powder micrographs. The smaller β, the more homogeneous the distribution. In addition to the milling time, the type of alloy and the size and composition of the aluminum powder particles have an influence. For example, smaller powders can achieve a low β more quickly.

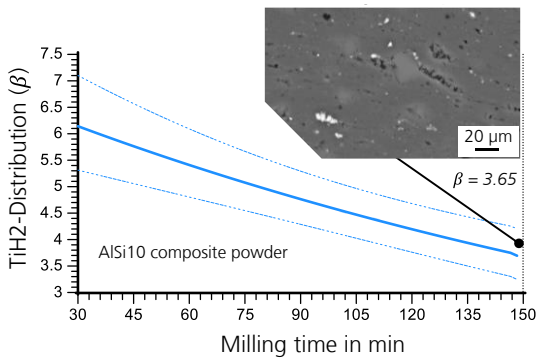

Figure 1. Prediction of TiH_2 distribution as function of milling time within a Simoloyer© ball mill determined by β-value. The more homogeneous the distribution.

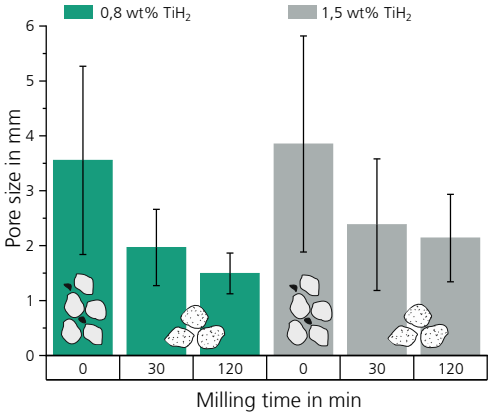

Figure 2. Foam pore size as function of milling time.

With better TiH_2 distribution, the final foam structure also becomes more homogeneous (Figure 2). A significant increase in the TiH2 content is, accordingly, not necessary. However, a certain amount of hydrogen is lost during milling, or the dehydrogenation is shifted to a lower temperature. The reason for the latter is the TiH2 comminution, which is demonstrable by DSC and was found by [1] in similar investigations. Further information regarding the work we have published in [2].

References

[1] E. Schumann, J.-F. Silvain, J.-L. Bobet, M. Bardet, Y. Lu, A. Kotousov, M. Lamirand-Majimel *Materials Chemistry and Physics*, **2016**, 173, 106–116.
[2] S. Siebeck, M. Trautmann, J. Hohlfeld, T. Hipke, G. Wagner *Key Engineering Materials*, **2019**, 809, 320–25.

Manufacturing of designed open cellular structures additive and via casting

C. Drebenstedt[1*] D. Kibaroglu[2], N.N. [1], N. N. [2]

[1] Fraunhofer IWU, [2] RWTH Aachen University
*Claudia.Drebenstedt@iwu.fraunhofer.de

In the project "ProZell" the aim is to manufacture special open-cellular structures for crash absorption in high manganese steels. The first step included the creation of concepts of different structures, the selection of the preferred variant and the implementation into a CAD-model.
The structures are manufactured following two different routes: additive manufacturing and investment casting. As base for the structure the f2cc,z structure and the additive route the studies [1, 2] are used. The manufactured structures will be tested via compression testing.
The target is to get the same structure with both routes and to compare their compression behaviour. Where else the additive structures have a size of 3 mm as unit cell, the casted structures start with a unit cell of 10 mm and is stepwise reduced to find the right parameters and the limitations of the process.
As next step the design of the structures shall be adapted according to the results. Additional the influence of different strut diameters (relative densities) and radii at the strut intersections will be studied.
For the casting the structures lost wax casting is used, like described in [3].

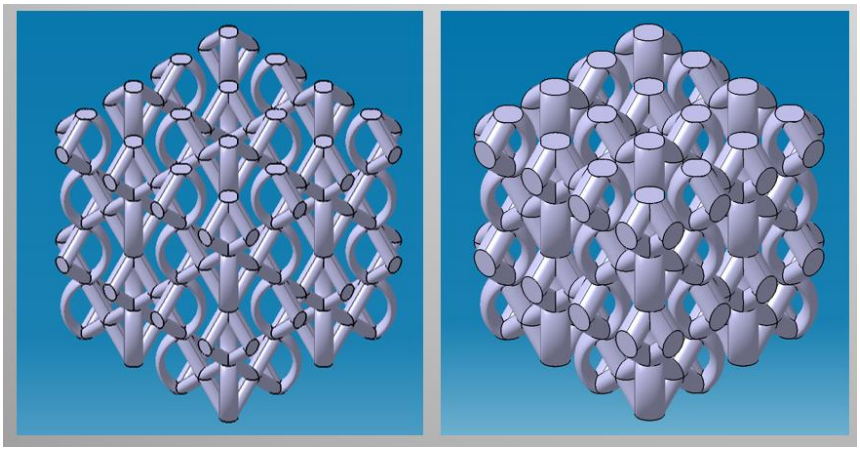

Figure 1. CAD model of the structure with two different strut diameters

References

[1] P. Köhnen; C. Haase; J. Bültmann; S. Ziegler; J. H. Schleifenbaum; W. Bleck, *Mechanical properties and deformation behavior of additively manufactured lattice structures of stainless steel*, Materials & Design, 2018, volume 145, page numbers 205-217.
[2] P. Köhnen, M. Létang, M. Voshage, J. H. Schleifenbaum, C. Haase:
Understanding the process-microstructure correlations for tailoring the mechanical properties of L-PBF produced austenitic advanced high-strength steel; Additive Manufacturing 30 2019
[3] J. Wang; S. R. Sama; P. C. Lynch; G. Manogharan, Design and Topology Optimization of 3D-Printed Wax Patterns for Rapid Investment Casting, Procedia Manufacturing, 2019, volume 34, page numbers 683-694.

Photopolymerization-assisted ice-templating of porous polysiloxane-derived ceramics with tailored pore morphology

K. Rauchenwald, J. Eßmeister, V. Bartsch, M. Mayr and T. Konegger

TU Wien, Institute of Chemical Technologies and Analytics
katharina.rauchenwald@tuwien.ac.at

While ceramics exhibit high thermal and chemical stability rendering them suitable candidates for catalyst carriers, conventional powder-based processing is somewhat limited in terms of obtaining porous parts. Catalyst carriers should ideally show hierarchical porosity and tailored pore shapes, as ordered macropores reduce the flow resistance and thus increase the product throughput, while mesopores further increase the surface area and the catalytic activity. In contrast to traditional powder-based routes, polymer-derived ceramics (PDCs) come with significant processing benefits. PDCs can be chemically modified in the precursor state and can be shaped as polymeric liquids. Novel shaping methods like ice-templating are in this regard particularly interesting, as porosity, surface area and pore morphology can be systematically optimized.

In this work, a photocurable poly-silsesquioxane (PSO) solution is combined with the ice-templating method to obtain directionally aligned and porous silicon oxycarbide (SiOC) monoliths for prospective catalysis applications. PSO is functionalized with acrylic groups as crosslinker. The modified preceramic polymer solution can be stabilized in its ice-templated state by light irradiation prior to solvent sublimation and pyrolysis, similarly to previous reports on poly-silazane-derived ceramics.(1, 2) Processing via ice-templating is optimized on a custom-made set-up to control the cooling rate and to monitor the freezing front velocity in a reproducible manner. The pore morphologies obtained by the use of cyclohexane and tert-butanol as macropore templates are studied, cooling rates of 1 to 10 K/min are applied, and the effect of different thermal gradients on the macropore alignment are investigated. Furthermore, the introduction of sacrificial porogens into PSO is evaluated for further increasing the specific surface area (Figure 1).

By adequate knowledge of the effect of selected process parameters on the final material morphology, it can be shown that ice-templating enables the generation and control of porosity at different length scales to create functional structures with hierarchical porosity. The obtained ceramics are thereby a promising starting point for the development of PDC-based catalysts for CO_2 utilization processes.

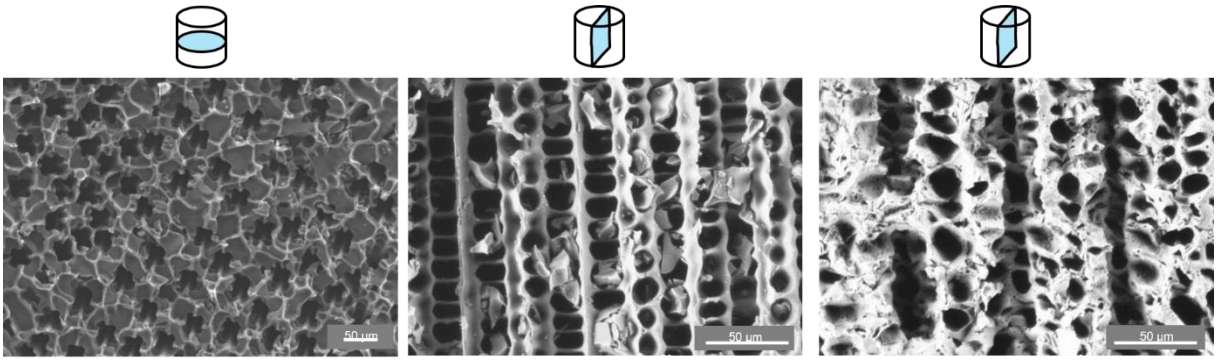

Figure 1. Electron micrographs of sections perpendicular and parallel to the freezing direction of ice-templated PSO-derived ceramics using cyclohexane as structure-directing solvent (left and middle: without sacrificial porogens; right: with polystyrene as a sacrificial porogen).

References

(1) Mikl, G., Obmann, R., Schörpf, S., Liska, R. and Konegger, T., 2019. Pore morphology tailoring in polymer-derived ceramics generated through photopolymerization-assisted solidification templating. Advanced Engineering Materials, 21(6), p.1900052.
(2) Obmann, R., Schörpf, S., Gorsche, C., Liska, R., Fey, T. and Konegger, T., 2019. Porous polysilazane-derived ceramic structures generated through photopolymerization-assisted solidification templating. Journal of the European Ceramic Society, 39(4), pp.838-845.

General manufacturing 1

Session Chairs

Dr.
Mike Tromm
Technoform Glass Insulation Hol…

60 Years Open-celled Ceramics Based on Replica Technique – Applications, Obstacles and Opportunities

D. Haase[1*], A. Füssel[1], J. Adler[1]

[1] Fraunhofer Institute for Ceramic Technologies and Systems IKTS,
*Daniela.Haase@ikts.fraunhofer.de

Thinking of open-celled ceramics we look back on development history of 60 years. Starting with the first patents for the production of ceramic foams in the 1960s, the Schwartzwalder process became established industrially for the production of molten metal filters [1]. From this time on versatile fields of applications, which are predestined for these special open-celled structures, have been identified and discussed in literature. This includes the use of ceramic foams as porous burners, structured catalyst supports, filters for wood-fired furnaces or automotive, bone substitute materials, solar receivers, heat exchangers, energy absorbers, preforms for metal-matrix composites, lightweight or acoustic construction components or direct heaters [2-4]. For such high-performance applications ceramic foams need to fulfil significantly higher requirements in terms of purity, mechanical strength, high-temperature and chemical resistance or structural design compared with the conventional quality for molten metal filtration. On this account the production technologies as well as the material variety of ceramic foams have developed rapidly in the past few decades and thus for many applications an industrial implementation was achieved.

Figure 1. Examples of applications for open-cell foam ceramics.

This lecture will give an overview about the current state of development of open-celled ceramic foams for various applications. Based on selected examples it will be shown for which applications an industrial implementation has been successfully realized and why some applications may never make it beyond proof of concept in research.
The reasons are complex. Especially for applications where only small variations in properties such as pressure drop, strength or geometrical surface are required, a high degree of exact adherence to geometrical and structural tolerances is necessary. With respect to the increased demand for high reproducibility, the replica technique is competing with progressively developing additive manufacturing technologies. However, the Schwartzwalder process is very efficient and may enter to new fields of application by advanced production and finishing concepts as well as the development and standardization of efficient analysis and quality assurance systems.

References

[1] K. Schwartzwalder, A. V. Somers; US Patent 309 0094, 1963.
[2] J. Adler, G. Standke; *Keramische Zeitschrift*, 2003, 10: 786-792.
[3] M. Scheffler, P. Colombo; *Wiley-VCH*, 2005, ISBN: 9783527313204.
[4] M.V. Twigg, J.T. Richardson; *Ind. Eng. Chem. Res.,* 2007, 46, 4166-4177.

Hierarchically porous ordered mesoporous silica COK-12 materials

U. Simon[1*], L.M. Henning[1], E.S. Dal Molin[1], G.J. Smales[2], J. Schmidt[3], M.G. Colmenares[1], M.F. Bekheet[1], A. Gurlo[1]

[1] Technische Universität Berlin, Faculty III Process Sciences, Institute of Material Science and Technology, Chair of Advanced Ceramic Materials, Straße des 17. Juni 135, 10623 Berlin, Germany, [2] Bundesanstalt für Materialforschung und -prüfung (BAM), Division 6.5 – Synthesis and Scattering of Nanostructured Materials, Unter den Eichen 87, 12205 Berlin, Germany, [3] Technische Universität Berlin, Faculty II Mathematics and Natural Sciences, Institute of Chemistry, Chair of Functional Materials, Straße des 17. Juni 135, 10623 Berlin, Germany
*ulla.simon@ceramics.tu-berlin.de

Ordered mesoporous materials with high surface areas and tailored pore structures are interesting for a variety of applications such as sorption, drug delivery, sensing, catalysis, and separation. As most materials are in powder form, besides tailoring micro- and mesoporosity, research focuses on shaping, e. g. into monoliths, for better handling and defined heat and mass transfer.
COK-12, invented by Jammaer et al. in 1999, shows high specific surface areas given by 2D hexagonally-ordered cylindrical mesopores approximately 6 nm in diameter. [1] The mesopores are tailored by a soft-templating approach using the amphiphilic triblock copolymer Pluronic P123 as structure-directing agent at room temperature and mild reaction conditions. Compared to other ordered mesoporous silica materials, the synthesis of COK-12 is simple and upscalable in batch and semi-continuous mode.

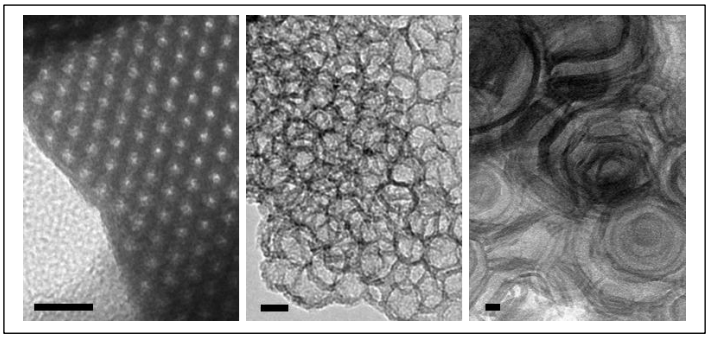

Figure 1. TEM images of the pore structure due to synthesis modifications: cylindrical mesopores (left), mesocellular foam (middle), and multilamellar vesicular structures (right). The scale bars are 20 nm.

Here we report a comprehensive overview on the tailoring of COK-12 materials. In the meso scale we show the tailoring of pore diameter and pore shape (cylindrical, mesocellular foam, and multilamellar vesicles) as well as surface functionalization with graphene oxide. [2,3] The structure properties are proven by nitrogen sorption analysis, small angle X-ray scattering, transmission electron microscopy, and X-ray photoelectron spectroscopy. Furthermore, we shape COK-12 into monoliths with introduced macroporosity by spark plasma sintering and additive manufacturing and use them successfully in water purification and as supports in catalysis applications.

References

[1] J. Jammaer, A. Aerts, J. D'Haen, J.W. Seo and J.A. Martens *Stud Surf Sci Catal*, 2010, 175, 681–684.
[2] L.M. Henning, D.D. Cubas, M.G. Colmenares, J. Schmidt, M.F. Bekheet, B.R. Pauw, A. Gurlo, U. Simon, *Microporous Mesoporous Mater*, 2019, 280, 133–143. 3
[3] L.M. Henning, U. Simon, G.J. Smales, G. Gurlo, M. Bekheet, *RSC Adv*, 2019, 62, 36271–36284.

Carbon fiber reinforced AZ91 magnesium foams produced using the melt foaming method

J. Isakovic[1*], H. Dieringa[1], N. Ben Khalifa[1,2]

[1] Helmholtz-Zentrum Hereon - Institute of Material and Process Design, [2] Leuphana University Lüneburg - Institute of Product and Process Innovation
*jonas.isakovic@hereon.de

Foam structures of AZ91 magnesium alloys have been widely investigated in the last decade [1]. The development of hybrid materials, in which materials such as aluminum or magnesium alloys are reinforced with nanoparticles or fibers, shows advantages in mechanical properties [2]. Due to its high specific strength and low density, magnesium is generally well suited as a structural material in lightweight construction. In this work, the influence of recycled carbon fibers on the properties of an AZ91 magnesium foam produced by a melt foaming process is analysed and discussed.

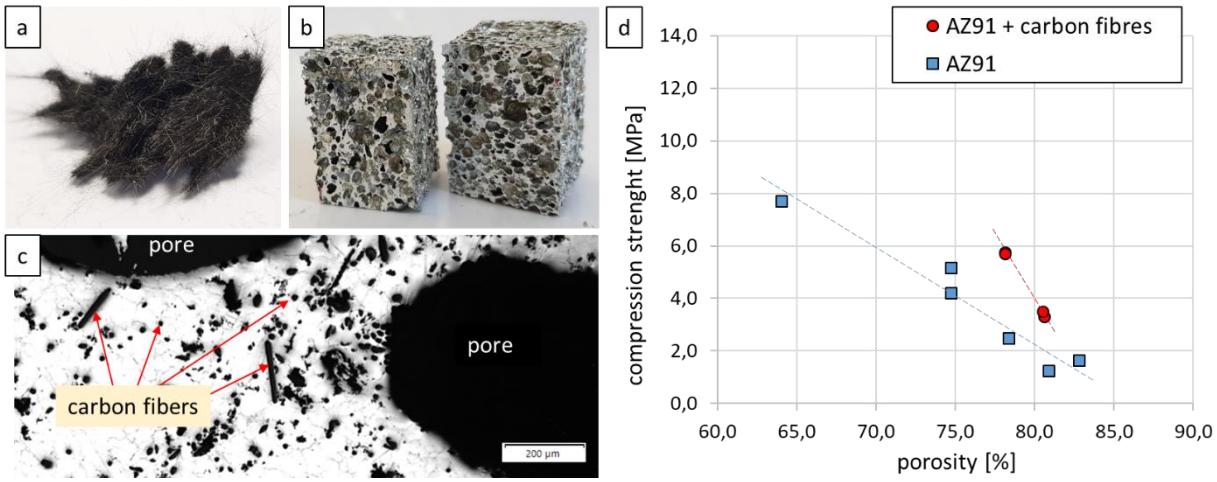

Figure 1. a) Bundle of recycled and milled carbon fibers, b) AZ91 foam samples with and without carbon fibers, c) Micrograph of the AZ91 + carbon fibers foam, d) Comparisons of the AZ91 foams with and without carbon fibers in a diagram showing compression strength over porosity.

The melt foaming process was carried out on a tube furnace in round conical casting moulds. The added carbon fibers, see figure 1a (product: "carboNXT milled pure / Mitsubishi Chemical Advanced Materials GmbH"), are 100 % recycled and coarse milled. According to manufacturer, they have a length of > 500 µm and a diameter of 6 µm (± 1 µm). In all experiments, the viscosity of the AZ91 melt was increased with 3 wt. % calcium to enhance the foaming process. In addition of 5 wt. % carbon fibers, 2 wt. % $CaCO_3$ as blowing agent was stirred into the melt at 700°C. After a holding time of 30 seconds, the mold was quenched in water. For comparison, foam without carbon fibers was produced in similar way. The AZ91-C_{rec} foam samples have a porosity of more than 75%, which is in line with other works with similar process parameters [3], whereas the AZ91 foam has a much wider spread in porosity, see figure 1d. In addition to the analysis of the porosity and the average pore size, a metallographic examination of the samples was carried out. According to figure 1c, the carbon fibers are rather homogeneously distributed and have different orientations. The AZ91-C_{rec} foams have a higher compression strength at the same porosity compared to the samples without carbon fibers, see figure 1d. Therefore, it is assumed that the carbon fibers are suitable for further improvement of foam processing and the mechanical properties of foam structures, which needs to be investigated more in detail.

References

[1] A. Kucharczyk, K. Naplocha,* J.W. Kaczmar, H.Dieringa, K.U. Kainer; *Adv. Eng. Mater.*, **2017**, *1700562*
[2] H. Dieringa, *Journal of Materials Science*, **2011**, *46,* 289 - 306.
[3] C.-H. Seo, M.-J. Jeong, I.-Y. Jung, B.-Y. Hur, *Materials Science Forum*, **2008**, *569,* 273-276

Ceramic foams for the catalytic emission reduction – chances and challenges

Andreas Roppertz[a], Frank Hoferecht[b]

a University of Applied Science Niederrhein, b Blue Fire GmbH

In the field of heterogeneous catalysis ceramic foams are the most prominent representatives of cellular materials. They exhibit extremely high porosities, with a significant degree of interconnectivity that results in low pressure-drop. Mass and heat transfer can be enhanced by high convection in the tortuous large pores. Furthermore, ceramic foam catalysts, unlike their honeycomb monolithic counterparts, have a considerable degree of radial mixing, which is an advantage in processes limited by heat transfer and can homogenize flow distribution. Reactions that require short contact times to control product selectivity or processes that are limited by heat transfer to or from the catalyst bed can benefit from the use of foam-based catalysts. Due to the previously mentioned beneficial behavior foam ceramics are used in several industrial relevant processes like Fischer-Tropsch synthesis or methanation.

Foam ceramics are also used in the field of catalytic emission reduction. Regarding small furnace the tightening of the 1st BImSchV often requires the application of catalysts inside the burning room in order to reduce carbon monoxide as well as hydrocarbon emissions. For this purpose mainly ceramic foams are applied what is not only due to their low price, but also due to the structure-related additional particle emission reduction behavior. Highly turbulent flow conditions caused by the pore structure allow this additional particle reduction, which is of great importance for small furnace. Depending on the structure and the prevailing flow conditions, the particle matter generated during combustion can be quantitatively separated. It must be emphasized that the application of catalysts within small furnace leads to different effects. On the one hand, the catalyst structure can influence the pressure conditions in the combustion chamber, what leads to potentially higher pollutant and particle emissions. On the other hand, the pore structure of the ceramic substrate controls the efficiency of particle separation. Therefore, the selection of a suitable catalyst system for simultaneous emission and particle reduction based on foam ceramics in small furnaces is a complex undertaking.

Designed gas diffusion barrier for producing skinless polymer foams by gas dissolution foaming

D. Cuadra-Rodríguez[1*], S. Barroso-Solares[2], M. A. Rodríguez-Pérez[3], J. Pinto[4]

[1] Cellular Materials Laboratory (CellMat), Condensed Matter Physics Department, University of Valladolid, Paseo Belén 7, 47011, Valladolid, Spain,
[2] BioEcoUVA Research Institute on Bioeconomy. University of Valladolid, Spain
*dcuadra@fmc.uva.es

Gas dissolution foaming is one of the most employed methods to fabricate micro and nanocellular polymers, which are materials composed of solid and gas phases. The process consists of a physical dissolution of the gas into the polymer under pressure conditions, a sharp drop of the pressure, and the foaming process by applying temperature [1]. The solubility and the diffusivity of the polymer-gas system are intrinsically related to the final cellular structure; thus, the study of the mechanisms involved in the diffusion process is critical to further enhance this process. Between the pressure drop and the foaming stage, a gas diffusion process out of the polymer is taken place due to the pressure difference, promoting a gas concentration decrease in the borders of the polymer. According to the gas concentration profile, three different regions appear in the resulting foam: a homogenous cellular core which represent the largest volume, a solid skin in the borders where gas concentration was not enough to foam, and a region which presents a cell size gradient between both previous zones [2]. Therefore, the reduction of the gas concentration in the borders hinders the foaming in this region, resulting in a polymer with a foamed core covered by non-foamed solid skins in the edges. This drawback avoids the exposure of the cellular structure to the external medium, limiting their physical properties [3], and their potential application of the cellular polymers in several fields, such as filtration, catalysis [4].

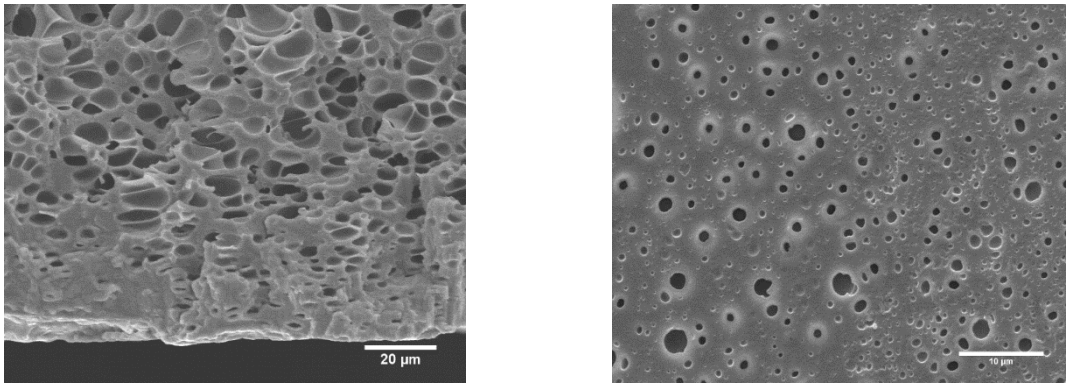

Figure 1. SEM micrographs of the cross section (left) and the surface (right) of a PMMA foam by employing the gas diffusion barrier during the foaming process.

In this work, a novel approach was designed to improve the gas dissolution foaming process in order to avoid the appearance of the non-foamed solids skins in the cellular polymers. The idea is based on a gas diffusion barrier placed over the surfaces of the polymer, which delays the diffusion during the pressure drop stage, remaining an appropriate gas concentration in the edges to obtain completely foamed polymers. Besides, this technique has allowed foaming systems with the same magnitude of the solid skins formed, it means in the micrometric range, which previously could not be foamed using this foaming technique.

References

[1] S. Costeux, CO2-blown nanocellular foams, J. Appl. Polym. Sci. 41293 (2014).
[2] V. Kumar, J.E. Weller, A model for the unfoamed skin on microcellular foams, Polym. Eng. Sci. 34 (1994) 169–173.
[3] J. Martín-de León, V. Bernardo, M.Á. Rodríguez-Pérez, Key Production Parameters to Obtain Transparent Nanocellular PMMA, Macromol. Mater. Eng. 302 (2017) 3–7.
[4] J. Germain, J.M.J. Fréchet, F. Svec, Nanoporous Polymers for Hydrogen Storage, Small. 5 (2009) 1098–1111.

Influence of pressure-induced temperature drop on the foaming behavior of amorphous polylactide (PLA) during autoclave foaming with supercritical CO_2

M. Dippold[1*], H. Ruckdäschel[1]

[1] University of Bayreuth
*marcel.dippold@uni-bayreuth.de

Foaming of thermoplastic polymers is often performed in high-pressure autoclaves to investigate the potential of various materials in a controlled environment. Blowing agents such as hydrocarbons, alcohols or inorganic gases are required to initiate nucleation and further expansion of the bulk material. The physical foaming of amorphous polylactide (PLA) by the dissolved simple gas carbon dioxide (CO_2) is an effective contribution to the sustainable development of foamed products [1].

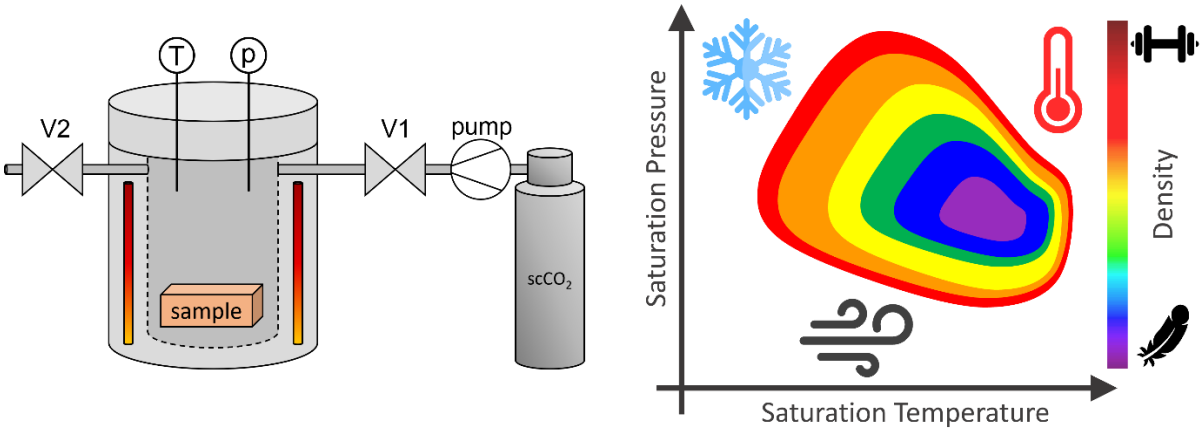

Figure 1. In autoclave foaming the area for low densities is bounded by three limits depending on saturation temperature and pressure.

Unlike complex extrusion or injection molding technologies, the autoclave process depends only on pressure, temperature, and time during saturation of the sample with the surrounding gas. Previous and current literature is mainly concerned with these precisely controllable parameters up to depressurization and, to some extent, on the pressure drop rate, without considering changes in temperature during pressure release.

As known from the rapid expansion of gases or liquids, a near adiabatic process with limited heat transfer is expected, similar to the depressurization within the autoclave process, resulting in a temperature drop of the expanding medium and cooling of the material [2]. A drop in temperature increases the viscosity of the polymer sample, which greatly affects the growth and stabilization of foam cells after nucleation [3]. Since the path of CO_2 from supercritical phase to ambient pressure is defined by its phase diagram and several thermodynamic phenomena, pressure and the resulting pressure drop rates are significantly affected during the process in addition to temperature.

Analysis of density as a function of saturation temperature and pressure during saturation allows identification of a "valley" bounded by three limits to high expansion rates. First two are known in literature and caused by (i) too low viscosity for stabilization and (ii) thermodynamically suppressed nucleation and further expansion at low saturation pressures. Third, expansion of the medium at high saturation pressures and low temperatures near the liquid phase of CO_2 leads to a rapid temperature drop (iii), which increases the resistance of the polymer to stretching.

References

[1] E.T.H. Vink *Industrial Biotechnology*, 2015, *11*, 167-180.
[2] S.T. Munkejord *Energy*, 2020, *211*.
[3] D. Gao *Journal of Cellular Plastics*, 2016, *52*, 175-187.

Investigation of modified PU-foam templates for the preparation of open-porous materials

A. Füssel[1*], D. Haase[1], J. Adler[1]

[1] Fraunhofer Institute for Ceramic Technologies and Systems IKTS,
*Alexander.Fuessel@ikts.fraunhofer.de

Reticulated polymer foam templates are characterized by sharp-edged triangular struts. They transfer this attribute to open-celled structures based on them, for instance, in the case of ceramic and metal foams prepared by the well-known and industrially established replica technique [1-3]. One characteristic element of these kind of foams is the hollow, triangular strut core left by the polymeric template after its decomposition during the heat treatment step. Moreover, the triangular strut shape can also be found in metal foams prepared by investment casting. In this process the polymeric foam template is filled with a flowable moulding material, which is dried, dewaxed and pyrolyzed, in order to generate a mould with a well-defined channel structure. This mould can be filled afterwards with liquid metal melt during the casting process. After removing the mould material, the result is a sharp-edged and highly open-porous metal foam.
In both examples, the mechanical strength of the resulting foam structure will be affected by the sharp-edged strut shape of the template, either by stress concentration or by the low portion of strut material per volume of the foam.
While a subsequent infiltration of pyrolyzed, pre-sintered or sintered foams can help to increase the strength of replica foams [4], another approach is used in case of investment casting: the thickening of the polyurethane template struts. Usually, this is done by a dip coating with liquid wax [5], but the powdering of meltable polymer granules on a previously applied adhesive layer has been reported too [6].

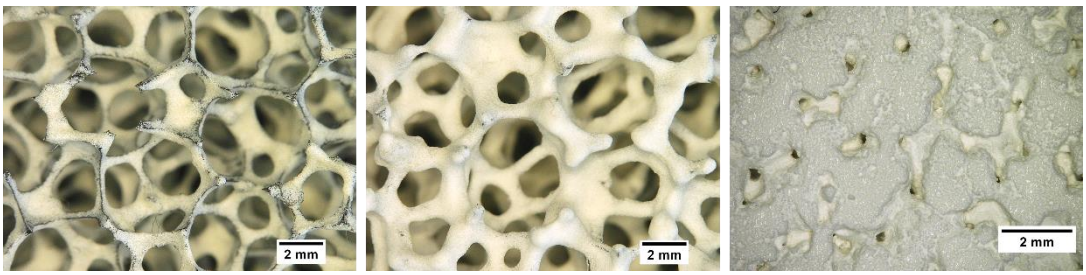

Figure 1. PU-foam template with thickened struts of two different loadings (left and middle) and compact Zeolite block with inner channel porosity based on such modified PU-foam template (right).

In this lecture, an alternative slurry-based technology for adjusting the strut thickness will be presented. This approach allows to adjust the strut thickness in a wide range (see fig. 1) and can be used for the preparation of replica foams as well as the creation of compact ceramic bodies consisting of a well-defined network of pore channels. The influence of the modification of the triangular cross-section to a more circular one, on the coating behaviour and the later mechanical properties of ceramic replica foams, will be discussed briefly. Also, as an alternative example of moulds for investment casting, the preparation of zeolite-based bricks for a thermochemical storage approach will be shown.

References

[1] K. Schwartzwalder, A. V. Somers, US Patent 309 0094, 1963.
[2] P. Colombo *Philosophical Transactions: Mathematical, Physical and Engineering Sciences*, 2006, *364*, 109-124.
[3] P. Quadbeck et al. *Adv. Eng. Mater.*, 2011, *13*, 1024-1030.
[4] U. F. Vogt et al. *Journal of the European Ceramic Society*, 2010, *30*, 3005-3011.
[5] I. Dani et al. *Procedia Manufacturing*, 2020, *43*, 10-17.
[6] A. M. Matz et al. *Advances in Materials Science and Engineering*, 2014, *2014*, 1-9.

Polycrystalline Superalloy Membranes Produced by Directional Coarsening Through Rolling and Ageing

C. Voelter[1*], J.M. Lück[1], J. Rösler[1]

[1] Institute for Materials Science, Technische Universität Braunschweig
*c.voelter@tu-braunschweig.de

Nickel-based superalloys are known for their use at high temperatures and loads. Due to the interaction of external loads and internal stresses caused by the misfit between precipitate and matrix, the so-called "rafting" occurs, with the precipitates coalescing into elongated rafts [1]. Since both the γ' rafts and the γ matrix are fully interconnected, i.e. a bicontinuous network has formed, this phenomenon can be used to produce open-porous metallic membranes [2]. For this purpose, the single-crystalline alloy CMSX-4 is thermo-mechanically treated under creep stress and then one of the two phases is electrochemically extracted.

In order to reduce costs and realize larger specimen dimensions, in addition to membranes made of single-crystalline, those made of polycrystalline starting material are studied. Recent publications investigate the development of superalloy membranes by incoherent growth of the particles [3]. This results in membranes with relatively large pores, a porosity of 44 % and an ultimate tensile strength of 120 MPa.

In this work, we show polycrystalline membranes with a directionally coarsened structure. By means of separate mechanical and thermal treatment, a rafted structure similar to the directionally coarsened one in CMSX-4 is also formed in the polycrystalline alloy. In contrast to the uniaxial creep load during the production of directionally coarsened single-crystalline membranes, a directional rafted structure is formed here from originally cubic γ' precipitates (figure 1a) by repeated rolling and ageing. Figure 1b shows the microstructure after thermo-mechanical treatment and figure 1c the surface of the open-porous membrane after the γ' phase was removed.

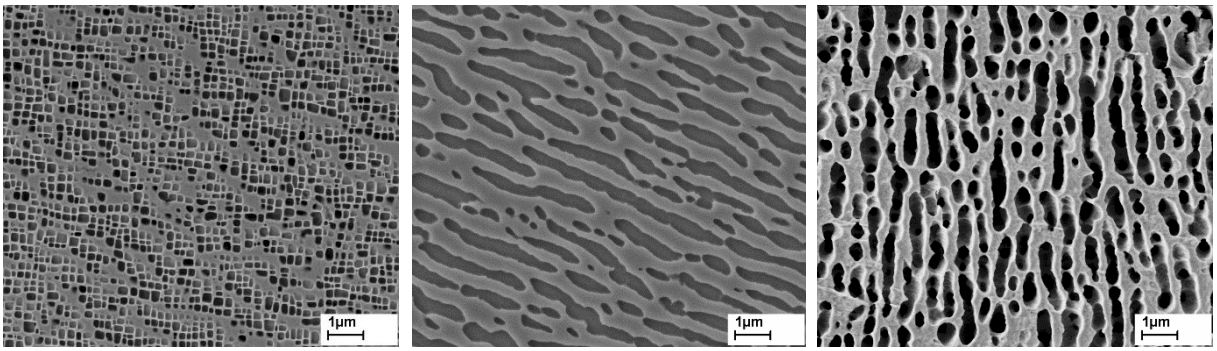

Figure 1. Microstructure after a) precipitation heat treatment [3], b) several passes of cold rolling and aging, and c) chemical extraction of the γ' phase resulting in an open porous structure.

The development of the microstructure during the thermo-mechanical treatment is shown by micrographs of the specimen and cross-sections of the extracted membranes, as well as quantitatively evaluated on the basis of the length-related flow resistivity. In addition, the mechanical properties are determined in tensile tests using an optical strain measurement system.

References

[1] T.M. Pollock; A.S. Argon *Acta Met. Mater.*, 1994, *42*, 1859–1874.
[2] J. Rösler; C. Voelter, *Adv. Eng. Mater.*, 2018, *20*, 1701011.
[3] C. Voelter; J. Rösler, *Materials*, 2021, *14*, 784.

Production and Mechanical Properties of Highly Porous Metal Structures Based on Elements Made from Aluminium Sheets

J. Baumeister[1*], L. E. Füllgraf[1], J. Weise[1]

[1] Fraunhofer Institute IFAM, Wiener Strasse 12, D-28359 Bremen, Germany
*joachim.baumeister@ifam.fraunhofer.de

After their development approximately 30 years ago, aluminium foams like Foaminal or aluminium foam sandwich (AFS) have found their way into industrial production. However, the application range is still limited. This is partly due to the specific property spectrum of foams; however, the main reason can be attributed to their relatively high production costs. These are caused by expensive raw materials and the complicated foaming process. In order to evade the latter, the advanced pore morphology (APM) foam was developed; which comprises the simple foaming of small foam elements, which are subsequently combined to larger components or foam fillings by means of polymer bonding. As the high raw material costs are still an issue, the present investigation focused on small quasi-porous elements made from aluminium sheet as alternative basis for the APM foams. Aluminium Raschig rings – known from random column packing in chemistry – were used in different sizes and combinations for the experiments. Bonding of the rings to obtain larger specimens was performed with cold-curing epoxy adhesive and thermoplastic polyamide. Quasi-static compression tests according to DIN 50134 were used for the determination of the mechanical properties. Results showed that the non-isotropic behavior of simple Raschig rings leads to non-optimal use of the deployed material in the foam for the absorption of deformation energy. Using combinations of Raschig rings, the non-isotropy can be weakened and the material efficiency can be increased.

Keywords: aluminium foam; APM; random column packing.

Rheology-driven design of pizza gas foaming

P.R. Avallone[1], P. Iaccarino[1,2], N. Grizzuti[1], R. Pasquino[1], E. Di Maio[1,2*]

[1] Dipartimento di Ingegneria Chimica, dei Materiali e della Produzione Industriale, University of Naples Federico II, P.le Tecchio 80, 80125 Naples, Italy, [2] foamlab, University of Naples Federico II, P.le Tecchio 80, 80125 Naples, Italy
*edimaio@unina.it

This paper investigates the production of a yeast-free pizza by gas foaming and the use of rheology to guide the process design. The novel process relies on the use of a gaseous blowing agent and a pressure program to form and stabilize bubbles during baking, avoiding the use of yeast and the associated lengthy leavening stage. The evolution of the dough structure during baking has been studied by a rheological characterization at leavening and baking conditions. These experimental pieces of information have been used to evaluate the time available for blowing agent sorption under pressure during early baking stage, and to guide the pressure release during the final baking, to achieve an optimally foamed pizza.

Figure 1. Foaming processing program (pressure vs. time - closed symbols) and the rheological cooking curves (open symbols).

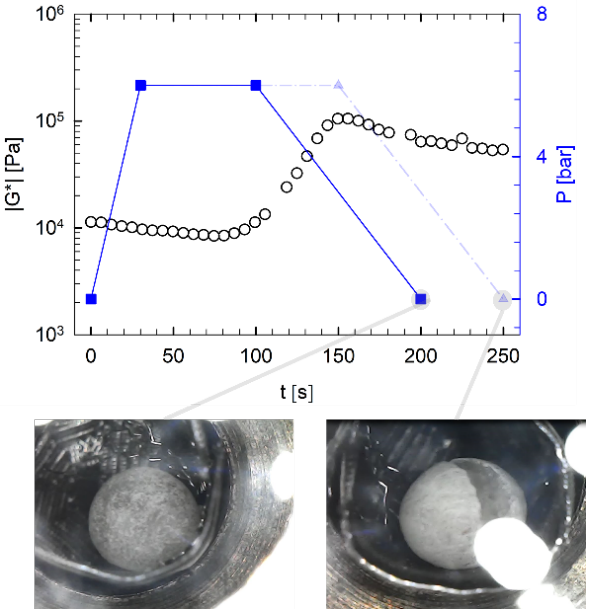

We designed a novel baking process for a yeast-free pizza dough, making use of the gas foaming by a physical blowing agent and a pressurized oven. A rheological testing campaign has been used to design the new process, which can be described in terms of baking&foaming. The evolution of the viscoelastic moduli of the dough at cooking temperature has allowed to define the time window for blowing agent sorption under pressure, and the depressurization stage to allow bubbles formation and growth. Mild pressures (as high as 6 bar) and a temperature of 145°C were required to bake&foam in ca. 4 minutes, consistently with the time required for the moduli buildup. A well-foamed pizza was achieved with densities and morphologies similar to the ones of a traditional dough with yeast. Moreover, the novel baking&foaming process parameters, as well as the physical blowing agent nature, can be suitably tuned to obtain a desired density and morphology of the final foamed product.

References

[1] P.R. Avallone et al. *Physics of Fluids*, 2022, *34* 033109.
[2] C. Brondi et al *J. Supercritical Fluids*, 2019, *154*, 104630.

Stabilization Mechanism of Aluminum Alloy Foams affected by Primary Crystals and Cell Wall Structures

Satomi Takamatsu[1*] (S. Takamatsu), **Takahiro Arai**[1] (T. Arai), **Shinsuke Suzuki**[1,2] (S. Suzuki)

[1] Department of Materials Science, Graduate School of Fundamental Science and Engineering, Waseda University, [2] Kagami Memorial Research Institute for Materials Science and Technology, Waseda University
*s-takamatsu@asagi.waseda.jp

Semi-solid route is one of the fabrication methods for aluminum alloy foams where the melt is thickened by primary crystals[1]. The primary crystals can inhibit the drainage in a cell wall of the foam by the clogging effect which is based on the percolation theory[2]. Clogged cell walls where the drainage is inhibited by this effect can hold other cell walls; thus a whole foam can keep stable. However, this effect was previously proved by two-dimensional observation. It is well known that the percolation threshold will differ depending on the observed dimension and the cell wall structures. Thus, it is crucial to confirm the clogging effect through the three-dimensional observation. Moreover, the cell wall structures of the stable foam should be evaluated to reveal what structure keeps the foam stable. The objective of this study is to prove the three-dimensional clogging effect and to evaluate the percolation thresholds of the cell wall structure.

Aluminum alloy foam was fabricated through the semi-solid route by adding TiH_2 as a blowing agent into Al-6.4mass%Si alloy in a semi-solid state and solidifying them. The inner structure of the foam was scanned by X-ray computed tomography and was reconstructed into the stack images with 20 μm intervals. The volume of each cell wall and primary crystals were calculated by integrating the cross-sectional areas of the cell wall measured by the stack images.

The three-dimensional percolation probability P_c was calculated by dividing the volume of primary crystals by that of each cell wall containing them. P_c for 322 out 532 cell walls exceeded the three-dimensional percolation threshold for the cell wall. According to the percolation theory, those cell walls are considered to be clogged. Additionally, the value of 61% for the percentage of clogged cell walls to all cell walls is larger than the two- and three-dimensional percolation threshold. Therefore, it is clear that the fabricated foam was stable, and the three-dimensional clogging effect was confirmed.

3D images obtained by X-ray CT showed five types of cell wall structures as shown in Figure 1. The difference in number of connected cell walls d was defined for classification and was calculated by subtracting the number of cell walls connected to the bottom of the observed cell wall n_b from that connected to the top n_t. Monte Carlo simulation was conducted to calculate the percolation threshold of each structure. The results showed that cell walls with large d have a small percolation threshold. This means the cell walls with large d can be clogged easily with a low fraction of solid. Therefore, it was revealed the foam having many cell walls with large d can be stable easily.

This study can be summarized as follows: The clogging effect works accurately in the three dimension. The cell wall structure defined as d can indicate the stability of a foam based on its percolation threshold.

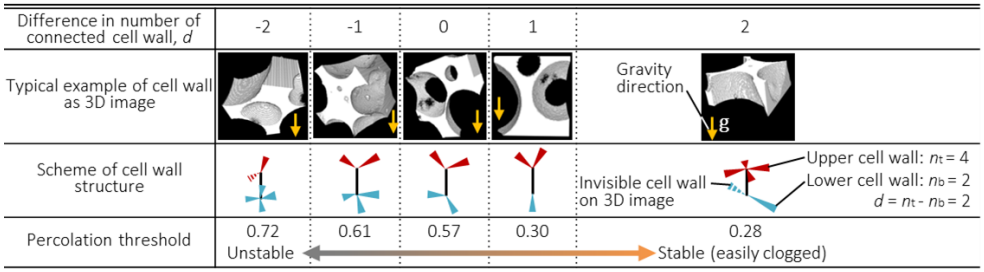

Figure 1. Typical examples of cell wall 3D image, their scheme and percolation threshold for each difference in number of connected cell wall d.

References

[1] T. Hanafusa, *et al.*; *Report of Hiroshima Prefectural Technology Research Institute Western Region Industrial Research Center*, **2020**, *10*, 847.
[2] S. Takamatsu, *et al.*; *Metals*, **2020**, *10*, 847.
[3] L.N. Smith, *et al.*; *Physical Review B*, **1979**, *20*, 3653.

Trabecular Metal: a history, materials and application

Y.Song, J.P. Anderson, J. Seebeck

Zimmer Biomet

Originating from an aviation industry innovation, porous tantalum material branded Trabecular Metal™ Material has been developed to an efficient bone replacement material and used clinically since 1997. It resembles trabecular bone in its cellular structure and weight-bearing characteristics making it an outstanding ingrow/ongrow solution. This highly porous, structural biomaterial enables rapid and extensive bone infiltration by approximating the mechanical and physical properties of the bone. Several studies are showing the great benefit for patients to serve heavy bone defects in joint replacements and revisions.

Trabecular Metal implants are fabricated using elemental tantalum metal to deposit with vapor deposition techniques on to a carbonized polyurethane foam (reticulated vitreous carbon (RVC)), which creates a metallic strut configuration. It consists of fully interconnecting pores with 70%-80% porosity which allows approximately 2-3 times greater bone ingrowth and double the interface shear strength compared to conventional porous coatings. The 3-D structure of the material provides inherent flexibility similar to bone, thereby reducing the risk for stress shielding. Additionally, the terminal struts on the surface of the TM components provide a high friction that increases primary implant stability.

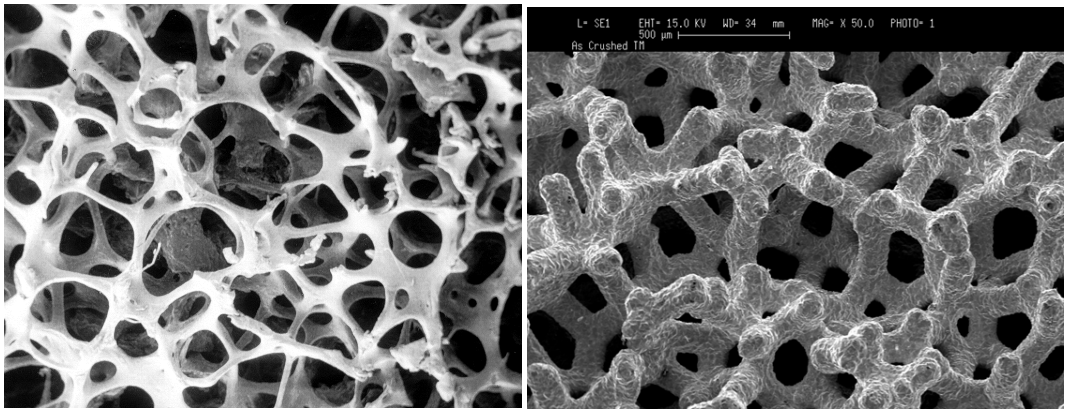

Figure 1. Microstructure of bone (left) and of trabecular metal (right)

The shape of the trabecular metal parts can be formed at polyurethane foam stage and produced as net shapes. They can also be machined after the CVD process to the required shape. The flexibility of this technique allows a variety in shapes of the final component. It permits trabecular metal to be used in many implant systems as augment, as well as attaching it to other titanium alloy or CoCr alloy implant parts as a bone ingrowth component. With various options of combinations, it provides the possibility to tailor individualized solutions for each patient.

Figure 2. Examples of implant with trabecular metal

This presentation will cover the development history of trabecular metal in the medical device industry, including details about the technology, and its application in various implant systems.

Joining and machining

In-situ integration of inserts into integrally manufactured sandwich structures

J. Faust[1], S. Geller[1], M. Gude[1]

[1] TU Dresden, Institute of Lightweight Engineering and Polymer Technology
Johann.Faust@tu-dresden.de

The potential of sandwich structures composed of fibre composite face sheets and a cellular polymer core has been known for years. In the past, such sandwich structures had to be manufactured by stacking and joining pre-manufactured layers and the sandwich core in a separate production step e.g. bonding or pressing, leading to time-consuming and expensive production methods. It has been shown in [1,2] that the efficiency of the process can be improved significantly by utilizing an expandable matrix that is injected in between textile face sheets which are impregnated by the expanding matrix in a closed mould, thus creating the sandwich structure within a one-step process. However, the problem of joining parts that are formed in the said manner by means of load application elements remained.
Therefore, a method has been developed that allows the in-situ integration of topologically optimized lightweight inserts that are tailored to the requirements of integral composite sandwich structures.

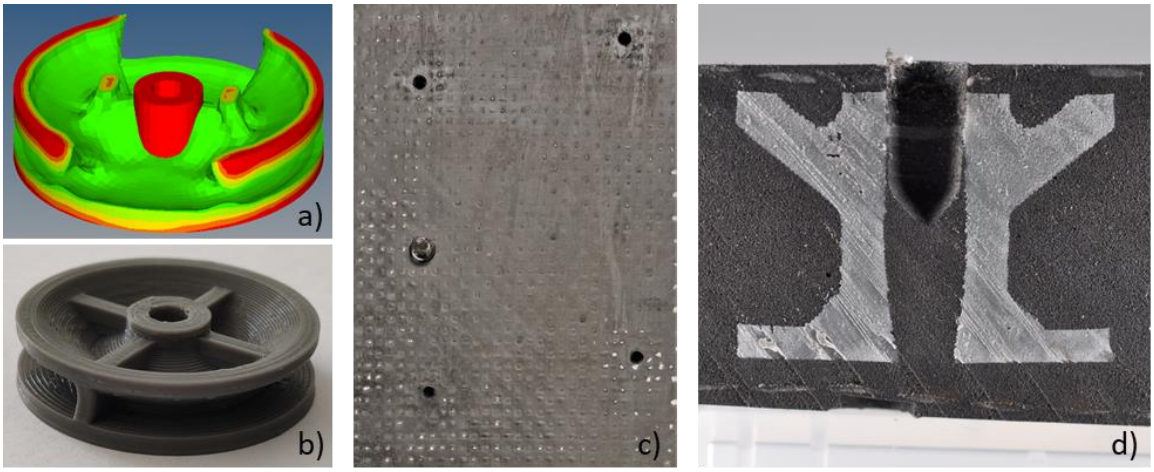

Figure 1. Insert as topology simulation result and 3D printed (a, b), in-situ integration of inserts in PU-core-sandwich-structures (c) and cross-section of structure-integrated inserts (d)

For the design of such inserts suitable to initiate loads into the sandwich structure, the different layers and their respective mechanical properties have to be taken into consideration. Studies showed that commercially available inserts made out of plastics or metal have limitations either in terms of integration in the sandwich foaming process or in their mechanical functionality. To solve the problem numerical topology optimization (fig. 1a) was performed to find the most optimal structure in terms of weight and pull-out resistance to a predefined screw geometry. The inserts were then 3D printed (fig. 1b) and integrated during the production process (fig. 1c). The results showed that the topologically optimized inserts were successfully integrated in the manufactured sandwich part and fully enclosed by the foam core (fig. 1d). Furthermore, pull-out-tests indicated that the mechanical properties of a so-fabricated joint are close or equal to those of a metal insert while featuring only a fraction of the weight.

References

[1] M. Gude; S. Geller; O. Weißenborn *Integral manufacture of fiber-reinforced sandwich structures with cellular core using a polyurethane spray-coat method*, 2014, *Proceedings of Cellular Materials Cellmat 2014*, Dresden, Deutschland, 22.-24. Oktober 2014
[2] O. Weißenborn; S. Geller; M. Gude *Prozessuntersuchungen zur Herstellung neuartiger Sandwichstrukturen im Polyurethan-Sprühverfahren*, 2017, *PU Magazin, volume 4*, p. 276-280

Mechanical engineering

Cellular metamaterial with axisymmetric chiral auxetic structure

Anja Mauko[1*] (A. Mauko), **Miran Ulbin**[1] (M. Ulbin), **Nejc Novak**[1] (N. Novak), **Matej Vesenjak**[1] (M. Vesenjak), **Zoran Ren**[1] (Z. Ren)

[1] University of Maribor, Faculty of Mechanical Engineering, Slovenia
*anja.mauko@um.si

Cellular metamaterials can be designed to have increased energy absorption capacity and higher specific stiffness while retaining light-weightiness. In this research, a unique cellular metamaterial with an axisymmetric chiral auxetic structure was designed, fabricated, and mechanically tested [1], [2]. The 3D chiral unit cell corresponds to the 10th eigenmode of the regular cubic unit cell. The 3D chiral unit cells were spatially scaled and distributed in the radial and axial directions to form the axisymmetric chiral auxetic structure (Figure 1). The unit cells were graded in the radial direction by scaling the length and amplitude of the horizontal struts from the inner to the outer layer of cells. The designed structure was fabricated using the powder fusion method (PBF) with basic material 316L and then experimentally tested in quasi-static and dynamic compression loading regimes, achieving strain rates from 0.005 s^{-1} to 1050 s^{-1}. The tested structure exhibited pronounced auxetic response with smooth deformation and gradually increasing load-carrying capability until final densification. Digital cameras observed the structures' deformation process, and the advanced Digital Image Correlation (DIC) method was used to analyse the full-field strain data. The computational model of the novel chiral auxetic structure was built and validated by the experimental results. The validated computational model was then used to optimise the axisymmetric chiral auxetic structure parameters to achieve the desired mechanical response.

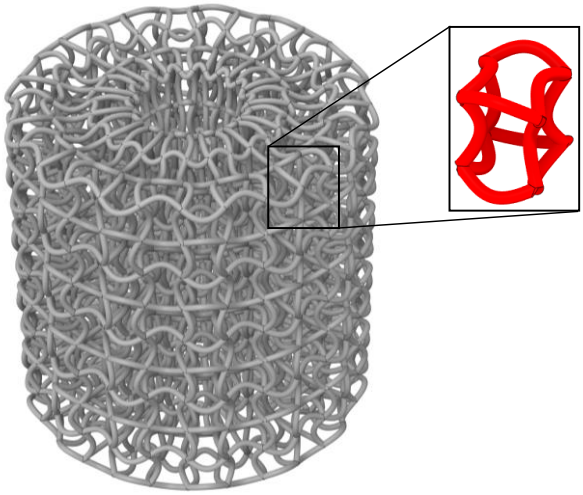

Figure 1. Axisymmetric chiral auxetic structure [2].

References

[1] Z. R. M. Vesenjak, N. Novak, "Axisymmetric chiral auxetic structure, EP21197296.3 patent pending," 2021.

[2] N. Novak, A. Mauko, M. Ulbin, L. Krstulović-Opara, Z. Ren, and M. Vesenjak, "Development and characterisation of novel three-dimensional axisymmetric chiral auxetic structures," *J. Mater. Res. Technol.*, vol. 17, pp. 2701–2713, Mar. 2022, doi: 10.1016/J.JMRT.2022.02.025.

Mechanical engineering 1

Session Chairs

Johannes Eßmeister
TU Wien

Bending and compression behaviour of Triply Periodical Minimal Surface (TPMS) structures-filled tubes

N.Novak[1*], O. Al-Ketan[2], M. Vesenjak[1] and Z. Ren[1]

[1] Faculty of Mechanical Engineering, University of Maribor, Slovenia
[2] Core Technology Platform, New York University Abu Dhabi, United Arab Emirates
*n.novak@um.si

The metal foam-filled tubes are one of the best energy-absorbing components in the field of crashworthiness, blast and impact protection due to their lightweight design and extraordinary energy absorption capabilities. The cores of foam-filled tubes can consist of different cellular or composite materials, providing different mechanical properties and deformation modes. Recent advances in additive manufacturing enable the fabrication of very complex and predesigned cellular geometries like Triply Periodical Minimal Surface (TPMS) structures [1-2].

The TPMS lattices were designed and generated using the software MSLattice [3]. The generated cores, empty tubes and TPMS-filled tubes were fabricated using the powder bed fusion system EOS M280 with atomised stainless steel 316L powder. Five types of samples were considered in this work: as-fabricated empty tube, 3D printed empty tube, TPMS core, ex-situ TPMS-filled tube and in-situ TPMS-filled tube.

Compression and three-point bending tests under quasi-static and dynamic loading conditions were performed for all samples. The validated computational models provide a framework for further computational design of multi-morphology (hybrid) lattices with spatially variable cell types.

A qualitative comparison of the quasi-static bending mechanical responses is shown in Figure 1. The results showed that the ex-situ and in-situ TPMS-filled tubes provide very similar responses, with a slightly stiffer elastic response of in-situ TPMS-filled tubes due to a better interface connection between the core and the tube. The specific energy absorption (SEA) of TPMS-filled tubes is increased up to 40 % at ex-situ TPMS-filled tubes and up to 46 % at in-situ TPMS-filled tubes if compared to the summed responses of core and empty tubes.

Under compression loading, the energy absorption of the axially loaded ex-situ and in-situ TPMS-filled structures is enhanced by 21 % and 44 % if compared to the as-fabricated empty tube, which has the highest SEA of empty tubes and the core. The SEA enhancement is much lower at transversal loading, where only the in-situ TPMS-filled tubes result in the SEA enhancement up to 12 %.

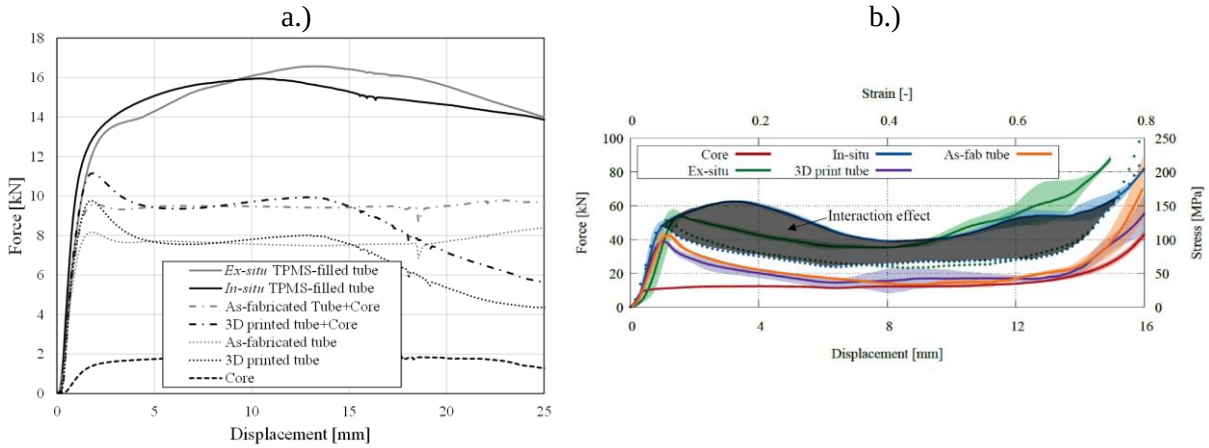

Figure 1. The bending (a) and compression (b) mechanical response of analysed samples.

References

[1] O. Al-Ketan *Additive Manufacturing*, 2018, *19*, 167-183.
[2] N.Novak *Composite Structures*, 2021, *266*, 1-10.
[3] O. Al-Ketan Mater. Des. Process. Commun., 2021, *3 (6)*, 1–10.

Medical devices and life science 1

Session Chairs

Prof. Dr.-Ing.
Peter Quadbeck
University of Applied Science O...

Biodegradable Iron-based Material for Customized Stent Structures

B. Paul[1*], M. Otto[1], J. Hufenbach[1,2]

[1] Institute for Complex Materials, Leibniz IFW Dresden, Dresden, Germany
[2] Institute of Materials Science, Technische Universität Bergakademie Freiberg, Freiberg, Germany
*b.paul@ifw-dresden.de

For manufacturing implants customized to the patient's need, additive manufacturing (AM) has a high potential. Hence, the processing of biodegradable metallic materials to fabricate new temporary implants with complex geometry and with adjusted mechanical and (bio)chemical properties is currently drawing increasing attention. Thereby, laser powder bed fusion (LPBF) – as a dominating metal AM process – presents an attractive technology. Regarding biodegradable materials, Fe-Mn-based alloys are promising candidates, besides Mg- or Zn-based systems, due to the broad range of mechanical properties, the high mechanical integrity during degradation as well as an excellent processability [1]. Especially, the processing of Fe-Mn-C-based alloys via LPBF is very attractive because very filigree structures can be realized due to their high strength. Such filigree structures are needed for e.g. stents to open up clogged vessels. Furthermore, owing to the LPBF processing, a relatively homogenous microstructure can be achieved leading to the desired uniform degradation.

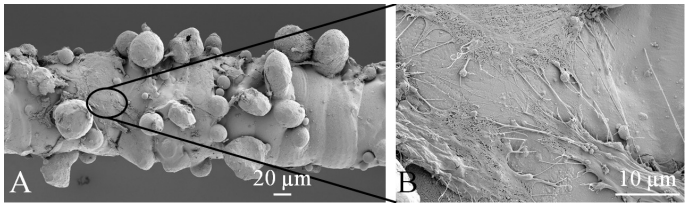

Figure 1. SEM images of Fe-30Mn-1C-0,02S stent structures with adherend endothelial cells after 1 day of cultivation.

In our group, a biodegradable Fe-30Mn-1C-0,02S alloy was developed and first stent prototypes were successfully processed via LPBF [2-6]. The stents with a generic structure could be expanded manually with a balloon catheter [5]. In 3-point-bending tests, those stents revealed superior mechanical properties in comparison to LPBF-processed stent structures made of clinically applied 316L SS [6]. Furthermore, generic stent structures were seeded with endothelial cells and cultivated for up to 14 days (Fig. 1 after 1 day of cultivation). Thereby, the influence of different degradation stages due to pre-incubation in cell culture medium on adhesion, viability and morphology of the endothelial cells was analyzed [6]. After 1 day of cultivation of endothelial cells on different degraded samples, no difference of the degradation stages was obvious. Only after longer cultivation of 7 to 14 days, the influence of the degradation layer became visible. Overall, biocompatibility of the alloy was confirmed and Fe-Mn-C systems are seen as promising candidates for potential application as temporary implant material.

Funding of this project by the DFG under project number HU 2371/1-1 is gratefully acknowledged.

References

[1] T. Niendorf, F. Brenne, P. Hoyer, D. Schwarze, M. Schaper, R. Grothe, M. Wiesener, G. Grundmeier, H.J. Maier, *Metall. Mater. Trans. A,* 2015, 46, 2829–2833.
[2] J. Hufenbach, H. Wendrock, F. Kochta, U. Kühn, A. Gebert, *Mater. Letters*, 2017, 186, 330-333.
[3] J. Hufenbach, F. Kochta, H. Wendrock, A. Voß, L. Giebeler, S. Oswald, S. Pilz, U. Kühn, A. Lode, M. Gelinsky, A. Gebert, *Mater. Design*, 2018, 142, 22-35.
[4] M. Otto, S. Pilz, A. Gebert, U. Kühn, J. Hufenbach, *Metals*, 2021, 11, 944.
[5] J. Hufenbach, J. Sander, F. Kochta, S. Pilz, A. Voss, U. Kühn, A. Gebert, *Adv. Eng. Mater.*, 2020, 2000182.
[6] B. Paul, A. Lode, A.-M. Placht, A. Voß, S. Pilz, U. Wolff, S. Oswald, A. Gebert, M. Gelinsky, J. Hufenbach, *ACS Appl. Mater. Interfaces*, 2022,14,439-451.

Simulation 1

Session Chairs

Dr.-Ing.
Daniela Haase
Fraunhofer Institute for Cerami...

Simulation and verification of mechanical properties of injection molded thermoplastic foam structures

D. Oikonomou*, H.-P. Heim

Institute of Material Engineering, Polymer Engineering, University of Kassel, 34125 Kassel, Germany;
oikonomou@uni-kassel.de (D. O), heim@uni-kassel.de (H.-P. H.)

Abstract

In this study, a chain of numerical simulation programs is performed to determine mechanical properties of foamed polymer samples. First, an injection moulding process is simulated by using the software "Moldex3D" to acquire morphological properties, such as porosity and cell size distribution (Figure 1). Real manufactured components represent the empirical part of this study and are produced as reference. Thus, the structural characterization of the porosity and cell size distribution serves as a verification basis for the simulated data of "Moldex3D". Subsequently, material and global mechanical properties such as cell size distribution as well tensile strength are modelled with the help of the software "Digimat". This program combines the material processing data from the injection moulding simulation as well as from the Digimat material database itself, which are both required for the structural mechanics modelling (Finite Element Analysis). Tensile test is used to reverse engineer and therefore to optimize the digital material data of Digimat. In addition, an initially neutral receiver mesh obtains the process and material data from the process simulation (Moldex3D) and the material modelling (Digimat). Consequently, mechanical properties are digitally calculated and simulated by using the software "Marc" under tensile loading and verified with the comparison of the experimental results.

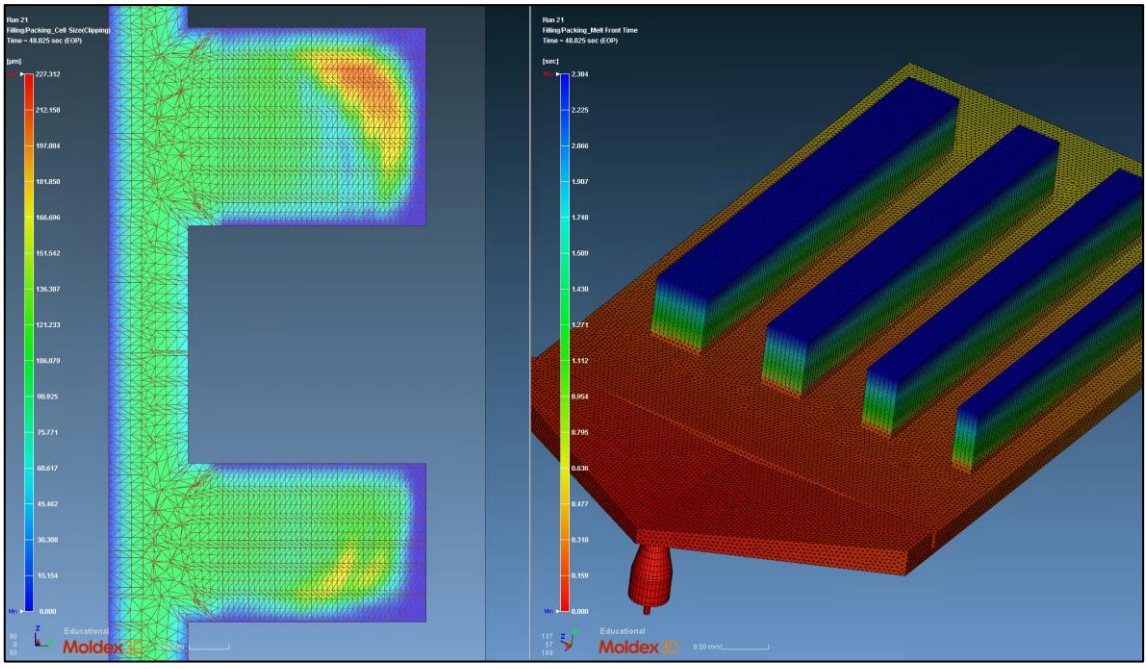

Figure 1 - Interface of the injection moulding simulation (Moldex3D)

Special Reticulate Session

Polyurethane based metal foams

P. Quadbeck [1], U. Jehring,[2] G. Pöhle[2], Alexander Füssel[3], Gisela Standke[3]

[1] Offenburg University of Applied Sciences, Badstraße 24, 77652 Offenburg, Germany
[2] Fraunhofer Institute for Manufacturing Technology and Advanced Materials (IFAM), Branch Lab Dresden, Winterbergstraße 28, 01277 Dresden, Germany
[3] Fraunhofer Institute for Ceramic Technologies and Systems IKTS, Winterbergstraße 28, 01277 Dresden, Germany

High porosity permeable materials have been manufactured on the basis of the highly uniform structure of foamed polyurethane since the early 1960s. The first steps in this direction were taken by the ceramic replication technique known as the "Schwartzwalder process". Such replication methods have been transferred to the production of open cell metal foams. For example, nickel foams based on electroplating processes have long been used on an industrial scale as current collectors in batteries. Similarly, roll-to-roll PVD processes are used to produce open cell foams of copper, nickel or iron, as well as various precious metals and refractory metals. Similarly, the CVD process is used to coat tantalum as a medical device, although here the focus is on the use of carbonized PU foams. Metal foams in alloyed form have also been created on the basis of such coating processes, for example by applying further layers or with particles that are subsequently alloyed by heat treatment.
Open-cell metal foams have also been produced by the replication method. Since the replication method is based on powder metallurgical technologies, foams made of a broad range of different materials may be fabricated, e. g. unalloyed or low alloyed steels, highly alloyed austenitic and ferritic steels, titanium alloys, or molybdenum. Finally, metal foams were produced by investment casting, which in principle have the same structures as the variants presented above, but have full web struts. Although all of these processes produce visually similar materials, the properties produced are sometimes very different. The paper compares the structures produced by the different processes and their properties, and shows some major application examples of these materials.

Structure, chemical and physical properties characterization

3D printing of hydrogel inks containing PHBV microparticles

E. Pacheco [1], M. Pérez-Recalde [1], B. Aráoz [1], and E. Hermida [1,*]

[1] Lab3Bio, ITECA, National University of San Martin, San Martin and CONICET, Buenos Aires, Argentina
* ehermida@unsam.edu.ar

3D printing has widely increased the development of cellular materials that emulate the extracellular matrix of different tissues [1]. Inks for 3D printing must fulfill certain biological and mechanical requirements: to be biocompatible and biodegradable, to have a shear-thinning behavior, to show at least 0,90 of printability, and to give scaffolds with similar mechanical properties to the tissue to be replaced. Furthermore, the addition of a drug delivery systems (DDS) to a scaffold is under development, seeking potential applications in pharmacology [2]. In this work, a sodium alginate-gelatin hydrogel with poly (hydroxybutyrate-co-hydroxyvalerate) (PHBV) microparticles was employed to produce 3D printed scaffolds.

The hydrogel was a blend made of 9% sodium alginate and 4.5% gelatin 4.5%; its liquid-like behavior led to a poor printability (Pr=0.81). This value could be improved to 0,94 by the addition 15 mM of $CaCl_2$. This ink, called Ink-Ca, was filled with PHBV spherical microparticles (MP) from 5 mg to 100 mg every 10 ml of ink. The MP were prepared by an emulsification/solvent technique [3]; their mean size, determined by microscopy, was 14±6 µm. Interestingly, the viscosity of the ink filled with MP decreased as the concentration increases: 1498, 1178 and 840 Pa.s for 0, 30 and 100 mg of MP/10 mL of ink.

Samples made of the Ink-Ca loaded with MP (5 mg, 15 mg, 30 mg, 50 mg and 100 mg) and crosslinked with $CaCl_2$ 0,5 M for 3 h at 25°C and overnight at 4°C showed an increase in the compression modulus from 400 kPa (without MP) to 550 kPa with 30 mg of MP. Higher concentrations of MP particles did not increase the compression modulus. Thus, 30 mg MP/10 mL enhances the compression modulus and higher concentrations could be suitable for drug delivery without loss in the mechanical behaviour.

When evaluated for 3D-printing, Ink-Ca/30 mg presented the same Pr (0,94) that the Ink-Ca. We manufactured scaffolds with infill 30% and 8 layers, by 3D printing, with the Ink-Ca and Ink-Ca/30 mg MP, to compare mechanical properties. These scaffolds were also crosslinked overnight with $CaCl_2$ 0,5M. In this case, again, the sample with MP increased the compression modulus (Ink-Ca 172±30 kPa, Ink-Ca/30 mg MP 270±30 kPa).

The results suggest that microparticles with alginate-gelatine hydrogel can be combined giving inks accurate for the application in 3D printing, and the microparticles produce changes in the microstructure both in ink form and in the scaffold form. 30 mg MP in this system is highlighted for DDS application for soft tissues.

References

[1] G, Savio; *Applied Bionics and Biomechanics*, **2018**, *vol. 2018*, https://doi.org/10.1155/2018/1654782.
[2] N, Pettinelli; *International Journal Of Biological Macromolecules*, **2016**, *vol. 146*, 110-118.
[3] Y, Farrag; *J Nanoparticle Research*, **2018**, *vol. 20-71,* https://doi.org/10.1007/s11051-018-4177-7.

Microstructural impact on the mechanical behavior of AlMg-Al_2O_3/SiO_2 syntactic foams under compressive loading

P. Kubelka[1*], N. Jost[1]

[1] Institute for Materials and Material Technologies (IWWT), Pforzheim University, Tiefenbronner Str. 65, D-75175 Pforzheim, Germany
*pierre.kubelka@hs-pforzheim.de

Metal matrix syntactic foams represent a highly relevant subject in the research field of closed-cell metal-ceramic composite foams. The composite nature of the material, with ceramic hollow spheres embedded within a metal matrix, represents a porous structure with superior strength in comparison to conventional metal foams, making them suitable for the use in a wide range of structural applications.

Al-based metal matrix syntactic foams are most commonly investigated, as they provide a high potential due to the combination of brittle ceramic hollow spheres with a ductile and low-density Al matrix. The possibility to change the compounds' interface and matrix properties by the presence of Mg in the matrix, enables an easy way to influence the foam's key aspects of porosity, microstructure and mechanical properties under compressive loading, starting at the production.[1]
Since past studies have solely investigated simple combinations of Al-based matrices and ceramic hollow spheres, there still is a huge research potential in studying the impact of different Mg contents in AlMg-based syntactic foams. Results from the microstructural characterization are compared with results of the compressive testings, in order to gain a holistic understanding of the influence of the Mg content on the interface and microstructure of AlMg-Al_2O_3/SiO_2 syntactic foams and their respective mechanical behavior under compressive loading. For this reason, syntactic foams, made of AlMg alloys with different Mg contents (min. 5 wt%) and two different kinds of oxide ceramic hollow spheres (Al_2O_3 and Al_2O_3/SiO_2), are produced, using a vacuum-pressure infiltration casting technique.[2] The modification of the Mg fraction positively influences the wetting behavior of the different ceramic spheres [3], resulting in a change of the metal-ceramic interfacial phase composition as well as the microstructure of the base matrix, investigated by light microscopy, scanning electron microscopy (SEM-EDS) and x-ray diffraction (XRD). The main reactions of SiO_2 with AlMg with higher Mg contents show the strongest impact on the microstructural change, by forming a diffusion zone on the interface with brittle oxides, silicides and ternary phases (Figure 1). In combination with the change of ductility and strength of higher Mg contents in the AlMg matrix, a strong dependence on the macroscopic deformation behavior can be detected.

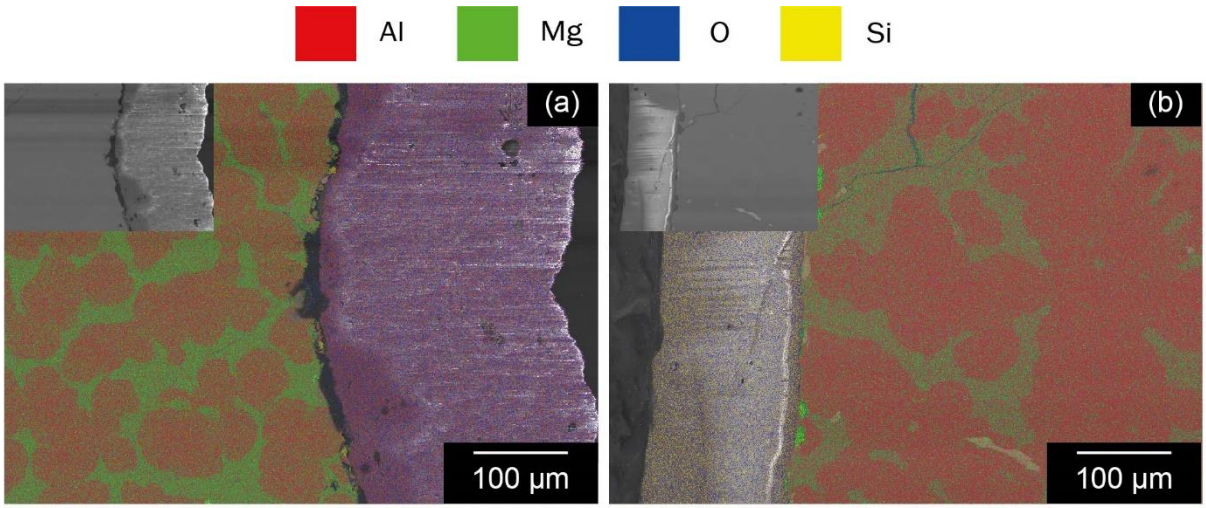

Figure 1. SEM-EDS mappings of Al, Mg, O and Si of AlMg syntactic foams with high Mg contents and two different ceramic hollow spheres: (a) alumina (Al_2O_3) hollow spheres and (b) kaolin (Al_2O_3/SiO_2) hollow spheres

References

[1] P. Kubelka, C. Wiener, N. Jost, *Materials Letters*, 2021, *287*, 129293
[2] P. Kubelka, A.M. Matz, N. Jost, *Proceedings of the 11th International Conference on Porous Metals and Metallic Foams (MetFoam 2019)*, 2020, 115-126
[3] A. Sangghaleh, M. Halali, *Applied Surface Science*, 2009, *255*, 8202-8206

Surface Modification of Nickel Foam by Iron-Powder Pack Treatment

A. Moloodi[1], A. Salehi[*1]

[1] Materials Research Group, Iranian Academic Center for Education, Culture and Research (ACECR), Khorasan Razavi, P.O. Box 91779-49367, Mashhad, Iran.
*am_salehi85@yahoo.com

In this study reticulated Ni foams were alloyed by iron-powder pack treatment, resulting in Ni–Fe foams. Nickel foams were embedded in a mixtures of iron, graphite, ammonium chloride and alumina powders and heated at 1050 °C for 8 h. Alumina added as an anti-sintering agent and ammonium chloride added as an activator in the powder mixtures. The volume ratio of iron, graphite, ammonium chloride and alumina powders was 7:3:1:9. Scanning electron microscopy (SEM) and energy dispersive spectrum (EDS) analysis were used to investigate the microstructures and the elemental composition of the Ni–Fe foams respectively.

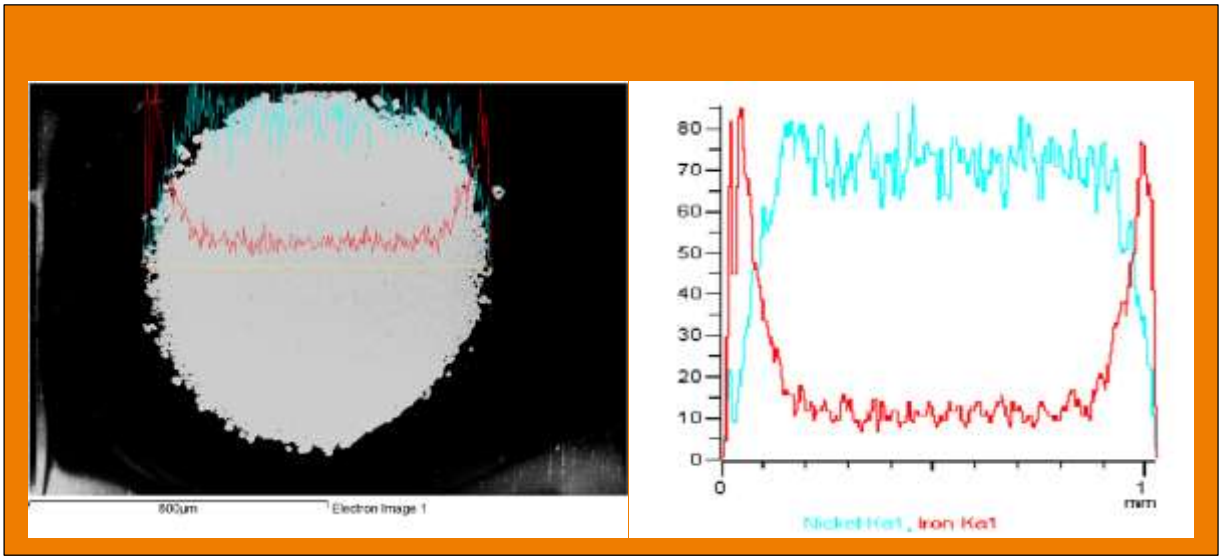

Figure 1. SEM and EDS analysis of Ni-Fe foams treated at 1050 °C/8 h.

In the present work, polyurethane sponge was used as the substrate. At first, polymeric foam was etched, then, samples were immersed in tin chloride and palladium chloride solutions in order to be sensitized and activated, respectively. Alternatively, an alkaline solution with hypophosphorous salt as reductant was employed to chemically plate the nickel. Mixtures of commercially available iron, graphite, ammonium chloride and alumina powders were put into an alumina crucible, and Ni foams were embedded in the mixtures.
Figure 1 shows the cross sections of the Ni–Fe foams. Pang et al [3] showed some boundaries between the Fe-rich layer and Ni-rich layer. While these boundaries are disappeared in the present work because of the long-time treatment (8 hours at 1050 °C), which indicates that the Fe–Ni interdiffusion process is happened during the pack treatment.

References

[1] Y Morizono, T Yamamuro, S Tsurekawa; Materials Transactions, 2020, 61, 2002-2007.
[2] A Salehi, A Moloodi, F Barzegar, Materials Science Forum, 2018, 933, 11-16
[3] Q. Pang, G.H. Wu, Z.Y. Xiu, G.Q. Chen, D.L. Sun; Materials Science and Engineering: A, 2012, 534, 699-706.
[4] M. Li, R. Jijie, A. Barras, P. Roussel, S. Szunerits, R. Boukherroub, Electrochimica Acta, 2019, 302, 1-9.

The effect of interfacial reaction on the peak strength in metal matrix syntactic foams

Cs. Kádár[1,2*], P. Kubelka[3], A. Szlancsik[1,2], N. Jost[3], I.N. Orbulov[1,2]

[1] Department of Materials Science and Engineering, Faculty of Mechanical Engineering, Budapest University of Technology and Economics, Műegyetem rkp. 3., H-1111 Budapest, Hungary,
[2] MTA–BME Lendület Composite Metal Foams Research Group, Műegyetem rkp 3., H-1111, Budapest, Hungary
[3]Institute for Materials and Material Technologies (IWWT), Pforzheim University, Tiefenbronner Strasse 65, D-75175 Pforzheim, Germany
*kadar@eik.bme.hu

Nowadays, one of the most important environmental and energy policy challenges is managing and mitigating climate change. The reduction of the greenhouse gas emissions caused by fossil fuels can be partly achieved by reducing the weight of cars and thus the amount of fuel used. Therefore, developing new materials with high specific strength is becoming increasingly important. Metal-matrix syntactic foams have the potential to use them in such applications.

This study investigated the peak strength (the first maximum or local maximum in stress right after the quasi-linear regime) of Mg and Al-based syntactic foams. We studied if the effect of the strength of the matrix material, the mechanical properties of the ceramic hollow spheres, and the effect of the interfacial can be separated. Commercially pure Al and commercially pure Mg were selected as matrix materials. Two kinds of ceramic hollow spheres (CHS) with different geometric properties and compositions were applied as filler materials for each matrix material. The small CHS had an average diameter of 1.45 mm and a wall thickness of 250 μm, containing 33 % Al_2O_3, 48 % amorphous SiO_2, and 19 % mullite. The large CHSs' diameter was 3.83 mm, and the CHSs' average wall thickness was 150 μm, containing 99.7% alumina. The peak strength value was found to be independent of the CHS type for the Al matrix, but for the Mg matrix, the different CHSs resulted in an increase of ~50% and ~100% in the peak strength. The difference in the peak strength was successfully modeled by the finite element method and explained as the results of the reaction of the Mg matrix and the CHS during manufacturing.

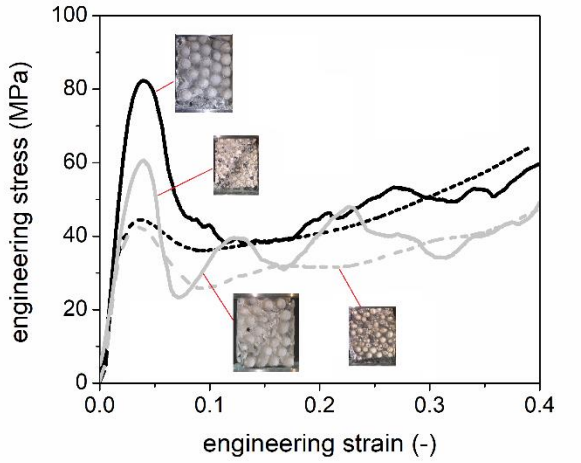

Figure 1. Typical stress-strain curves of the four different kinds of syntactic foams. The continuous and dashed lines belong to the Mg and Al matrix, respectively. The inserted photos show the surface of the foams at 15 % deformation.

Structure, chemical and physical properties characterization 1

Session Chairs

Dr.
Csilla Wiener
Budapest University of Technol...

Thermophysical properties of porous Ti_2AlC and Ti_3SiC_2 produced by powder metallurgy

S.A. Tsipas[1*], E. Tabares[1], T. Weissgaerber[2], T.Hutsch[2], F. Sket[3], B. Velasco[1]

[1]Departamento de Ciencia e Ingeniería de Materiales e Ingeniería Química, IAAB, Universidad Carlos III de Madrid, Avda. de la Universidad, 30, 28911 Leganés, Madrid, Spain,
[2]Fraunhofer Institute for Manufacturing Technology and Advanced Materials IFAM, Branch Lab Dresden, Winterbergstr. 28, D-01277 Dresden, Germany
[3]Institute IMDEA Materials, Calle Eric Kendel 2, Madrid 28906, Spain

*stsipas@ing.uc3m.es

MAX phase materials have caught the attention of researchers due to their unique combination of properties; their nanolaminated structure gives this family of materials the excellent attributes characteristic of both metal and ceramic compounds. MAX phase foams have a great potential for various applications where tailored functional and mechanical properties are required, such as high electrical and thermal conductivity, high elastic stiffness and low thermal expansion coefficient. In this study, Ti_2AlC and Ti_3SiC2 MAX phase foams with controlled porosity and pore size, where produced. The foams where produced from powders using crystalline carbohydrate as space holder. Consolidation was performed by cold isostatic pressing followed by complete dissolution of the water-leachable space-holder and pressureless vacuum sintering. The physicochemical properties of porous was studied in depth in order to access their suitability of applications such as catalytic devices on vehicles, heat exchangers or impact resistant structures. The study was performed on isostatic consolidated samples with different amount (20–60 vol%) and size of space holder (250–1000 μm) and in samples without space holder. Oxidation tests were performed at different temperatures for each material depending on their maximum service temperature. In order to understand the oxidation mechanism, oxidation kinetics were analysed to determine the influence of size and amount of porosity in each case. Electrical and thermal conductivity where studied at room temperature and at temperature up to 1000 °C. Gas permeability and the coefficient of thermal expiation was also measured for all foams produced. It is established that these porous MAX phases have suitable properties for their use as catalytic substrates, heat exchanges, high temperature filters or volumetric solar receivers.

A detailed study of the heat transfer mechanisms in micro-and nanocellular PMMA: modelling of the thermal conductivity

I. Sánchez-Calderón[1*], V. Bernardo[2], M.A. Rodríguez-Pérez[1]

[1] CellMat Laboratory. Campus Miguel Delibes. Faculty of Science. Condensed Matter Physics Department. University of Valladolid, Paseo de Belén 7, 47011, Valladolid, Spain.
[2] CellMat Technologies S.L., Paseo de Belén 9-A, 47011, Valladolid, Spain
*ismaelsc@fmc.uva.es

Cellular polymers are of great technological interest in sectors such as construction and automotive because of their low thermal conductivity, weight, and cost[1]. Nowadays, modern society needs specific materials for each application. Therefore, it is necessary to produce new and advanced materials as technology evolves. In this framework, a new generation of cellular polymers with enhanced properties was developed during the last decade: the so-called nanocellular polymers [1]. Nanocellular polymers are porous materials characterized by cell sizes below 1 micron. These materials have aroused great attention owing to their very interesting combination of properties. For instance, as a result of their nanometric cell size, these materials present a reduced thermal conductivity of the gas phase due to the Knudsen effect (**Figure 1**) [2–4].

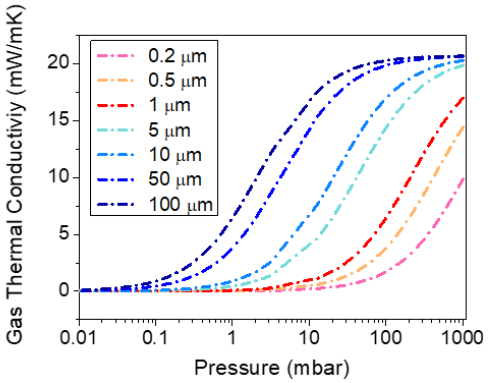

Figure 1. Gas thermal conductivity reduction due to the Knudsen effect.

There are plenty of theoretical works hypothesizing the thermal insulation performance of nanocellular polymers. However, there is a lack of experimental results, especially at low densities. Thus, in the present work, we aim to study the thermal conductivity of low-density micro-and nanocellular poly(methyl-methacrylate) (PMMA) to evaluate the heat transfer mechanisms acting on these structures. A collection of samples covering densities from 100 to 230 kg/m^3 and cell sizes of 400-4000 nm are prepared by gas dissolution foaming. The thermal conductivity is measured using a heat flow meter. The results are analyzed to understand the contribution of each transfer mechanism to the total thermal conductivity. The conclusions of this work allow identifying the real potential of nanocellular polymers and the next challenges to be accomplished to improve their performance.

References

[1] J. Martín-de León, V. Bernardo, M. Rodríguez-Pérez, Nanocellular Polymers: The Challenge of Creating Cells in the Nanoscale, Materials (Basel). 12 (2019) 797. https://doi.org/10.3390/ma12050797.
[2] Z.-Y. Li, C.-Y. Zhu, X.-P. Zhao, A theoretical and numerical study on the gas-contributed thermal conductivity in aerogel, Int. J. Heat Mass Transf. 108 (2017) 1982–1990. https://doi.org/10.1016/j.ijheatmasstransfer.2017.01.051.
[3] B. Notario, J. Pinto, M.A. Rodriguez-Perez, Nanoporous polymeric materials: A new class of materials with enhanced properties, Prog. Mater. Sci. 78–79 (2016) 93–139. https://doi.org/10.1016/j.pmatsci.2016.02.002.
[4] B. Notario, J. Pinto, E. Solorzano, J.A. de Saja, M. Dumon, M.A. Rodríguez-Pérez, Experimental validation of the Knudsen effect in nanocellular polymeric foams, Polymer (Guildf). 56 (2015) 57–67. https://doi.org/10.1016/j.polymer.2014.10.006.

Adaptation of the pore morphology of freeze-cast SiOC screens for gas-liquid phase separation

Pedro Henrique da Rosa Braun[1*], Kurosch Rezwan[1, 2], Michaela Wilhelm[1]

[1] University of Bremen, Advanced Ceramics, Am Biologischen Garten 2, IW3, Germany, [2] MAPEX—Center for Materials and Processes, University of Bremen, Am Fallturm 1, Bremen, Germany

*pedrohe1@uni-bremen.de

A macroporous SiOC pore structure for phase-separation requires balanced mechanical and mass transport properties that can be created via unidirectional solution-based freeze-casting of preceramic polymer. In this work, cyclohexane (CH) and tert-butyl alcohol (TBA) or a mixture of both were used as a template media in freeze-casting to achieve a permeable pore morphology with high mechanical stability. The results show that using only CH or TBA produces dendritic or prismatic pore structures, respectively, while a mixture of these solvents creates honeycomb-like pore structures. Variations in the amount of TBA led to pore window sizes between 11-57 µm and consequently water permeabilities from 4.4×10^{-13} to 1.4×10^{-11} m². The dendritic pore structure has the highest compressive strength (39 MPa) due to its smallest pore sizes (16-20 µm) and secondary dendrites, and was selected to

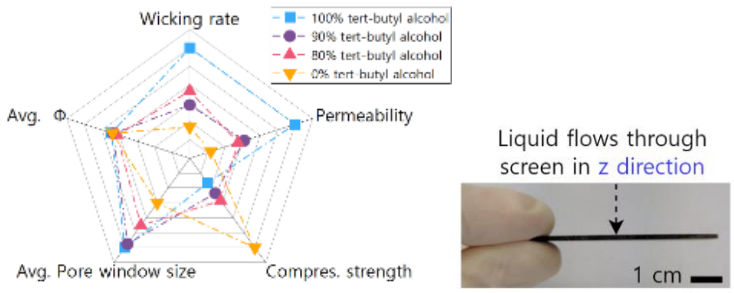

Figure 1. Radar plot (left) indicating the properties from the pore structure and its correlation with the mass transport and mechanical properties for different weight amount of TBA used in the initial mixture of solvents. SiOC screen (right) used for gas-liquid phase separation

produce crack-free porous screens for air-hydrofluoroether phase separation. The pore window size of the screens varied between 6-35 µm depending on the freezing temperature (-20, -80 or -120°C). The calculated bubble point diameter varied between 17 and 42 µm and is consistent with the largest pore window size of each screen, indicating the absence of cracks in the screen and its suitability for gas-liquid phase separation.

Aluminium-Foam-Sandwiches – Correlation between foam structure and mechanical performance

Tillmann Robert Neu*[1,2], Korbinian Heim[3], Hans-Wolfgang Seeliger[3], Paul Hans Kamm[1,2], Nadine von der Eltz[1], John Banhart[1,2], Francisco García-Moreno[1,2]
1 Technische Universität Berlin, Hardenbergstr. 36, 10623 Berlin, Germany
2 Helmholtz-Zentrum Berlin für Materialien und Energie, Hahn-Meitner-Platz 1, 14109 Berlin, Germany
3 pohltec metalfoam GmbH, Robert-Bosch-Str. 6, 50769 Köln
*t.neu@tu-berlin.de

Aluminium foam sandwich panels composed of an AlSi8Mg4 foam core and 6082 alloy sheets ('AFS') are available now in sizes up to a few square metres. A problem in production is how to cope with non-uniformities of the foam structure. Non-destructive quality control methods are desired for possible large-scale application such as in the automotive industry and for safety-relevant parts. We have investigated large industrial AFS panels and used X-ray radiography as a method to identify weak spots in the foam core. For this purpose, we use the false colour representation of the standard deviation or the logarithm of the intensity values of the X-ray images as shown in Figure 1 in order to identify possible defects.

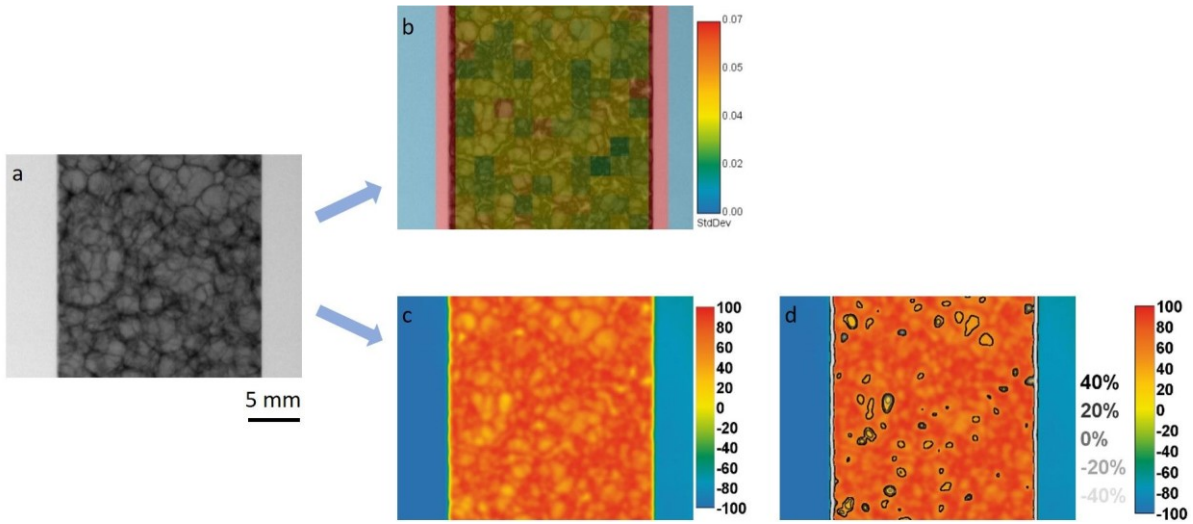

Figure 1. a) X-ray radiography b) colour overlay on the radiography based on the standard deviation of the logarithmic grey values in a 50 × 50 pixel grid c) False colour image of the X-ray image after logarithmisation of the grey values and d) image from c with additional contour lines.

For samples in which defects have been identified, the correlation with failure in tensile and bending tests has been investigated. The properties of a large number of samples tested in compression, tension and bending have been determined and presented in property tables. Furthermore, the protective effect of the AFS has been tested in impact and crash scenarios. We conclude that with X-ray radiography we can identify flawed and potentially weak. In 50% of all tensile test samples, no such defects are discovered and the foams appear uniform. In the other cases defects occur. Of these about 50 % give rise to a predictable localised failure, in the other cases not.

Cellular materials offer a wide spectrum of applications such as catalyst support structures, lightweight materials, energy adsorption or energy storage materials. Due to several ways of processing and different materials, a wide range of material properties e.g. thermal conductivity, mechanical strength or damping can be adjusted, measured and verified, with regard to the expected properties. Especially in heterogeneous and homogeneous porous structures and their composites, only global effective material properties can be determined and measured. For example, the knowledge on the predominating influence of the microstructure on the global properties is the key for designing materials with desired properties. To fill this gap and enable a "look-in" a microstructure model derived from µ-CT measurements (see highlights in Figure 1) carried out at certain processing steps can be used as model for FEM-calculations. In this context, the representative volume of interest (REVOI) in particular plays a decisive role in order to be able to determine the global and not only local characteristics. By combining Minkowski and structural parameters, the REVOI can be determined as a function of the cellular structure.

Combining estimated material properties by experiment with microstructure models offers the possibility to carry out different simulations over different hierarchical levels in order to design the structures for future applications of porous ceramics.

a) b)

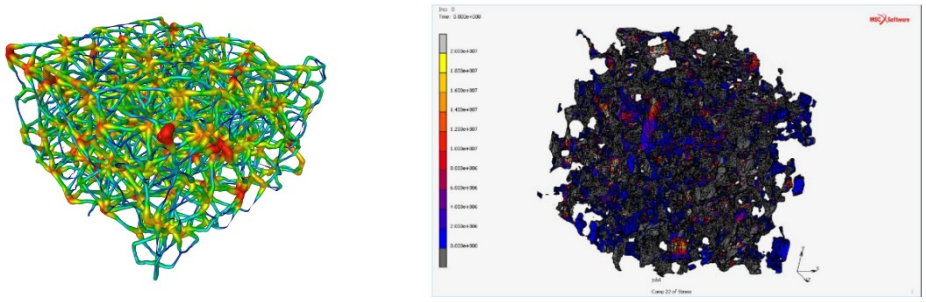

Figure 1: a) Pore network of a 30ppi replica foam, b) FEM-Simulation of stress distribution in a MAX-Phase gel casted foam

Latest references:

Biggemann, J., Pezoldt, M., Stumpf, M., Greil, P., Fey, T. **Modular ceramic scaffolds for individual implants**, Acta Biomaterialia 80 (2018) 390–400

Fey, T., Stumpf, M., Chmielarz, A., Colombo, P., Greil, P., Potoczek, M. **Microstructure, thermal conductivity and simulation of elastic modulus of MAX-phase (Ti_2AlC) gel-cast foams** , Journal of European Ceramic Society 38 (10) (2018) 3424-3432

Stumpf, M., Travitzky, N., Greil, P., Fey, T. **Sol-gel infiltration of complex cellular indirect 3D printed alumina**, Journal of the European Ceramic Society 38 (2018) 3603–3609

Fey, T., Betke, U., Rannabauer, S. and Scheffler, M., **Reticulated Replica Ceramic Foams: Processing, Functionalization, and Characterization**, Adv. Eng. Mater., 2017, 19(10), 1700369

Correlation between microstructural and macroscopic mechanical properties of polyurethane foams

A. Greß (Speaker)[1]*; L. Griem[2]; P. Altschuh[3]; T. Feser[1]; E. Beeh[1]; B. Nestler[3]; T. Siefkes[1]
[1]German Aerospace Center - Institute of Vehicle Concepts, Stuttgart; [2]Karlsruhe Institute of Technology -Institute of Applied Materials, Karlsruhe; [3]University of Applied Sciences Karlsruhe - Institute of Digital Materials Science; *alexander.gress@dlr.de

Mechanical properties of structural foams are largely influenced by the manufacturing process. Depending on the manufacturing process, the foam type (e.g. open-pored/closed-pored), its density and its orientation are defined. These quantities, however, only define the global structural properties. Due to the inhomogeneous process, no adequate statement can yet be made about the real microstructure. Nevertheless, if a mechanical load is applied to a foam, the generated inhomogeneous stress field depends on its actual microstructure, which is characterized by specific values such as pore distribution, mean pore size, spatial gradients in the pore size distribution, pore arrangement and geometry of cell walls. Irregularities in these microstructural descriptors caused by the foaming process can lead to local differences in mechanical properties.

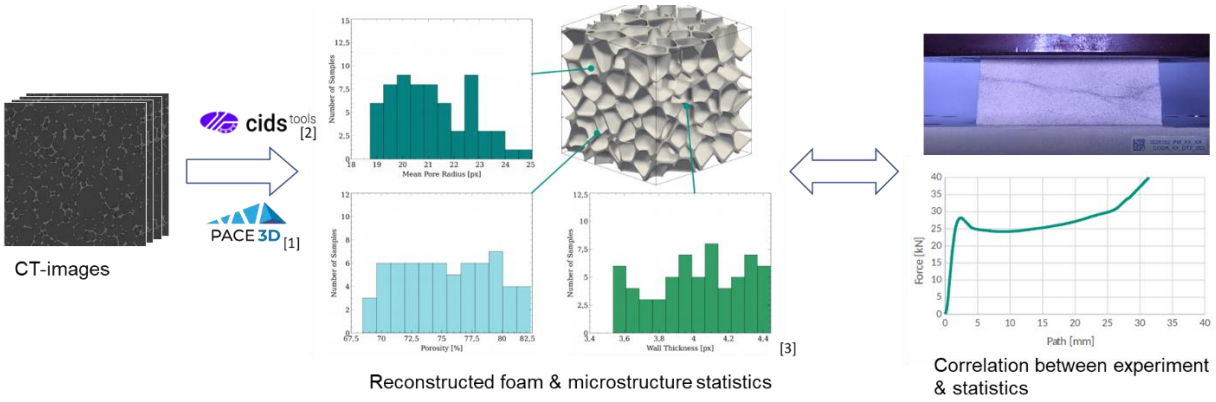

Figure 1. Schematic approach for connecting the microstructure with the mechanical properties

The objective of the current research is linking the above-mentioned microstructural properties and the resulting macroscopic mechanical material behaviour of structural foams by using artificial intelligence (AI) based digital methods. For this purpose, polyurethane (PU)-foams of varying densities are analysed to create a suitable database. For each of the investigated foam densities, the dependency of the microstructure and the mechanical properties according to the sampling position are investigated. First, the mechanical properties of tension and compression load are experimentally determined in parallel and perpendicular spatial direction as well as for varying positions along the foaming directions. The microstructure properties of the real PU-foams are determined using computer tomography scans. Afterwards, the microstructures are reconstructed using computer algorithms incorporated in the phasefield simulation framework Pace3D in order to generate digital twins. Applying various data science methods and micromechanics simulations, the morphological characteristics and the mechanical properties of the digital microstructures are determined. The results from experiments and computational methods are compared and correlations between the mechanical tests and the microstructure analyses are derived. In forthcoming research, this correlation of microstructure and mechanical behaviour will be explained and predicted using AI-based methods.

References

[1] J. Hötzer, et al., 2018
[2] A. Koeppe, F. Bamer and B. Markert, 2019
[3] L. Griem et al., Identifying structure-property linkages in polyurethane foams to characterize their mechanical properties using machine learning, MSE Conference, 2022

ERROR
Determination of In-situ Experimental Mechanical Properties of Injection Molded Thermoplastic Foam Structures

https://externalpublic.ams3.cdn.digitaloceanspaces.com/13/c0cc282c-62f6-42e1-9979-652fd358f893/KÃžbra-GÃžzel_Abstract_CellMAT2022_submitted.pdf
https://dgm.inventum.de/eventItems/75357583-ee7e-4cdf-9e41-9dd7aaf0bfd3

High density aluminium foams

N. Babcsan[1]*; R. Bozzo[2]; M. DeAngelis[2]; J. Babcsan Kiss[1]

[1]Innobay Hungary Ltd., Miskolc (Hungary), [2]Cymat Technologies Ltd., Mississauga (Canada)

*norbert.babcsan@gmail.com

Aluminium foams have the most productive technology and versatile properties among the metal foams. At the Canadian Cymat company we developed Smart Metal HD aluminium foams which maximum density of 1.3 g/cm3 is in the aluminium *matrix syntactic foam* value range. This is the upper limit of the cellular aluminium where the material compression strength still remains constant up to even 40% strain. With this high density the aluminium foam compression strength increased to a level which was not achievable until know. Mechanical and microstructural studies of high density aluminium foams between 0.4 and 1.3 g/cm3 will be shown in which range the aluminium foam became castable without destroying the cellular structure.

Improvement of the cell structure of water foamed LSR

S. Marl[1*], K. Klier[1], A. Rüppel[1], M. Hartung[1], R.-U. Giesen[1], H.-P. Heim[1]

[1] University of Kassel, Institut für Werkstofftechnik, Kunststofftechnik
*Svenja.marl@uni-kassel.de

Liquid silicone rubber (LSR) has good chemical and physical properties, in particular, it is biocompatible and weatherproof and it can be used between -50 °C and 200 °C. It is used in the automotive sector, for households, babycare and medical devices. However, it is more expensive than other elastomers. For this reason, the density should be reduced to get lower the price of parts. By producing LSR foams, the density can be reduced to below 1 g/cm³. [1] Besides, the haptics of the components and the thermal insulation properties are improved.
LSR is processed by liquid injection molding (LIM). Due to this processing method, the blowing agent has to expand inside the hot mold (150 °C up to 200 °C) to create the foam structure. A possible blowing agent is water, which can be mixed in the uncured LSR before the injection molding process. [1] The cell structure with water as a blowing agent is very inhomogeneous because there are unfoamed areas and foamed areas. This structure can be influenced by the mold temperature and it can be improved by adding an additive to the water.

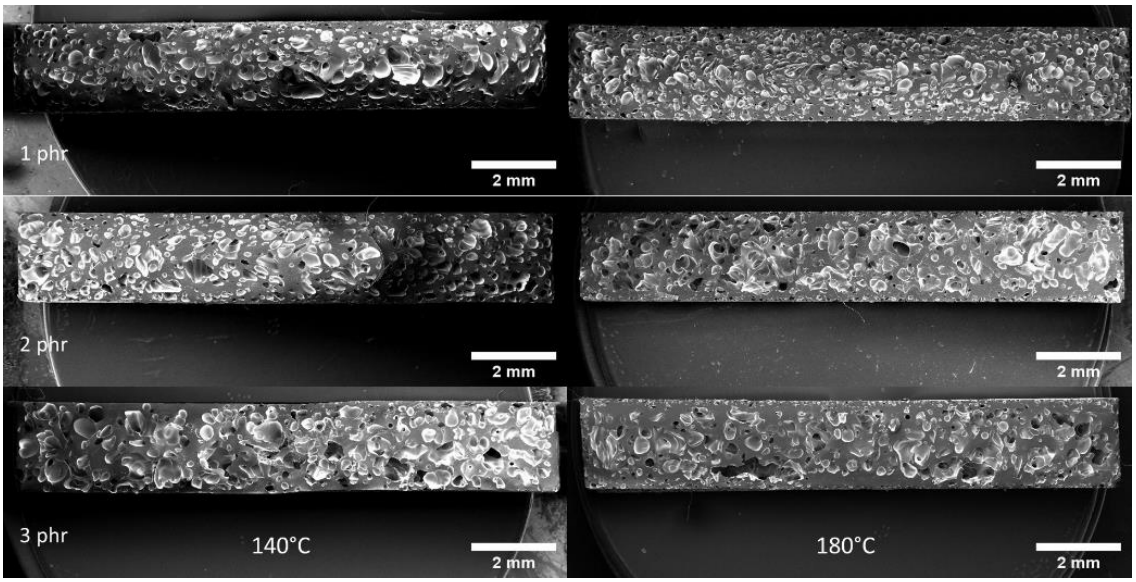

Figure 1. SEM images of the foam structure for different proportions of blowing agent (top: 1 phr, center: 2 phr, bottom: 3 phr) as a function of mold temperature (left: 140 °C, right: 180 °C)

References

[1] S. Marl; A. Rüppel; M. Hartung; K. Klier; R.-U. Giesen; H.-P. Heim *Advanced Engineering Materials* **2021**, 1–20.

Polyurethane aerogels: lightweight, transparency and super-insulation in one material

B. Merillas[1*], J. Martín-de-León[1], F. Villafañe[2], M. A. Rodríguez-Pérez[1,3]

[1] Cellular Materials Laboratory (CellMat), Condensed Matter Physics Department, Faculty of Science, University of Valladolid, Campus Miguel Delibes, Paseo de Belén 7, 47011 Valladolid, Spain,
[2] GIR MIOMeT-IU Cinquima-Química Inorgánica. Faculty of Science, University of Valladolid, Campus Miguel Delibes, Paseo de Belén 7, 47011 Valladolid, Spain
[3] BioEcoUVA Research Institute on Bioeconomy, University of Valladolid, Spain
*b.merillas@fmc.uva.es

Nowadays, aerogels are becoming one of the most promising materials owing to their combination of exceptional properties. Their low densities, huge surface areas, low speed of sound and insulation performance make them suitable for a wide range of applications in several sectors [1],[2]. Nevertheless, most research is focused on silica aerogels, having a relevant drawback: their brittleness and lack of stiffness. Therefore, aerogels composed by other matrixes are being actively searched for.
In this work, organic aerogels based on polyisocyanurate-polyurethane have been synthesized and characterized in detail [3]. These aerogels showed tailorable structures and, thus, properties through changes in the catalyst concentration. By the study of the structure-properties relationship, the influence of the different structural parameters (particles and pores) on the different properties was assessed. The obtention of polyurethane aerogels showing transparency for the very first time, while presenting tunable mechanical properties and superinsulation was achieved (see Figure 1). Thermal conductivity values as low as 12 mW/mK for densities around 160 kg/m^3 were reached, much lower than the conventional thermal insulators, opening a broad spectrum of potential applications in the building sector such as glazing windows, automotive and aeronautical sectors, or even for energy management.

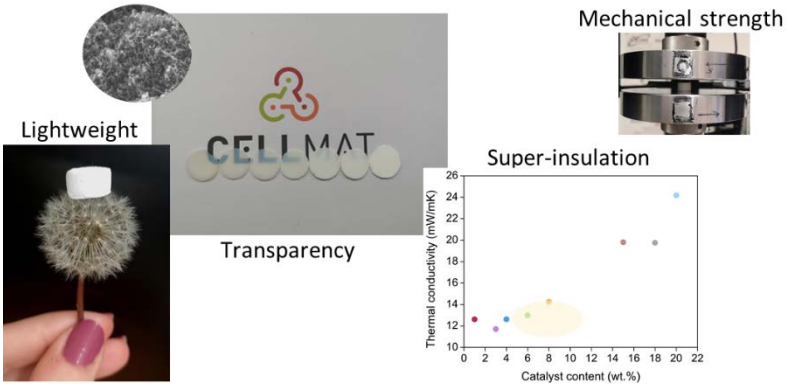

Figure 1. Main properties of the polyurethane aerogels under study.

References

[1] Aegerter, M.A. Leventis, N. Koebel M. Aerogels Handbook., Springer US, **2011**. 79–101.
[2] Smirnova I, Gurikov P., J Supercrit Fluids, **2018**, 134, 228–33.
[3] Merillas B, Martín-de León J, Villafañe F, Rodríguez-Pérez MA., ACS Appl Polym Mater., **2021**, 3(9), 4607–4615.

Predicting formation of deformation band via path search in porous metals with unidirectional pores

M. Sawada[1*], S. Suzuki[1]

[1] Waseda University
*m.sawada@toki.waseda.jp

During compression of porous metals, compressive stress remains constant even though compressive strain increases. However, stress shows a sudden increase/decrease when there is a significantly large local deformation such as deformation bands. A deformation band is a series of locally deformed cell walls. It is reported that a dense joint region of cell walls can prevent the bands to expand.[1] Yet, prediction of the specific location of the bands in a specimen is needed to further prevent the formation of deformation bands. Calculating the stress concentration factor for each cell wall is one of the ways to estimate the relative amount of local deformation. The exact location of deformation bands could possibly be predicted by performing a path search on a strain map. Thus, the objective of this research was to predict locally deformed cell walls and deformation bands from the initial geometry.

Porous metals with penetrating unidirectional pores were employed for the specimen since *in situ* observation of all cell walls is possible with them. Two cubic specimens with different edge lengths of 25 and 39 mm were prepared which will be referred to as L25 and L39. Pores were randomly distributed with maintaining a porosity of approximately 35 pct. The compressive behavior of the specimens was numerically analyzed with finite element code Abaqus/Standard, Explicit 2018. The material properties in the analysis were mainly obtained from the experimental compression test of a non-porous A6061 aluminum alloy that was annealed at 415 °C for 2.5 h which was performed in our previous study.[2]

In order to estimate the amount of local deformation, the stress concentration factor of each cell wall was calculated in accordance with the research by Howland and Isida.[3,4] In addition, the factor was calibrated to flatten the horizontal distribution of the factor. The cell walls that have a relatively large factor were mostly corresponding to the cell walls with large local deformation at the compressive strain e = 1.0 pct. Then, a path search was performed on a map of equivalent plastic strain $\overline{\varepsilon_p}$ at e = 1.0 pct. All paths that connect vertical edges of the specimen were evaluated to find the path that has the maximum mean of $\overline{\varepsilon_p}$ in a path. Fig.1 (*a*) shows the $\overline{\varepsilon_p}$ mean in a path of all candidate paths. The Rank 1 path which is shown as the red band in the Fig. 1 (*b*) corresponded to the actual formation of the macroscopic deformation band at e = 12.0 pct for L25. There was no obvious deformation band in L39 so that Rank 1 path was not corresponding to anything in that specimen. This difference is considered to be caused by the difference in distribution of the $\overline{\varepsilon_p}$ mean; deviation in L25 is significantly larger than that in L39 which presumably enlarged deformation selectiveness in the specimen.

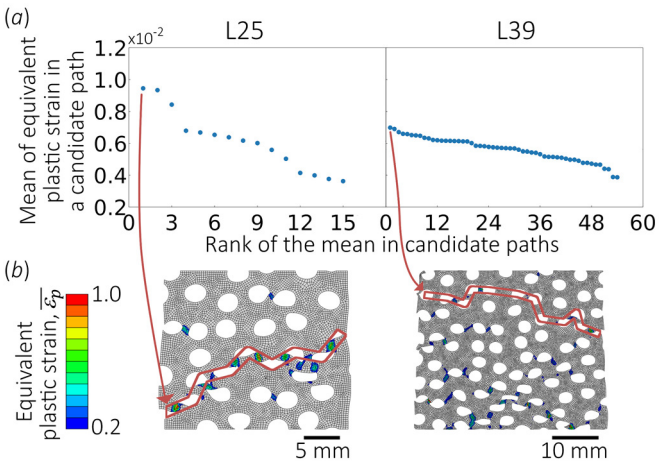

Figure 1. Results of path search on a map of equivalent plastic strain $\overline{\varepsilon_p}$. (*a*) Distribution of $\overline{\varepsilon_p}$ mean in a path for all candidate paths, (*b*) Correspondence between the path with the largest $\overline{\varepsilon_p}$ mean (=Rank 1 path) and local strain concentrations at the compressive strain e = 12.0 pct.

References

[1] Z. Fan et al.; *Scr. Mater.*, 2018, vol. 142, pp. 32–5.
[2] M. Sawada et al.; *Mater. Trans.*, 2020, vol. 61, pp. 1782–9.
[3] R.C.J. Howland; *Proc. R. Soc. London. Ser. A - Math. Phys. Sci.*, 1935, vol. 148, pp. 471–91.
[4] M. Isida; *Trans. Japan Soc. Mech. Eng.*, 1959, vol. 25, pp. 1118–24.

The mechanical properties of titanium-based foams

Cs. Kádár[1*],P. Jenei[2], S.M. Hung[3], C.J. Kuo[3], R. Gorejová[4], R. Oriňaková[4], H. Choe[5], J. Gubicza[2]

[1] Department of Materials Science and Engineering, Faculty of Mechanical Engineering, Budapest University of Technology and Economics, Műegyetem rkp. 3., H-1111 Budapest, Hungary
[2]Department of Materials Physics, Eötvös Loránd University, Budapest, P.O.B. 32, H-1518, Hungary
[3]CellMobility Inc., 11F, Sec.4, Nanjin E. Rd., Taipei, China
[4] Department of Physical Chemistry, Institute of Chemistry, Faculty of Science, Pavol Jozef Šafárik University in Košice, Moyzesova 11, 041 54, Košice, Slovak republic
[5]School of Materials Science and Engineering, Kookmin University, 77 Jeongneung-ro, Seongbuk-gu, Seoul, 02707, Republic of Korea
*wiener.csilla@gpk.bme.hu

Titanium-based metal foams have gained a lot of attention recently, due to their high strength, biocompatibility, and high corrosion resistance, making them promising candidates for clinical use, such as orthopedic scaffolds. Titanium foams also have the potential to use them as structural materials e.g. in the aerospace industry, since the high relative strength is coupled with the mechanical stability at high temperatures.

In this study, the compressive properties and failure modes of freeze-casted titanium foams with different densities at various strain rates were investigated. We recorded the acoustic emission response and the surface deformation during compression and found no changes in deformation mechanisms in the investigated strain rate interval (from 0.001 s^{-1} to 0.5 s^{-1}). The relationship between the relative density and the stiffness modulus can usually be described for metal foams as a power-law relationship, where the exponent is 1 and 2 depending on the governing deformation mode. For our foams this exponent 4.6 that could not be explained by the existing models. Similarly, the power law exponent for the strength – relative density function according to the compression and Gibson-Ashby models is 1 and 1.5, respectively; however, we measured 5. To explain our measured high exponent, we propose the high power exponent to be the consequence of the changes in the deformation mechanism; for low relative density it deforms by the bending of the cell edges or struts, while for higher relative densities the compressive model should be applied.

Thermal conductivity reduction in nanocellular PMMA by addition of graphite nanoplatelets as IR blocker

A. Sillero-Navajas[1*], J. Martín-de-León[1], M.A. Rodríguez-Pérez[1]

[1] Cellular Materials Laboratory (CellMat), Condensed Matter Physics Department, University of Valladolid, Campus Miguel Delibes, Paseo de Belén n°7, 47011 Valladolid, Spain

*angel.silnav@gmail.com

Nowadays, cellular polymers find extensive use in a wide variety of applications owing to their versatility and desirable properties. Among these is the heat insulation sector, with an ever-growing demand for enhanced materials that meet the current energy efficiency needs. In recent years, nanocellular polymers, which are defined as cellular polymers with cell sizes below the micron, have become a topic of great interest in the pursuit of materials with the ability to reach lower thermal conductivities. This leap to the nanometric scale leads to the confinement of the gaseous phase into the tiny cells. As the mean free path of air molecules becomes comparable to the cell size, they are more likely to collide with cell walls than with one another, resulting in a reduction of the gaseous thermal conductivity. This phenomenon is known as the Knudsen effect.[1,2]

However, on top of the challenges involved in producing these advanced materials, the remarkable reduction in thermal conductivity originally expected for nanocellular polymers has proven difficult to achieve in practice. Even though thermal radiation can be neglected for microcellular materials, this mechanism starts to play an important role in heat transfer once the cell size is reduced, which could counteract Knudsen effect. For this reason, new research about this subject should also explore ways to limit the radiation contribution, such as with the use of additives or filler particles as infrared (IR) blocker.[3,4]

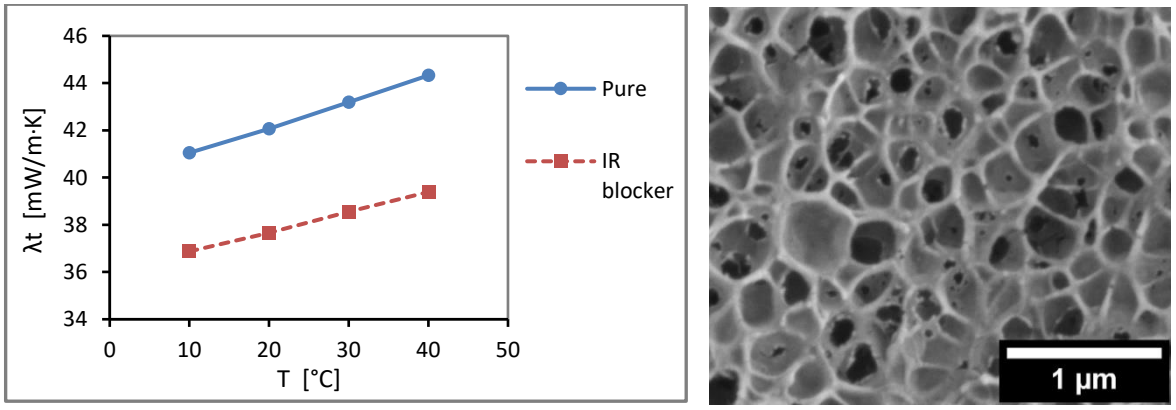

Figure 1. Experimental thermal conductivity of two cellular PMMA with similar cellular structure with and without infrared blockers (left) and scanning electron microscopy micrograph of nanocellular PMMA with infrared blockers (right).

In the present work, micro- and nanocellular composites based on poly(methylmethacrylate) (PMMA) and graphite nanoplatelets (GNP) have been produced for the first time by means of the gas dissolution foaming method, with CO_2 as a physical blowing agent (Figure 1 right). Materials containing three distinct types of GNP have been characterized, and the influence of these fillers on the resulting cellular structure and thermal conductivity has been studied. These results confirm the IR-blocking behavior of GNP in nanocellular polymers (Figure 1 left), and show the potential of the proposed approach for further reducing the thermal conductivity of this new family of insulating materials.

References

[1] S. Costeux. *J. Appl. Polym. Sci.*, **2014**, *131*(23), 41293.
[2] B. Notario et al. *Polymer*, **2015**, *56*, 57–67.
[3] M. Arduini et al. *Cellular Polymers*, **2016**, *35*(2), 49–66.
[4] V. Bernardo et al. *Colloids and Surfaces A*, **2020**, *600*, 124937.

Sustainability and recycling 1

Session Chairs

Dr.-Ing.
Tobias Fey
Friedrich-Alexander-Universität ...

INITIAL AND AGED THERMAL CONDUCTIVITY OF POLYISOCYANURATE (PIR) FOAMS WITH DIFFERENT HFO CONTENTS

Patricia Torres-Regalado[1,2*] (P.Torres) and Miguel. A. Rodríguez-Pérez[2](M.A.Rodríguez)

[1] CellMat Technologies S.L., Paseo de Belen 9A, 47011 Valladolid, Spain,[2] CellMat Laboratory, University of Valladolid, Valladolid, Spain.
*p.torres@fmc.uva.es; marrod@fmc.uva.es

Nowadays, rigid foams based on polyurethane (RPU) are a fundamental part of our lives, since they are used as thermal insulating materials in many fields such as for instance construction, refrigeration, and piping/tubing industries. These foams with a closed cellular structure are one of the most popular foam insulators mainly due to the combination of high insulating capability and excellent mechanical properties. Inside the group of RPU foams is included polyisocyanurate (PIR) foams which are produced using raw materials and formulations similar to those of RPU foams, except that the isocyanate index is higher, and the polyol used is based on polyester instead of polyether [1], [2]. PIR foams are typically considered an improved solution in comparison with traditional RPU, due to their lower thermal conductivity, improved flame retardancy and higher temperatures of use [3], [4].

Hydrofluorolefins (HFOs) are a new class of more environmentally friendly refrigerants displaying a zero Ozone Depletion Potential (ODP), low Global Warming Potential (GWP) and low flammability. They are a greener alternative to the previous generations of traditional blowing agents, including chlorofluorocarbons (CFCs), hydrochlorofluorocarbons (HCFCs) and hydrofluorocarbons (HFCs). These blowing agents are unsaturated organic compounds that comprise hydrogen, fluorine, and carbon. Unlike traditional blowing agents, which are saturated, HFOs are olefins, also known as alkenes [5].

In this work we present a study of polyisocyanurate (PIR) foams synthesized with the HFO 1233zd(E) (LBA). The effect of LBA content on the density, cellular structure, mechanical properties and thermal conductivity upon aging of polyisocyanurate foams has been evaluated. The obtained results showed that the foams produced with higher LBA content have lower density. In addition, all foams have similar cell sizes (around 900 microns) and the use of LBA as blowing agent induced the generation of foams with a very homogeneous cellular structure.

The initial thermal conductivity and the aged thermal conductivity has been studied using an accelerated laboratory test method that allows predicting the thermal conductivity up to 25 years by measuring for 90 days. The initial values of the thermal conductivity were very low, in the range of 20 to 22 mW/mK. These values increase to reach values in the range 30 to 32 mW/mK after the aging process. (figure 1). The rate of aging has been correlated with the content of HFO used to produce the foam and with the temperature reached during foaming. A higher amount of HFO allows producing foams with a slower aging of the thermal conductivity.

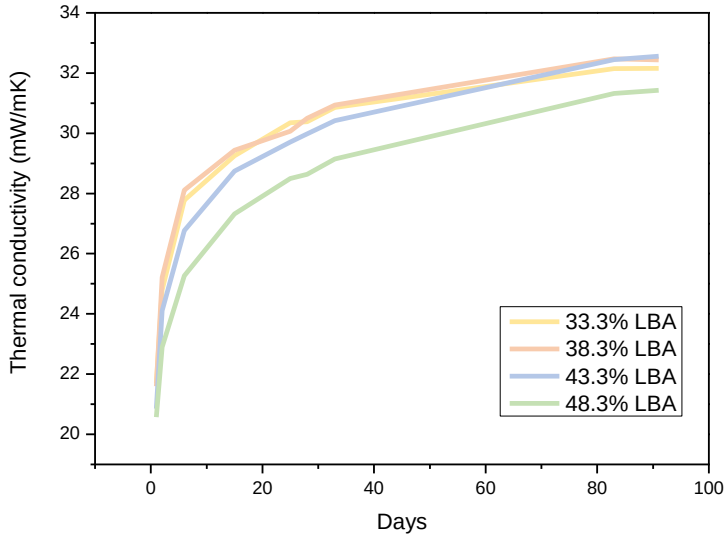

Figure 1. Thermal conductivity evolution between day 0 and day 90 of PIR foams produced uisng different contents of HFO.

As a final conclusion, it can be said that LBA is a good alternative to replace traditional foaming agents, due to the strong improvement achieved for the aged thermal conductivity values when it is used for the production of PIR foams. The results obtained in this work shows how using HFO in combination with PIR systems opens the possibility of producing more efficient and environmentally sustainable foams.

References

[1] R. Heath, Isocyanate-Based Polymers: Polyisocyanurates and their Copolymers, **2017**, page 799-835.
[2] E. Sharmin and F. Zafar, Polyurethane: An Introduction, **2012**, page 3–16.
[3] M. Kurańska, A. Prociak, S. Michałowski, and K. Zawadzińska, The influence of blowing agents type on foaming process and properties of rigid polyurethane foams, **2018**, page 672–678.
[4] M. Jelena and B. Umberto, Microstructure and blowing agent concentration analysis in accelerated aged polyurethane & polyisocyanurate insulation, **2019**, vol. 609, no. 6.
[5] R. S. Grossman, Auto Seating Lightweighting Using Solstice® Liquid Blowing Agent (HFO 1233zd(E)), **2016**, vol. 9, no. 3.

Studying the stabilization mechanisms in non-crosslinked natural rubber latex foams

C. Amezúa[1*], L.O. Salmazo[1], A. López[1], M.A. Rodríguez[1]

[1] Cellular Materials Laboratory (CellMat), Condensed Matter Physics Department, Faculty of Science, University of Valladolid, Campus Miguel Delibes, Paseo de Belén 7, 47011 Valladolid, Spain
*clara.amezua@fmc.uva.es

Natural rubber latex foams (NRLFs) are flexible foams that are used in comfort products such as mattresses and pillows [1]. The chemistry participating in the synthesis of NRLFs needs the use of vulcanizing agents, such as sulfur, to cross-link the polymeric matrix, and thus, promote the stability of the solid fase of the foams [2]. Therefore, in spite of the bioderived character of natural latex, the final foam is not easily degradable. Nowadays, the industrial and academic interest on looking for more sustainable and environmentally friendly substitutions to cross-linked materials encourages the development of new synthesis routes for these foams.

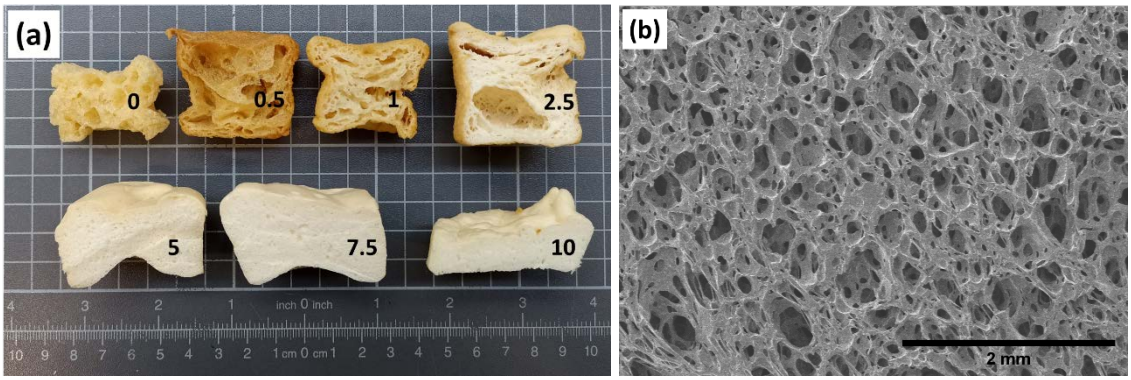

Figure 1. (a) Macroscopic structure of the egg white powder series of foams changing the amount of protein from 0 to 10 phr and (b) SEM micrograph of a latex foam stabilized with egg white powder and corn starch.

In this work, we develop non-crosslinked NRLFs using egg white powder and corn starch as stabilizer additives The foams are produced by a two-stage foaming process in which the liquid blend natural latex-stabilizer additive is firstly aerated with a whipping machine and secondly dehydrated via microwave radiation, which is able to promote rapid heating and water evaporation and save more energy than the conventional heating methods [3]. The density and the main structural parameters of both the liquid and solid foams are studied to understand the effects of the protein and starch in the stabilization mechanisms involved in the synthesis of these foams.
The two-stage foaming process and the presence of proteins, starch or combinations of both allow to obtain flexible and non-crosslinked NRLFs with open cellular structures, like those of the conventional cross-linked product.

References

[1] Z.M. Ariff, *Journal of Materials Research and Technology*, **2020**, 9, 9929–9940
[2] S. Pinrat, *Journal of Physics: Conference Series*, **2022**, 2175, 012038
[3] N.S.A. Zauzi, *Materials Today: Proceedings*, **2019**, 17, 1001–1007

Authors

Y

Z

D

V

IMPRINT – IMPRESSUM
CellMAT 2022 - 7th International Conference on Cellular Materials
Editor: Prof. Dr.-Ing. Peter Quadbeck, University of Applied Science Offenburg, Germany

Postanschrift:
DGM - Deutsche Gesellschaft für Materialkunde e.V.
Marie-Curie-Straße 11-17
53757 Sankt Augustin

T +49 (0) 69 75306 750
F +49 (0) 69 75306 733
E-Mail: dgm@dgm.de
Web: www.dgm.de

ISBN- 978-3-88355-428-0